

Journal Information

Maejo International Journal of Science and Technology (ISSN 1905-7873 © 2014), the international journal for preliminary communications in Science and Technology is the first peer-refereed scientific journal of Maejo University (www.mju.ac.th). Intended as a medium for communication, discussion, and rapid dissemination of important issues in Science and Technology, articles are published online in an open access format, which thereby gives authors the chance to communicate with a wide range of readers in an international community.

Publication Information

MIJST is published triannually. Articles are available online and can be accessed free of charge at <http://www.mijst.mju.ac.th>. Printed and bound copies of each volume are produced and distributed to selected groups or individuals. This journal and the individual contributions contained in it are protected under the copyright by Maejo University.

Abstracting/Indexing Information

MIJST is covered and cited by Science Citation Index Expanded, SCOPUS, Journal Citation Reports/Science Edition, Zoological Record, Directory of Open Access Journals (DOAJ), CAB Abstracts, ProQuest, Google Scholar and EBSCO.

Contact Information

Editorial office: Maejo International Journal of Science and Technology (MIJST), 1st floor, Orchid Building, Maejo University, San Sai, Chiang Mai 50290, Thailand

Tel: +66-53-87-3880; Fax: +66-53-49-8133

E-mail: duang@mju.ac.th



MAEJO INTERNATIONAL JOURNAL OF SCIENCE AND TECHNOLOGY

Editor

Duang Buddhasukh, Maejo University, Thailand.

Associate Editors

Jatuphong Varith, Maejo University, Thailand.
Wasin Chareerntanankul, Maejo University, Thailand.
Niwooti Whangchai, Maejo University, Thailand.
Morakot Sukchotiratana, Chiang Mai University, Thailand.
Nakorn Tippayawong, Chiang Mai University, Thailand.

Editorial Assistants

James F. Maxwell, Chiang Mai University, Thailand.
Jirawan Banditpuritat, Maejo University, Thailand.

Editorial Board

Emeritus Prof. John Bremner
Dr. Pei-Yi Chu
Asst. Prof. Ekachai Chukeatirote
Prof. Richard L. Deming
Prof. Cynthia C. Divina
Prof. Mary Garson
Prof. Kate Grudpan
Dr. Soon Min Ho
Assoc. Prof. Duangrat Inthorn
Prof. Minoru Isobe
Prof. Dr. Sriman N. Iyengar
Professor Dr. Prakash Naraian Kalla
Dr. Nakul Karkare
Prof. Kunimitsu Kaya
Assoc. Prof. Margaret E. Kerr
Prof. Tanongkiat Kiatsirirot
Asst. Prof. Dr. Ignacy Kitowski
Asst. Prof. Andrzej Komosa
Prof. Dr. Monai Krairiksh
Asst. Prof. Pradeep Kumar
Asst. Prof. Dr. Sunil Kumar
Prof. Dr. T. Randall Lee
Asst. Prof. Ma. Elizabeth C. Leoveras
Prof. Dr. Subrata Mallick
Dr. Subhash C. Mandal
Prof. Amarendra N. Misra
Dr. Robert Molloy
Prof. Mohammad A. Mottaleb
Asst. Prof. Anand Nayyar
Engr.Obeta Nwachkwu
Assoc. Prof. Dr. Kaew Nualchawee
Prof. Dr. Yoko Oki
Prof. Stephen G. Pyne
Dr. Khaled Nabih Rashed
Prof. Renato G. Reyes
Prof. Dr. Hidehiro Sakurai
Dr. Waya Sengpracha
Prof. Dr. Sung le Shim
Asst. Prof. Dr. Satish K. Singh
Prof. Paisarn Sithigorngul
Prof. Anupam Srivastav
Prof. Maitree Suttajit
Asst. Prof. Thanaphong Thanasaksiri
Asst. Prof. Narin Tongwittaya
Prof. Keshav D. Verma
Assoc. Prof. Niwoot Whangchai
Assoc. Prof. Malinee Wongnawa
Asst. Prof. Dr. Kusum Yadav
Dr. Mahdi Zowghi

University of Wollongong, NSW, Australia.
Changhua Christian Hospital, Taiwan, R.O.C.
Mae Fah Luang University, Thailand.
California State University Fullerton, Fullerton CA
Central Luzon State University, Philippines.
The University of Queensland, Australia.
Chiang Mai University, Thailand.
INTI International University, Malaysia
Mahidol University, Thailand.
Nagoya University, Japan.
VIT University, India.
University, Bikaner, Campus Jaipur, India.
York Hospital, PA, USA.
Tohoku University, Japan.
Worcester State College, Worcester, MA.
Chiang Mai University, Thailand.
University of Maria-Curie Sklodowska, Poland.
University of Maria-Curie Sklodowska, Poland.
King Mongkut's Institute of Technology Ladkrabang, Thailand.
Jaypee University of Information Technology, India.
National Institute of Technology, Jharkhand, India.
University of Houston, USA.
Central Luzon State University, Philippines.
Siksha O Anusandhan University, India.
Jadavpur University, India.
Fakir Mohan University, Orissa, India.
Chiang Mai University, Thailand.
Northwest Missouri State University, USA.
KCL Institute of Management and Technology, India.
Enugu State University of Science and Technology, Nigeria.
Geoinformatics and Space Technology Development of Agency, Thailand.
Okayama University, Japan.
University of Wollongong, Australia.
National Research Centre, Giza, Egypt.
Central Luzon State University, Philippines.
Institute for Molecular Science, Myodaiji, Japan.
Silpakorn University, Thailand.
University of Seoul, Korea.
Jaypee University of Engineering and Technology, India.
Srinakharinwirot University, Thailand.
College of Engineering and Technology, India.
Naresuan University (Payao Campus), Thailand.
Chiang Mai University, Thailand.
Maejo University, Thailand.
S.V. (P.G.) College, Aligarh, India.
Maejo University, Thailand.
Prince of Songkla University, Thailand.
Salman Bin Abdulaziz University, Kingdom of Saudi Arabia.
Sharif University of Technology, Tehran, Iran.

Consultants

Asst. Prof. Chamnian Yosraj, Ph.D., President of Maejo University
Assoc. Prof. Thep Phongparnich, Ed. D., Former President of Maejo University
Assoc. Prof. Chalermchai Panyadee, Ph.D., Vice-President in Research of Maejo University

**MAEJO INTERNATIONAL JOURNAL
OF SCIENCE AND TECHNOLOGY**

*The International Journal for the Publication of Preliminary
Communications in Science and Technology*





MAEJO INTERNATIONAL JOURNAL OF SCIENCE AND TECHNOLOGY

Volume 8, Issue 1 (January – April 2014)

CONTENTS

	Page
Editor's Note	
<i>Duang Buddhasukh, Editor-in-Chief</i>	i
Statistical optimisation of culture conditions for biocellulose production by <i>Komagataeibacter</i> sp. PAP1 using soya bean whey <i>Amornrat Suwanposri, Pattaraporn Yukphan, Yuzo Yamada and Duangjai Ochaikul</i> *	1-14
On certain Banach spaces of difference sequences of fuzzy real numbers <i>Hemen Dutta</i>	15-19
Flexural performance of foam concrete containing pulverised bone as partial replacement of cement <i>Funso Falade, Efe Ikponmwosa* and Christopher Fapohunda</i>	20-31
An efficient Hantzsch synthesis of 1,4-dihydropyridines using <i>p</i> -toluenesulfonic acid under solvent-free condition <i>Masoud Nasr-Esfahani*, Morteza Montazerzohori and Razieh Raeati</i>	32-40
An alternative synthesis of (±)-phenylephrine hydrochloride <i>Wipanoot Baison, Aphiwat Teerawutgulrag*, Pakawan Puangsombat and Nuansri Rakariyatham</i>	41-47
Wave run-up on sandbag slopes <i>Thamnoon Rasmeeasmuang*, Wanich Chuenjai and Winyu Rattanapitikon</i>	48-57

An adaptive radial basis function neural network (RBFNN) control of energy storage system for output tracking of a permanent magnet wind generator <i>Abu H. M. A. Rahim</i>	58-74
Factors affecting release of ethanol vapour in active modified atmosphere packaging systems for horticultural products <i>Weerawate Utto</i>	75-85
On a fuzzy approach for the evaluation of golf players <i>Micael S. Couceiro*</i> , <i>Fernando M. L. Martins</i> , <i>Filipe M. Clemente</i> , <i>Gonçalo Dias and Rui Mendes</i>	86-99
Cultivation options for indoor and outdoor growth of <i>Chaetoceros gracilis</i> with airlift photobioreactors <i>Watadta Ritcharoen</i> , <i>Puchong Sriouam</i> , <i>Piyanate Nakseedee</i> , <i>Patthama Sang</i> , <i>Sorawit Powtongsook</i> , <i>Kunn Kungvansaichol and Prasert Pavasant*</i>	100-113

**MAEJO INTERNATIONAL JOURNAL
OF SCIENCE AND TECHNOLOGY**

Volume 8, Issue 1 (January – April 2014)

Author Index

Author	Page	Author	Page
Baison W.	41	Pavasant P.	100
Chuenjai W.	48	Powtongsook S.	100
Clemente F. M.	86	Puangsoombat P.	41
Couceiro M. S.	86	Rahim A. H. M. A.	58
Dias G.	86	Rakariyatham N.	41
Dutta H.	15	Raeati R.	32
Falade F.	20	Rasmeemasmuang T.	48
Fapohunda C.	20	Rattanapitikon W.	48
Ikponmwosa E.	20	Ritcharoen W.	100
Kungvansaichol K.	100	Sang P.	100
Martins F. M. L.	86	Sriouam P.	100
Mendes R.	86	Suwanposri A.	1
Montazerozohori M.	32	Teerawutgulrag A.	41
Nakseedee P.	100	Utto W.	75
Nasr-Esfahani M.	32	Yamada Y.	1
Ochaikul D.	1	Yukphan P.	1

Instructions for Authors

A proper introductory e-mail page containing the title of the submitted article and certifying its originality should be sent to the editor (Duang Buddhasukh, e-mail: duang@mju.ac.th). The manuscript proper together with a list of suggested referees should be attached in separate files. The list should contain at least 5 referees with appropriate expertise. Three referees should be non-native from 3 different countries. Each referee's academic/professional position, scientific expertise, affiliation and e-mail address must be given. The referees should not be affiliated to the same university/institution as any of the authors, nor should any two referees come from the same university/institution. The editorial team, however, retain the sole right to decide whether or not the suggested referees are approached.

Failure to conform to the above instructions will result in non-consideration of the submission.

Please also ensure that English and style is properly edited before submission. UK style of spelling should be used. Authors who would like to consult a professional service can visit www.proof-reading-service.com, www.editage.com, www.bioedit.co.uk (bioscience and medical papers), www.bioscienceeditingsolutions.com, www.scribendi.com, www.letpub.com, www.papersconsulting.com, www.sticklerediting.com, Cambridge Proofreading (<http://proofreading.org/>), www.ProofreadingServices.com, www.horizonproofreaders.org, www.manuscript-proofreading.com, [Quality Proofreading](http://QualityProofreading.com), [Help.Plagtracker](http://Help.Plagtracker.com), www.ninjaessays.com/editing/, <http://bid4papers.com/editing-services.html> or www.enago.com.

Important : Manuscript with substandard English and style will not be considered.

Warning : Plagiarism (including self-plagiarism) may be checked for at *the last* stage of processing and, if detected, will result in a rejection and blacklisting.

Manuscript Preparation

Manuscripts must be prepared in English using a word processor. MS Word for Macintosh or Windows, and .doc or .rtf files are preferred. Manuscripts may be prepared with other software provided that the full document (with figures, schemes and tables inserted into the text) is exported to a MS Word format for submission. Times or Times New Roman font is preferred. The font size should be 12 pt and the line spacing 'at least 17 pt'. A4 paper size is used and margins must be 1.5 cm on top, 2.0 cm at the bottom and 2.0 cm on both left and right sides of the paper. Although our final output is in .pdf format, authors are asked NOT to send manuscripts in this format as editing them is much more complicated. Under the above settings, a manuscript submitted should not be longer than **15 pages** for a full paper or **20 pages** for a review paper.

A template file may be downloaded from the *Maejo Int. J. Sci. Technol.* homepage. ([DOWNLOAD HERE](#))

Authors' full mailing addresses, homepage addresses, phone and fax numbers, and e-mail addresses homepages can be included in the title page and these will be published in the manuscripts and the Table of Contents. The corresponding author should be clearly identified. It is the corresponding author's responsibility to ensure that all co-authors are aware of and approve of the contents of a submitted manuscript.

A brief (200 word maximum) Abstract should be provided. The use in the Abstract of numbers to identify compounds should be avoided unless these compounds are also identified by names.

A list of three to five keywords must be given and placed after the Abstract. Keywords may be single words or very short phrases.

Although variations in accord with contents of a manuscript are permissible, in general all papers should have the following sections: Introduction, Materials and Methods, Results and Discussion, Conclusions, Acknowledgments (if applicable) and References.

Authors are encouraged to prepare Figures and Schemes in colour. Full colour graphics will be published free of charge.

Tables and Figures should be inserted into the main text, and numbers and titles supplied for all Tables and Figures. All table columns should have an explanatory heading. To facilitate layout of large tables, smaller fonts may be used, but in no case should these be less than 10 pt in size. Authors should use the Table option of MS Word to create tables, rather than tabs, as tab-delimited columns are often difficult to format in .pdf for final output.

Figures, tables and schemes should also be placed in numerical order in the appropriate place within the main text. Numbers, titles and legends should be provided for all tables, schemes and figures. Chemical structures and reaction schemes should be drawn using an appropriate software package designed for this purpose. As a guideline, these should be drawn to a scale such that all the details and text are clearly legible when placed in the manuscript (i.e. text should be no smaller than 8-9 pt).

For bibliographic citations, the reference numbers should be placed in square brackets, i.e. [], and placed before the punctuation, for example [4] or [1-3], and all the references should be listed separately and as the last section at the end of the manuscript.

Format for References

Journal :

1. D. Buddhasukh, J. R. Cannon, B. W. Metcalf and A. J. Power, "Synthesis of 5-n-alkylresorcinol dimethyl ethers and related compounds *via* substituted thiophens", *Aust. J. Chem.*, **1971**, *24*, 2655-2664.

Text :

2. A. I. Vogel, "A Textbook of Practical Organic Chemistry", 3rd Edn., Longmans, London, **1956**, pp. 130-132.

Chapter in an edited text :

3. W. Leistritz, "Methods of bacterial reduction in spices", in "Spices: Flavor Chemistry and Antioxidant Properties" (Ed. S. J. Risch and C-T. Ito), American Chemical Society, Washington, DC, **1997**, Ch. 2.

Thesis / Dissertation :

4. W. phutdhawong, "Isolation of glycosides by electrolytic decolourisation and synthesis of pentinomycin", *PhD Thesis*, **2002**, Chiang Mai University, Thailand.

Patent :

5. K. Miwa, S. Maeda and Y. Murata, "Purification of stevioside by electrolysis", *Jpn. Kokai Tokkyo Koho* **79 89,066 (1979)**.

Proceedings :

6. P. M. Sears, J. Peele, M. Lassauzet and P. Blackburn, "Use of antimicrobial proteins in the treatment of bovine mastitis", Proceedings of the 3rd International Mastitis Seminars, **1995**, Tel-Aviv, Israel, pp. 17-18.

Websites :

7. S. Simon, "What is an odds ratio?", **2008**, <http://www.childrensmercy.org/stats/definitions/or.htm> (Accessed: October 2011).

Manuscript Revision Time

Authors who are instructed to revise their manuscript should do so within **45** days. Otherwise the revised manuscript will be regarded as a new submission.

Manuscript Processing Time

As a result of a large number of submissions, there may be a long delay in the evaluation or publication of a paper. A duration of at least 6-8 months between submission and acceptance (or rejection) can normally be expected.

Maejo International Journal of Science and Technology

ISSN 1905-7873

Available online at www.mijst.mju.ac.th

Editor's Note

Dear all valued authors,

The two most important things for a submitted manuscript are, as a matter of principle, that it has a novel contribution and that it is scientifically sound. Primarily, we let the referees judge on these after some time period.

The next most important thing on our list is the language. Unfortunately, it happens to be the first thing we focus on when a submission is received in order to screen oncoming papers.

We therefore cannot overemphasise the importance of a properly edited manuscript with respect to language. In many cases, this can be achieved by the authors themselves (although with some additional care). Alternatively, for those authors who are less apt, a professional service may be sought. We have listed quite a number of them on our website for those who require one.

Full Paper

Statistical optimisation of culture conditions for biocellulose production by *Komagataeibacter* sp. PAP1 using soya bean whey

Amornrat Suwanposri¹, Pattaraporn Yukphan², Yuzo Yamada³ and Duangjai Ochaikul^{1,*}

¹ Department of Biology, Faculty of Science, King Mongkut's Institute of Technology Ladkrabang, Chalongkrung Rd. Ladkrabang, Bangkok, 10520, Thailand

² BIOTEC Culture Collection (BCC), Bioresources Technology Unit, National Centre for Genetic Engineering and Biotechnology, National Science and Technology Development Agency, Phaholyothin Road, Klong 1, Klong Luang, Pathumthani 12120, Thailand

³ Shizuoka University, 836 Ohya, Suruga-ku, Shizuoka 422-8529, Japan

* Corresponding author, e-mail: Suwanposri@hotmail.com; kodaungj@kmitl.ac.th

Received: 6 March 2013 / Accepted: 14 January 2014 / Published: 15 January 2014

Abstract: A low-cost medium based on soya bean whey (SBW) was prepared as a by-product from agriculture and optimised for biocellulose (BC) production by *Komagataeibacter* sp. PAP1. The optimal conditions for BC production are: pH 6.21, 1.61% ethanol concentration (v/v) and 28.4°C. The use of optimised medium based on SBW increased BC production 3.6 fold compared to standard Hestrin-Schramm (HS) medium. The BC film produced from the optimised medium was stronger and more impermeable to water vapour and oxygen compared to the one produced from the standard HS medium. These properties allow SBW film to be developed into eco-friendly food packaging for oxygen-sensitive products. Its high water absorption capacity allows its use in biomedical application such as wound dressing. Our results demonstrate that SBW can be used as an alternative low-cost substrate for BC production on commercial scale.

Keywords: biocellulose, bacterial cellulose, soya bean whey, *Komagataeibacter*

INTRODUCTION

Cellulose is one of the most important biopolymer substances and has been widely used in many industries because of its renewability, low cost and high abundance on earth. However, the most industrially used cellulose is derived from higher plants and is usually contaminated with hemicellulose, lignin and other plant components. To obtain pure cellulose, plant-derived cellulose (PC) is purified using chemical pulping and isolation/purification processes which involve the use of sodium hydroxide, sulphuric acid and other chemical reagents. These processes generate a large

amount of liquid waste with high biological oxygen demand (BOD) and chemical oxygen demand (COD) that causes severe environmental pollution [1]. Hence, researchers are interested in developing biotechnological processes to produce cellulose from alternative sources such as micro-organisms.

Bacterial cellulose or biocellulose (BC) is an extracellular cellulose produced by some acetic acid bacteria in the genus *Komagataeibacter* (formerly *Gluconacetobacter*) [2] such as *K. xylinus*, *K. nataicola*, *K. hansenii* and *K. swingsii* [3-5]. BC has high purity and has been considered as an alternative source of cellulose because of its clear advantages compared to PC in microfibrillar nanostructure, high mechanical strength, high elasticity, conformability, thermal stability, high water and liquid absorption, low toxicity, excellent biological affinity, and biodegradability [6-8]. Additionally, compared to PC, isolation and purification of BC is relatively simple and does not need intense chemical processes with high waste production. These unique qualities have attracted much attention to the use of BC as an alternative material in several special applications such as functionalised paper sheets, fire retarding agent, wound dressing for severely damaged skin and electronic paper [9-11]. However, BC is currently priced higher than PC. A promising approach to reduce the cost of production of BC and maximise its yield is optimisation of culture conditions and use of agricultural by-products or waste as substrate.

Soya bean whey (SBW) is a pale yellow liquid by-product which is produced from the pressing of coagulated soya bean milk in tofu production. SBW is 79-90% of soya bean milk [12] and has a high BOD (13,730 ppm) after 5 days of incubation [13]. It is a rich source of nutrient containing protein, starch, fat and sugars such as glucose, fructose, sucrose, raffinose and stachyose [14], which can be utilised as substrate for microbial fermentation [12]. Many studies have shown that SBW can be used as an inexpensive substrate in the production of peptide-enriched functional food, fungal mycelial protein and nisin, a high-value food preservative [12, 15, 16]. A few studies have reported of its use in BC production by *Komagataeibacter* sp. [17-19].

The microbial productivity of BC depends on culture conditions such as the composition of the medium (carbon, nitrogen and supplementary substances), pH, temperature and cultivation method [20]. It is difficult to determine the most important factors and to optimise the culture condition. One-factor-at-a-time is a conventional method for medium optimisation. It is time-consuming and expensive, and often leads to misinterpretation of results when interactions between different components take place [6]. Statistical experimental design has been applied to minimise error in determining the effect of parameters and it indicates the simultaneous, systematic and efficient variation of all parameters [21]. Response surface methodology (RSM) is a collection of mathematical and powerful statistical technique commonly used to determine the optimal culture conditions for multiple variables with a minimum number of experiments [22]. This technique had been successfully applied for designing media in the production of probiotics, bacterial cellulose, enzymes, organic acids and antibiotics [23-26].

In a previous study, we have reported the isolation of bacterial cellulose producer from tropical fruits found in Thailand [27]. We found that *Komagataeibacter* sp. PAP1 was the most potent BC producer. In this study, the BC productivity of this strain is improved by optimising culture conditions using RSM. We also report the use of SBW as a low-cost substrate for production of BC and the characterisation of BC film obtained from optimised medium based on SBW as compared with that obtained from standard Hestrin-Schramm (HS) medium. Characteristics, namely morphology, mechanical properties, water vapour transmission rate, oxygen gas transmission rate, water absorption capacity and colour appearance, are presented.

MATERIALS AND METHODS

Bacterial Strain and Raw Material

Komagataeibacter sp. PAP1 was used as BC producer. The bacterium was isolated from rotten papaya (*Carrica papaya*) and identified by morphological, physiological and biochemical characterisations as well as 16S rRNA gene sequence analysis [27]. The isolate could utilise almost all general carbon sources and gave the maximum BC yield in the standard HS medium [3] containing 2% (w/v) mannitol (3.50 g/L) or ethanol (3.43 g/L) as the sole carbon source. Optimal growth was obtained at 25-30°C, pH 4.5-7.0 and colonies appeared on a standard HS agar plate after 2-3 days [27].

For long-time storage of the isolate, glycerol stocks of the micro-organism were prepared in a medium containing 2.5% (w/v) glucose, 0.5% (w/v) peptone, 0.3% (w/v) yeast extract and 20% (v/v) glycerol, and maintained at -80°C until further use.

SBW was provided by a small tofu processing factory in Ladkrabang district, Bangkok, and kept at -10°C. Moisture content, protein content, fat, ash, total carbohydrate and lactose in SBW were analysed using standard methods according to AOAC [28]. The pH of SBW was measured using a pH meter (Cyberscan pH 2000, Utech Cybernetics, Singapore).

Preparation of Starter Culture

Komagataeibacter sp. PAP1 was cultivated on standard HS agar at 30°C for 48 hr. Two loopfuls of the bacterium were transferred into 300 mL of a sterilised starter medium in a 500-mL Erlenmeyer flask. The starter medium consisted of 5% (w/v) sucrose, 1% (w/v) ammonium sulfate and 0.1% (v/v) acetic acid. The volume of the starter medium was adjusted to 300 mL using SBW and the pH of the medium adjusted to 4.5 using 6N NaOH. The starter culture was carried out statically at 30°C for 48 hr.

Production of BC Using Medium Based on SBW

The filtered SBW was adjusted to different pHs by glacial acetic acid and 6N NaOH. Subsequently, it was sterilised at 110°C for 20 min. and then supplemented with different volumes of sterilised ethanol according to each experimental run (Table 1). The BC production was performed in 250-mL Erlenmeyer flasks containing 90 mL of the medium based on SBW (Table 2). Each flask was inoculated with 10 mL of the starter culture and incubation was done at different temperatures for 7 days under static condition. BC pellicles formed were washed three times with distilled water, treated with 2% (w/v) NaOH and sterilised at 121°C for 15 min. to eliminate residual bacterial cells and medium components. Purified cellulose pellicles were washed again thrice with distilled water and dried in a hot air oven at 65°C until constant weight was obtained. The BC production yield was expressed as dry weight of BC per volume of culture medium (g/L).

Experimental Design and Statistical Analysis

The effects of three independent variables ($k = 3$), namely initial pH of culture medium (X1), ethanol concentration (X2) and incubation temperature (X3), on BC production by *Komagataeibacter* sp. PAP1 were elucidated using a central composite design (CCD) of RSM. Each independent variable was analysed at five levels, i.e. the lower limit ($-\alpha$), low (-1), central (0), high (+1) and upper limit ($+\alpha$) (Table 1). The upper and the lower limits of each independent variable were set at a distance of 1.682 ($2^{k/4} = 1.682$) from the design centre. For statistical analysis, the three independent variables were coded according to the following equation [29]:

$$X_i = (A_i - A_c) / \Delta A_i \quad (1)$$

where X_i is the independent variable code value; A_i , the independent variable actual value in the original units; A_c , the independent variable actual value at the centre point in the original units; and ΔA_i , the step change in the original units.

Table 1. Code levels and the actual values of the factors of the three independent variables at five levels of CCD

Independent variable	Code	Actual value of factor at CCD level of:				
		$-\alpha$ (-1.682)	-1	0	+1	$+\alpha$ (+1.682)
Initial pH of culture medium	X1	2.64	4	6	8	9.36
Ethanol concentration (% v/v)	X2	0	0.75	2	3.25	4.10
Incubation temperature (°C)	X3	21.6	25.0	30.0	35.0	38.4

Six replications were performed at the centre point and the number of experimental runs was calculated from the equation [30]:

$$N = 2^k + 2k + c \quad (2)$$

where N is the number of experimental run; k , the number of independent variable; and c , the number of replication at the centre point.

The response data (yield of BC) from each experimental run was analysed by multiple linear regression using the PASW Statistics software (Version 18.0). Based on these results, a regression model was developed to predict the effect of combined variables on BC production by *Komagataeibacter* sp. PAP1. The responses can be predicted by the following second-order polynomial regression equation [29]:

$$Y = B_0 + B_1(\text{pH}) + B_2(\text{E}) + B_3(\text{T}) + B_{11}(\text{pH})^2 + B_{22}(\text{E})^2 + B_{33}(\text{T})^2 + B_{12}(\text{pH}*\text{E}) + B_{13}(\text{pH}*\text{T}) + B_{23}(\text{E}*\text{T}) \quad (3)$$

where Y is the predicted response (yield of BC, g/L); B_0 , the intercept term; B_1 - B_3 , the linear coefficients; B_{11} , B_{22} , B_{33} , the quadratic coefficients; B_{12} , B_{13} , B_{23} , the cross product coefficients; and pH, E and T, the initial pH of culture medium, ethanol concentration (% v/v) and incubation temperature (°C) respectively. The quality of fit of the model was tested by an analysis of variance (ANOVA) and the coefficient of determination (R^2). A value of $R^2 > 0.75$ indicates aptness of the model [29]. The response surface and contour plots were constructed with Statistica software (trial version) to indicate an optimal condition using the fitted second-order polynomial equations obtained by holding one of the independent variables constant and changing the levels of the other two variables [31].

Growth and BC Production under Optimal Conditions

To verify the predicted responses, the growth and BC production of *Komagataeibacter* sp. PAP1 were studied in 250-mL Erlenmeyer flasks under optimal conditions for 14 days. The viable bacterial cells were examined everyday using spread plate technique. The cell suspensions used for plating were obtained by vigorously shaking the culture flasks to release the bacterial cells from the cellulose pellicles [32]. Then the flasks were serially diluted with 0.1% (w/v) peptone, and 0.1 mL of each dilution was spread onto an agar plate containing an optimised medium based on SBW.

Colonies were counted after three days of incubation using a Reichert Darkfield Quebec colony counter (Model 13332600, Reichert Analytical Instruments Inc., USA).

Comparison of BC Production in Optimised SBW Medium and Standard HS Medium

Ten mL of the 48-hr starter culture were transferred to a 250-mL Erlenmeyer flask containing 90 mL of optimised medium based on SBW or standard HS medium, 2% (w/v) glucose, 0.5% (w/v) yeast extract, 0.5% (w/v) peptone, 0.27% (w/v) disodium hydrogen phosphate and 0.12% (w/v) citric acid (pH of mixture = 6.0). The culture was incubated statically for 7 days at an optimal temperature for the optimised medium based on SBW, or at 30°C for standard HS medium. After incubation, the yields of BC from each culture medium were analysed.

Preparation of BC Film

The BC samples produced in both media were immersed in 0.5% (v/v) ammonium hydroxide overnight and washed thrice with tap water. Subsequently, the BC pellicles were boiled for 30 min. to remove ammonium hydroxide and washed thrice again with tap water [33]. The pellicles were squeezed to remove water using a pressing machine and then dried at 65°C for 3 hr.

Characterisation of BC Film

Mechanical properties

The BC films were examined for tensile strength, Young's modulus and elongation at break using a universal testing machine (TA plus, Lloyd Instruments Ltd., England) at a test speed of 0.25 mm/min. according to Thai Industrial Standard (TIS. 1353) [34]. Rectangular specimens for measurements were cut from samples with a gauge length of 30 mm. Five specimens were made to average the results.

Water vapour transmission rate

The water vapour transmission rate was analysed using a Lyssy L 80-4000 water vapour permeation tester (Lyssy AG, Switzerland), and test conditions followed ASTM E398-13 [35] in the humidity detection sensor method.

Oxygen gas transmission rate

The oxygen gas transmission rate was determined using an Illinois 8008 oxygen permeation tester (Illinois Instruments Inc., USA), and test conditions followed the procedure of ASTM D3985-05 [36] in the coulometric sensor method.

Water absorption capacity

The water absorption capacity was examined using the procedure of ASTM D570-98 [37]. Each dried sample (2.54 × 7.62 cm) was immersed in distilled water at 23°C until equilibrium. The swollen sample was removed from water and excess water at the surface was wiped off. The sample was weighed and the water absorption capacity (%) was calculated ($= \frac{(\text{wet weight} - \text{dry weight})}{\text{dry weight}} \times 100$).

Colour analysis

To investigate the colour appearance of samples, L*, a* and b* values were measured by the CIELAB colour system with a colourimeter (Minolta CR-300, Konica Minolta, USA), where L* is the lightness with a scale from 0 (black) to 100 (white); and a* and b* are the colour directions: +a*, red direction; -a*, green direction; +b*, yellow direction; and -b*, blue direction.

Scanning electron microscopy

The BC samples produced in both culture media were cut and coated with gold (Fine coater, model JEC-12000, JEOL Ltd., Japan). A scanning electron microscope (JSM S410, JEOL Ltd., Japan) was used at 5 KV for sample examination with 5,000× and 30,000× magnifications.

Statistical analysis

Comparison of BC yields from optimised medium based on SBW versus standard HS medium was statistically analysed by student's t-test using PASW Statistics software (Version 18.0).

RESULTS AND DISCUSSION**Optimisation of Medium Based on SBW**

In this study, SBW consisted of 98.87% moisture, 0.34% protein, 0.02% fat, 0.51% ash, 0.26% total carbohydrate and 0.02% lactose (pH 4.5). In general, the medium composition and environmental factors affect bacterial cell growth and product formation [20]. Three main fermentation factors, namely initial pH of culture medium (X1), concentration of carbon source (X2) and incubation temperature (X3), were chosen for the optimisation of BC production by *Komagataeibacter* sp. PAP1 in SBW. In our previous study [27], mannitol and ethanol gave the highest BC yield, but on cost consideration ethanol was selected as carbon source in this study. CCD was used to identify the optimal condition for the medium. The experimental design and BC yields obtained from different treatment combinations for BC production are summarised in Table 2. BC yields were determined using multiple regression analysis with $p \leq 0.05$ and used to generate second-order regression model capable of predicting the amounts of BC yield (Y) as a function of the three independent variables. The derived regression equation (2) for the optimisation of the medium based on SBW becomes:

$$Y = 3.946372 + 0.077053 (\text{pH}) + 0.163093 (\text{E}) - 0.483914 (\text{T}) - 0.730344 (\text{pH})^2 - 0.609879 (\text{E})^2 - 0.791462 (\text{T})^2 - 0.054291 (\text{pH} \cdot \text{E}) - 0.099458 (\text{pH} \cdot \text{T}) + 0.141458 (\text{E} \cdot \text{T}) \quad (4)$$

The quality of fit of the quadratic polynomial equation was examined using R^2 and probability (p) values. The R^2 value was found by calculation to be 0.835, indicating that 83.50% of the variation in BC yields could be explained by the model (Table 3). The p value was found to be significant ($p < 0.05$) and no significant lack of fit ($p > 0.05$) was noticed. As shown in Table 4, statistical analysis indicates significant effects of ethanol concentration and incubation temperature on BC production. The generated second-order regression model is adequate in predicting the BC yield. From the linear coefficients of second-order equation above, initial pH of the culture medium and ethanol concentration show a positive effect on BC synthesis, whereas incubation temperature yields a negative result.

Table 2. Experimental design and results of BC yield using central composite design

Treatment	Code variable level			Response (BC yield, g/L)	
	X1	X2	X3	Observed	Predicted
1	-1	-1	-1	2.67±0.02	2.05
2	-1	-1	+1	1.61±0.04	0.99
3	-1	+1	-1	2.24±0.02	2.20
4	-1	+1	+1	1.59±0.03	1.71
5	+1	-1	-1	3.10±0.02	2.51
6	+1	-1	+1	1.49±0.03	1.06
7	+1	+1	-1	2.29±0.04	2.44
8	+1	+1	+1	1.40±0.02	1.56
9	-1.682	0	0	1.29±0.02	1.76
10	+1.682	0	0	1.81±0.02	2.01
11	0	-1.682	0	0.83±0.02	2.33
12	0	+1.682	0	2.95±0.05	2.50
13	0	0	-1.682	2.09±0.06	2.53
14	0	0	+1.682	0.67±0.02	0.90
15	0	0	0	3.60±0.06	3.95
16	0	0	0	3.81±0.06	3.95
17	0	0	0	4.00±0.04	3.95
18	0	0	0	4.01±0.04	3.95
19	0	0	0	4.01±0.02	3.95
20	0	0	0	4.35±0.03	3.95

Table 3. Analysis of variance (ANOVA) of BC yields

Source	SS	DF	MS	F-value	p-value
Model	67.073	9	7.453	34.154	0.000
Residual	10.910	50	0.218		
Total	77.983	59			

Note: SS = Sum of square, DF = Degree of freedom, MS = Mean square
 $R^2 = 0.835$

Table 4. Analysis of variance (ANOVA) of effects of three independent variables on BC yields

Code	Coefficient	t- value	p-value
Constant	3.946	35.880	.000
X1	.077	1.055	.296
X2	.163	2.234	.030
X3	-.484	-6.628	.000
X1X2	-.054	-.569	.572
X1X3	-.099	-1.043	.302
X2X3	.141	1.484	.144
X1X1	-.730	-10.264	.000
X2X2	-.610	-8.571	.000
X3X3	-.791	-11.123	.000

Note: X1 = initial pH of culture medium, X2 = ethanol concentration, X3 = incubation temperature

The second-order regression model was used to develop response surface plots (Figure 1). Figure 1a shows the response surface curve of BC production as a function of initial pH of the culture medium and ethanol concentration by keeping the incubation temperature at 30°C (central level). The BC yield increases with elevated pH and ethanol concentration up to 6 and 2% respectively. Further increase in both variables leads to opposite effects. Maximum BC production of 3.30 g/L is obtained at pH 6.21 and 1.61% ethanol.

Figure 1b shows the response surface curve of BC production as a function of initial pH and incubation temperature by keeping the concentration of ethanol at 2% (central level). The BC yield increases with incubation temperature up to 30°C (central level) and then decreases. The maximum BC yield of 3.53 g/L is obtained at initial pH of 6.21 and incubation temperature of 28.4°C.

Figure 1c shows the effect of ethanol concentration and incubation temperature on BC yield at initial pH 6 (central level). The BC yield increases with ethanol concentration and temperature up to 2% and 30°C respectively, and then decreases. The maximum BC yield of 3.42 g/L is obtained at 1.61% ethanol and 28.4°C. Based on Equation (4), the optimal values of initial pH, ethanol concentration and incubation temperature are 6.21, 1.61% and 28.4°C respectively, with a maximum BC yield of 4.03 g/L.

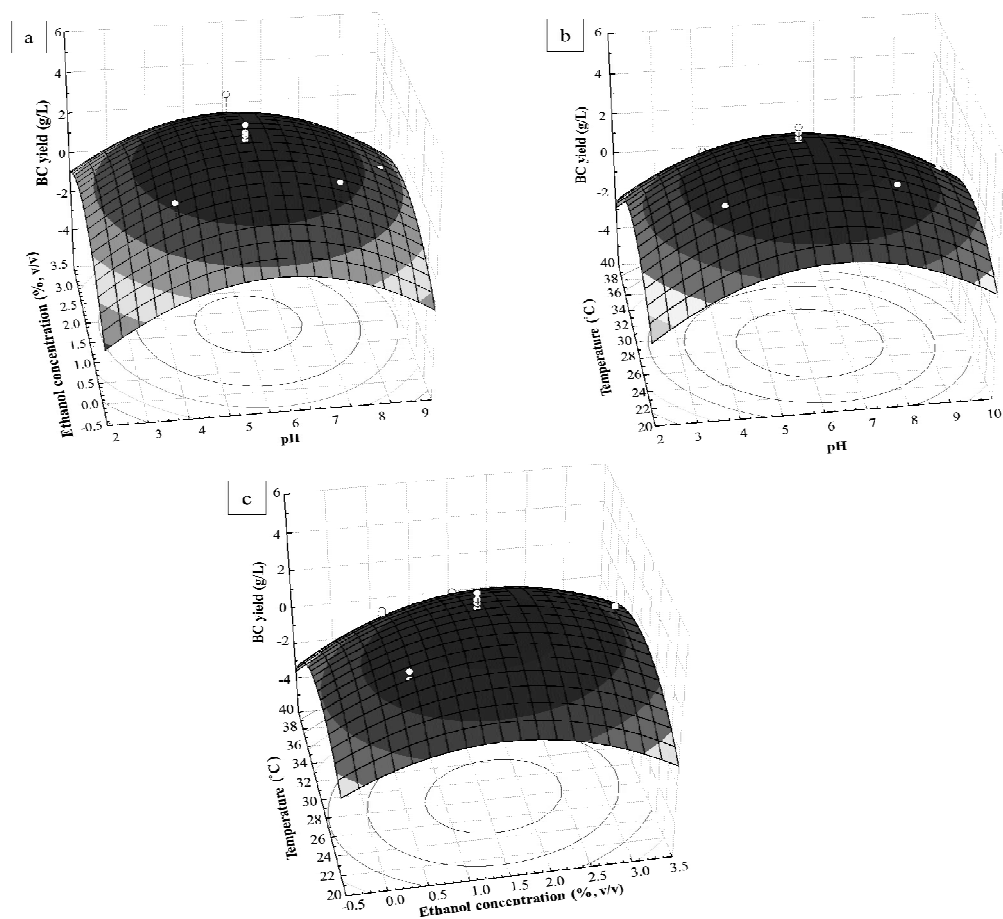


Figure 1. Three-dimensional response surface plots and contour plots of BC yield by *Komagataeibacter* sp. PAP1: (a) effect of ethanol concentration and initial pH of culture medium; (b) effect of initial pH of culture medium and temperature; (c) effect of ethanol concentration and temperature

To verify the predicted response, *Komagataeibacter* sp. PAP1 was cultivated in the optimised medium based on SBW under static condition for 14 days. As shown in Figure 2, bacterial cells of isolate PAP1 increased rather slowly during the first two days and then increased exponentially from the third to seventh day. A stationary phase was observed after seven days of cultivation, and the viable cell count reached a maximum value of 8.2×10^7 cfu/mL. The production of BC began from the first day of cultivation and increased rapidly from the third day. A maximum BC production of 4.10 g/L was obtained on the seventh day of cultivation, after which it stabilised. This result shows that BC production by *Komagataeibacter* sp. PAP1 is growth-associated. The pH of the culture medium decreased from 6.21 at the beginning to less than 3.50 after 14 days of cultivation. Under these conditions, the BC yield was relatively close to the predicted response (Table 2). Thus, they were used as optimal conditions in this study.

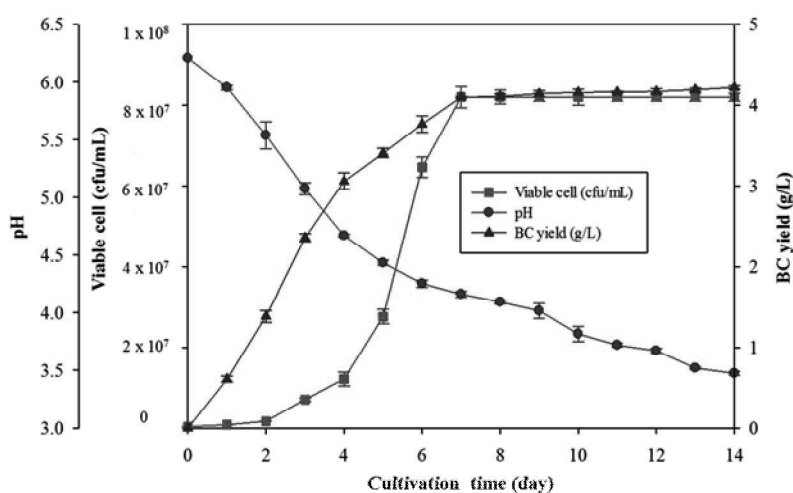


Figure 2. Growth and BC production of *Komagataeibacter* sp. PAP1 in optimised medium based on SBW

Comparison of BC Production

As shown in Table 5, BC yields indicate that the optimised medium based on SBW is better than the standard HS medium. The yield of BC in the former medium was 4.14 ± 0.02 g/L, 3.6 times higher than that (1.15 ± 0.03 g/L) obtained in the latter medium, the difference being highly significant ($p < 0.01$). The results suggest that SBW has some accelerative properties which increase cell growth and BC production [17]. The high productivity of BC in the optimised medium based on SBW, compared to standard HS medium, may significantly lower its production cost. The results obtained in this study are consistent with those in previous studies. Castro *et al.* [5] showed that pineapple peel juice as medium gave higher BC yield than did HS medium (2.80 vs 2.10 g/L) using *Gluconacetobacter swingsii*. Using waste from beer fermentation broth as raw material, Ha *et al.* [38] found that in a 120-hr cultivation, the medium from the waste and the HS medium yielded 4.52 and 0.45 g/L of BC respectively. In contrast, Carreira *et al.* [39] showed a low level of BC production of 0.08, 0.1, 0.1 and 0 g/L using cheese whey, grape skin aqueous extract, crude glycerol and sulfite pulping liquor respectively. Such low BC yields are likely to be due to the presence of inhibitors derived from industrial processes, which obstruct bacterial cell growth and BC production.

Table 5. Comparison of BC yields in two media

Medium	BC yield (g/L)
Optimised medium based on SBW	4.14 ± 0.02*
Standard HS medium	1.15 ± 0.03

Note: Results obtained are the mean of triplicates ± SD. Data were analysed using student's t-test.

* Highly significant ($p < 0.01$)

Characterisation of BC Film

Structure

The morphology of BC film examined by scanning electron microscopy shows three-dimensional porous network structures consisting of randomly arranged ribbon-shaped ultrafine fibrils (Figure 3). The BC fibrils have transverse dimensions ranging 26-63 nm, which are smaller than fibrils from PC [40]. The results are in accordance with previously reported BC structure [41-42]. Figures 3a-b show SBW film as thicker ribbon-shaped fibrils compared to HS film (Figures 3c-d). The reticulated structure of BC is tightly combined in SBW film but loose in HS film.

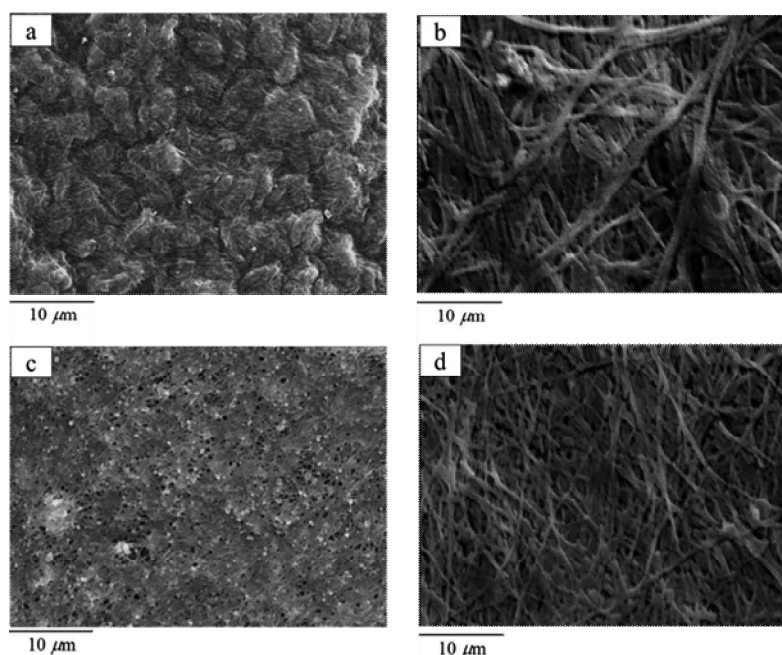


Figure 3. Structure of BC film produced from optimised SBW medium with magnification 5,000× (a) and 30,000× (b), and from standard HS medium with magnification 5,000× (c) and 30,000× (d)

Mechanical properties

The mechanical properties of both SBW and HS films are shown in Table 6. The SBW film shows an increase of 108% in tensile strength and 841% in Young's modulus over those of the HS film. The elongation at the break of SBW film (3.28%) was 3.4 times less than that of HS film (11.17%). The high Young's modulus of film made from BC can be explained by the structure of the BC pellicle, which has ribbon-shaped fibrils that are more easily oriented in one plane when they are pressed [43]. Furthermore, wider ribbons give higher tensile strength and Young's modulus because of increasing effective cross-sectional area and number of 1,4 covalent bonds [44]. The tensile strength and Young's modulus values of BC films produced in this study are relatively high compared to previous reports [44-45].

Table 6. Properties of BC film

Property	SBW film	HS film
Tensile strength (MPa)	49.16	23.58
Young's modulus (MPa)	2498.69	265.51
Elongation at break (%)	3.28	11.17
Water vapour transmission rate (g/m ² /day)	1986	2549
Oxygen gas transmission rate (cm ³ /m ² /day)	23.1	173
Water absorption capacity (%)	232.29	257.83

Barrier properties and water absorption

Barrier properties, viz. water vapour transmission rate and oxygen gas transmission rate, are listed in Table 6. The SBW film gives 22% lower water vapour transmission rate than does HS film and also acts as an efficient barrier to oxygen compared with HS film (23.1 vs 173 cm³/m²/day). Similar to the present study, Rani *et al.* [45] found the BC film produced from grape medium to be a better barrier to oxygen (415.27 cm³/m²/day) than one produced from the HS medium (1962.67 cm³/m²/day). They also found that the BC film has a higher water vapour transmission rate and lower oxygen gas transmission rate (2448.28 g/m²/day and 415.27 cm³/m²/day) when compared with a synthetic polymer (18-20 g/m²/day and 8000-1400 cm³/m²/day).

Both SBW and HS films show great water absorption property. The water absorption capacity of both kinds of film is over 2 times of their weight (Table 6). This is because BC has a three-dimensional porous network structure which can maintain a large amount of water [10, 46].

Colour appearance

Both SBW and HS films were opaque and white, as evident from the L* values being shifted slightly towards the lighter side (Table 7), suggesting that no bleaching is required for either film. The results compare well with a previous report on the utilisation of coconut water and pineapple water for BC production by *Acetobacter xylinum* strains [47]. The BC sheets produced from both kinds of agricultural waste exhibited a white colour and an opaque yellow colour respectively, thus needing no de-colourisation.

Table 7. Results of colour analysis of BC film

Sample	CIE Lab value ± Standard error		
	L*	a*	b*
SBW film	57.72 ± 0.34	-2.06 ± 0.17	-5.49 ± 0.06
HS film	58.56 ± 0.10	-1.19 ± 0.03	-5.31 ± 0.21

CONCLUSIONS

This study has demonstrated that soya bean whey can be efficiently used as a substrate for BC production. It has also shown that the BC film obtained shows good properties in the terms of mechanical strength, barrier to water vapour and oxygen, water absorption capacity and colour.

ACKNOWLEDGEMENTS

The authors are grateful to the National Science and Technology Development Agency and King Mongkut's Institute of Technology Ladkrabang for supporting this work.

REFERENCES

1. S. U. Pokalwar, M. K. Mishra and A. V. Manwar, "Production of cellulose by *Gluconacetobacter* sp.", *Rec. Res. Sci. Technol.*, **2010**, 2, 14-19.
2. Y. Yamada, P. Yukphan, H. T. L. Vu, Y. Muramatsu, D. Ochaikul, S. Tanasupawat and Y. Nakagawa, "Description of *Komagataeibacter* gen. nov., with proposals of new combinations (*Acetobacteraceae*)", *J. Gen. Appl. Microbiol.*, **2012**, 58, 397-404.
3. S. Hestrin and M. Schramm, "Synthesis of cellulose by *Acetobacter xylinum*. 2. Preparation of freeze-dried cells capable of polymerizing glucose to cellulose", *Biochem. J.*, **1954**, 58, 345-352.
4. P. Lisdiyanti, R. R. Navarro, T. Uchimura and K. Komagata, "Reclassification of *Gluconacetobacter hansenii* strains and proposals of *Gluconacetobacter saccharivorans* sp. nov. and *Gluconacetobacter nataicola* sp. nov.", *Int. J. Syst. Evol. Microbiol.*, **2006**, 56, 2101-2111.
5. C. Castro, R. Zuluaga, J. L. Putaux, G. Caro, I. Mondragon and P. Gañán, "Structural characterization of bacterial cellulose produced by *Gluconacetobacter swingsii* sp. from Colombian agroindustrial wastes", *Carbohydr. Polym.*, **2011**, 84, 96-102.
6. M. Shoda and Y. Sugano, "Recent advances in bacterial cellulose production", *Biotechnol. Bioprocess Eng.*, **2005**, 10, 1-8.
7. D. Klemm, D. Schumann, U. Udhardt and S. Marsch, "Bacterial synthesized cellulose-artificial blood vessels for microsurgery", *Prog. Polym. Sci.*, **2001**, 26, 1561-1603.
8. P. Ross, R. Mayer and M. Benziman, "Cellulose biosynthesis and function in bacteria", *Microbiol. Molec. Biol. Rev.*, **1991**, 55, 35-58.
9. A. H. Basta and H. El-Saied, "Performance of improved bacterial cellulose application in the production of functional paper", *J. Appl. Microbiol.*, **2009**, 107, 2098-2107.
10. W. K. Czaja, D. J. Young, M. Kawecki and R. M. Brown Jr, "The future prospects of microbial cellulose in biomedical applications", *Biomacromolec.*, **2007**, 8, 1-12.
11. J. Shah and R. M. Brown Jr, "Towards electronic paper displays made from microbial cellulose", *Appl. Microbiol. Biotechnol.*, **2005**, 66, 352-355.
12. A. Singh and R. Banerjee, "Peptide enriched functional food adjunct from soy whey: a statistical optimization study", *Food Sci. Biotechnol.*, **2013**, 22, 65-71.
13. M. Monajjemi, A. L. N. Aminin, A. R. Ilkhani and F. Mollaamin, "Nano study of antioxidant activities of fermented soy whey prepared with lactic acid bacteria and kefir", *Afr. J. Microbiol. Res.*, **2012**, 6, 426-430.
14. W. Y. Fung, Y. P. Woo and M. T. Liong, "Optimization of growth of *Lactobacillus acidophilus* FTCC 0291 and evaluation of growth characteristics in soy whey medium: A response surface methodology approach", *J. Agric. Food Chem.*, **2008**, 56, 7910-7918.
15. D. Mitra, A. L. Pometto III, S. K. Khanal, B. Karki, B. F. Brehm-Stecher and J. H. van Leeuwen, "Value-added production of nisin from soy whey", *Appl. Biochem. Biotechnol.*, **2010**, 162, 1819-1833.
16. H. Falanghe, A. K. Smith and J. J. Rackis, "Production of fungal mycelial protein in submerged culture of soybean whey", *Appl. Microbiol.*, **1964**, 12, 330-334.
17. X. Lu, Y. Qian and T. Yan, "Bacterial cellulose production by soybean whey based medium", *KMITL Sci. J.*, **2004**, 4, 100-107.
18. X. Lu, Y. Qian and L. X. Dong, "Application of bacterial cellulose to low-fat sausage", *Food Sci.*, **2005**, 26, 272-274.

19. S. Photisarach, "Optimization of bacterial cellulose production from *Acetobacter xylinum* Agr60 cultured in tofu whey", *Master Thesis*, 2011, Chiang Mai University, Thailand.
20. P. R. Chawla, I. B. Bajaj, S. A. Survase and R. S. Singhal, "Microbial cellulose: fermentative production and applications", *Food Technol. Biotechnol.*, 2009, 47, 107-124.
21. B. N. Gawande and A. Y. Patkar, "Application of factorial designs for optimization of cyclodextrin glycosyltransferase production from *Klebsiella pneumoniae* AS-22", *Biotechnol. Bioeng.*, 1999, 64, 168-173.
22. G. E. P. Box and J. S. Hunter, "Multi-factor experimental designs for exploring response surfaces", *Ann. Math. Statist.*, 1957, 28, 195-241.
23. A. Jagannath, A. Kalaiselvan, S. S. Manjunatha, P. S. Raju and A. S. Bawa, "The effect of pH, sucrose and ammonium sulphate concentrations on the production of bacterial cellulose (nata-de-coco) by *Acetobacter xylinum*", *World J. Microbiol. Biotechnol.*, 2008, 24, 2593-2599.
24. Q. K. Beg, V. Sahai and R. Gupta, "Statistical media optimization and alkaline protease production from *Bacillus mojavensis* in a bioreactor", *Process Biochem.*, 2003, 39, 203-209.
25. K. Adinarayana, P. Ellaiah, B. Srinivasulu, R. B. Devi and G. Adinarayana, "Response surface methodological approach to optimize the nutritional parameters for neomycin production by *Streptomyces marinensis* under solid-state fermentation", *Process Biochem.*, 2003, 38, 1565-1572.
26. S. Barrington and J. W. Kim, "Response surface optimization of medium components for citric acid production by *Aspergillus niger* NRRL 567 grown in peat moss", *Bioresour. Technol.*, 2008, 99, 368-377.
27. A. Suwanposri, P. Yukphan, Y. Yamada and D. Ochaikul, "Identification and biocellulose production of *Gluconacetobacter* strains isolated from tropical fruits in Thailand", *Maejo Int. J. Sci. Technol.*, 2013, 7, 70-82.
28. W. Horwitz and G. W. Latimer Jr. (Ed.), "Official Methods of Analysis of AOAC International", 18th Edn., Gaithersburg (MD), 2005, pp.59-61.
29. A. Pal and F. Khanum, "Production and extraction optimization of xylanase from *Aspergillus niger* DFR-5 through solid-state-fermentation", *Bioresour. Technol.*, 2010, 101, 7563-7569.
30. F. Rigas, V. Dritsa, R. Marchant, K. Papadopoulou, E. J. Avramides, and I. Hatzianestis, "Biodegradation of lindane by *Pleurotus ostreatus* via central composite design", *Environ. Int.*, 2005, 31, 191-196.
31. C. Malisorn and W. Suntornsuk, "Optimization of β -carotene production by *Rhodotorula glutinis* DM28 in fermented radish brine", *Bioresour. Technol.*, 2008, 99, 2281-2287.
32. D. Mikkelsen, B. M. Flanagan, G. A. Dykes and M. J. Gidley, "Influence of different carbon sources on bacterial cellulose production by *Gluconacetobacter xylinus* strain ATCC 53524", *J. Appl. Microbiol.*, 2009, 107, 576-583.
33. N. Suwannapinunt, J. Burakorn and S. Thaenthane, "Effect of culture conditions on bacterial cellulose (BC) production from *Acetobacter xylinum* TISTR976 and physical properties of BC parchment paper", *Suranaree J. Sci. Technol.*, 2007, 14, 357-365.
34. Thai Industrial Standards Institute, "Standard Test Methods for Paper and Paper Board", Industrial Standards Institute, Ministry of Industry, Bangkok, 1997, pp.1-6.
35. ASTM International, "Standard test method for water vapor transmission rate of sheet materials using dynamic relative humidity measurement", 2013, <http://enterprise2.astm.org/DOWNLOAD-/E398.1272742-1.pdf> (Accessed: December 2013).

36. ASTM International, "Standard test method for oxygen gas transmission rate through plastic film and sheeting using a coulometric sensor", 2010, <http://enterprise2.astm.org/DOWNLOAD-/D3985.1272742-1.pdf> (Accessed: December 2013).
37. ASTM International, "Standard test method for water absorption of plastics", 2010, <http://enterprise2.astm.org/DOWNLOAD/D570.1272742-1.pdf> (Accessed: December 2013).
38. J. H. Ha, O. Shehzad, S. Khan, S. Y. Lee, J. W. Park, T. Khan and J. K. Park, "Production of bacterial cellulose by a static cultivation using the waste from beer culture broth", *Korean J. Chem. Eng.*, 2008, 25, 812-815.
39. P. Carreira, J. A. S. Mendes, E. Trovatti, L. S. Serafim, C. S. R. Freire, A. J. D. Silvestre and C. P. Neto, "Utilization of residues from agro-forest industries in the production of high value bacterial cellulose", *Bioresour. Technol.*, 2011, 102, 7354-7360.
40. R. J. Moon, A. Martini, J. Nairn, J. Simonsen and J. Youngblood, "Cellulose nanomaterials review: Structure, properties and nanocomposites", *Chem. Soc. Rev.*, 2011, 40, 3941-3994.
41. O. Shehzad, S. Khan, T. Khan and J. K. Park, "Physicochemical and mechanical characterization of bacterial cellulose produced with an excellent productivity in static conditions using a simple fed-batch cultivation strategy", *Carbohydr. Polym.*, 2010, 82, 173-180.
42. C. Castro, R. Zuluaga, C. Álvarez, J.-L. Putaux, G. Caro, O. J. Rojas, I. Mondragon and P. Gañán, "Bacterial cellulose produced by a new acid-resistant strain of *Gluconacetobacter* genus", *Carbohydr. Polym.*, 2012, 89, 1033-1037.
43. P. Chen, S. Y. Cho and H. J. Jin, "Modification and applications of bacterial celluloses in polymer science", *Macromol. Res.*, 2010, 18, 309-320.
44. S. Keshk, "Physical properties of bacterial cellulose sheets produced in presence of lignosulfonate", *Enzyme Microb. Technol.*, 2006, 40, 9-12.
45. M. U. Rani, K. Udayasankar and K. A. A. Appaiah, "Properties of bacterial cellulose produced in grape medium by native isolate *Gluconacetobacter* sp.", *J. Appl. Polym. Sci.*, 2011, 120, 2835-2841.
46. W. Tang, S. Jia, Y. Jia and H. Yang, "The influence of fermentation conditions and post-treatment methods on porosity of bacterial cellulose membrane", *World J. Microbiol. Biotechnol.*, 2010, 26, 125-131.
47. S. Kongruang, "Bacterial cellulose production by *Acetobacter xylinum* strains from agricultural waste products", *Appl. Biochem. Biotechnol.*, 2008, 148, 245-256.

Full Paper

On certain Banach spaces of difference sequences of fuzzy real numbers

Hemen Dutta

Department of Mathematics, Gauhati University, Guwahati-781014, India

E-mail: hemen_dutta08@rediffmail.com

Received: 27 April 2013 / Accepted: 20 January 2014 / Published: 24 January 2014

Abstract: Some sets of difference sequences of fuzzy real numbers which have Banach subspaces are introduced and investigated. Further, it is shown that these subspaces are isometric with some subsets of the sets of null, convergent and bounded sequences of fuzzy real numbers.

Keywords: fuzzy real numbers, sequence of fuzzy real numbers, difference sequences, isometry

INTRODUCTION

The concept of fuzzy sets and fuzzy set operations was first introduced by Zadeh [1] and subsequently several authors have studied various aspects of the theory and applications of fuzzy sets. Bounded and convergent sequences of fuzzy numbers were introduced by Matloka [2], who showed that every convergent sequence is bounded. Nanda [3] studied the spaces of bounded and convergent sequence of fuzzy numbers and showed that they are complete metric spaces. Çakan and Şengönül [4] studied the space of convergent and bounded sequence of fuzzy numbers and showed that they are Banach spaces under a suitable norm. Altmok *et al.* [5] introduced the notions of lacunary almost statistical convergence and lacunary strongly almost convergent sequences. In comparison with the classical sequence spaces, several authors have extended such notions to sequences of fuzzy numbers. One may see also Savaş [6] for sequence of fuzzy numbers.

The notion of difference sequence of complex numbers was introduced by Kizmaz [7]. Later on Et and Colak [8], Tripathy and Et [9], Tripathy *et al.* [10], Dutta [11-13], Dutta and Bilgin [14], Başarır *et al.* [15] and some others have defined difference sequences by introducing different difference operators. In this article the author uses some difference operators which generalise all previous such operators and extends the notion of difference sequences to sequences of fuzzy numbers using these most generalised difference operators. First, some well known definitions are given.

Let D denote a set of all closed bounded intervals $A = [A_1, A_2]$ on real line R . Let A, B be two closed bounded intervals (i.e. $A, B \in D$). Then we define:

$$A \leq B \text{ if and only if } A_1 \leq B_1 \text{ and } A_2 \leq B_2, \text{ and}$$

$$d(A, B) = \max(|A_1 - B_1|, |A_2 - B_2|).$$

Then d is a metric on D . It is well known that (D, d) is a complete metric space and ' \leq ' is a partial order relation in D .

A fuzzy real number X is a fuzzy set on R , i.e. a mapping $X : R \rightarrow I (= [0,1])$ associating each real number t with its grade of membership $X(t)$. A fuzzy real number X is called *convex* if $X(t) \geq X(s) \wedge X(r) = \min(X(s), X(t))$, where $s < t < r$. If there exists $t_0 \in R$ such that $X(t_0) = 1$, then the fuzzy real number X is called *normal*. A fuzzy real number X is said to be *upper-semi-continuous* if, for each $\varepsilon > 0$, $X^{-1}([0, a + \varepsilon))$ for all $a \in I$ is open in the usual topology of R . The set of all upper-semicontinuous, normal, convex fuzzy real numbers is denoted by $R(I)$. Throughout the article, by a fuzzy real number we mean that the number belongs to $R(I)$.

The α -level set $[X]^\alpha$ of the fuzzy real number X , for $0 < \alpha \leq 1$, is defined as $[X]^\alpha = \{t \in R : X(t) \geq \alpha\}$; for $\alpha = 0$, it is the closure of the strong 0-cut. Throughout the article α means $\alpha \in [0, 1]$ unless otherwise stated.

A fuzzy real number X is called *non-negative* if $X(t) = 0$ for all $t < 0$. The set of all non-negative fuzzy real numbers is denoted by $R^*(I)$.

Let $\bar{d} : R(I) \times R(I) \rightarrow R$ be defined by:

$$\bar{d}(X, Y) = \sup_{0 \leq \alpha \leq 1} d([X]^\alpha, [Y]^\alpha).$$

Then \bar{d} defines a metric on $R(I)$. In fact $(R(I), \bar{d})$ is a complete metric space. The additive identity and multiplicative identity in $R(I)$ are denoted by $\bar{0}$ and $\bar{1}$ respectively.

For any two elements X, Y of $R(I)$, let us define:

$$X \leq Y \text{ if and only if } [X]^\alpha \leq [Y]^\alpha \text{ for any } \alpha \in [0, 1].$$

A subset E of $R(I)$ is said to be bounded above if there exists a fuzzy real number M , called an upper bound of E , such that $X \leq M$ for every $X \in E$. M is called the least upper bound or supremum of E if M is an upper bound and the smallest of all upper bounds. A lower bound and the greatest lower bound or infimum are defined similarly. E is said to be bounded if it is bounded both above and below.

If (M, ρ) is a linear metric space, then it is known that $g(x) = \rho(x, \theta)$ is a norm on M , where θ is the zero element in M .

Now let $\bar{\theta}$ be a fuzzy number such that $\bar{\theta}(x) = 0$ for all $x \in R$; then

$$\|X\| = \bar{d}(X, \bar{\theta})$$

is a norm on $R(I)$. Also, it is easy to show that $R(I)$ is a complete normed linear space, i.e. the space is a Banach space.

A sequence $X = (X_k)$ of fuzzy real numbers is a function X from the set N of all positive integers into $R(I)$. The fuzzy real number X_k denotes the value of the function at $k \in N$ and is called the k^{th} term or general term of the sequence.

The set of convergent sequences is denoted by c^F . A sequence $X = (X_k)$ of fuzzy numbers is said to be convergent to the fuzzy real number X_0 , written as $\lim_k X_k = X_0$, if for every $\varepsilon > 0$ there exists $n_0 \in N$ such that

$$\|X_k - X_0\| < \varepsilon, \text{ for } k \geq n_0.$$

A sequence $X = (X_k)$ of fuzzy real numbers is said to be a Cauchy sequence if, for every $\varepsilon > 0$, there exists $n_0 \in N$ such that

$$\|X_k - X_l\| < \varepsilon, \text{ for } k, l \geq n_0.$$

The set of bounded sequences is denoted by ℓ_∞^F . A sequence $X = (X_k)$ of fuzzy real numbers is said to be bounded if the set $\{X_k: k \in N\}$ of fuzzy numbers is bounded; equivalently,

$$\sup_k \|X_k\| < \infty.$$

NEW DEFINITIONS AND RESULTS

Let r and s be two non-negative integers and $v = (v_k)$ be a sequence of non-zero reals. Then we define the following new definitions and spaces.

A sequence $X = (X_k)$ of fuzzy numbers is said to be $\Delta_{(v,r)}^s$ -convergent to the fuzzy real number X_0 , written as $\lim_k \Delta_{(v,r)}^s X_k = X_0$, if for every $\varepsilon > 0$ there exists $n_0 \in N$ such that

$$\|\Delta_{(v,r)}^s X_k - X_0\| < \varepsilon \text{ for } k \geq n_0,$$

where $(\Delta_{(v,r)}^s X_k) = (\Delta_{(v,r)}^{s-1} X_k - \Delta_{(v,r)}^{s-1} X_{k-r})$ and $\Delta_{(v,r)}^0 X_k = v_k X_k$ for all $k \in N$, which is equivalent to the following binomial representation:

$$\Delta_{(v,r)}^s X_k = \sum_{i=0}^s (-1)^i \binom{s}{i} v_{k-ri} X_{k-ri}.$$

In this expansion, we take $v_k = 0$ and $X_k = \bar{0}$ for non-positive values of k . (1)

Let $c^F(\Delta_{(v,r)}^s)$ denote the set of all $\Delta_{(v,r)}^s$ -convergent sequences of fuzzy real numbers. In particular if $X_0 = \bar{0}$ in the above definition, we say $X = (X_k)$ to be $\Delta_{(v,r)}^s$ -null sequence of fuzzy real numbers and we denote the set of all $\Delta_{(v,r)}^s$ -null sequences of fuzzy real numbers by $c_0^F(\Delta_{(v,r)}^s)$.

A sequence $X = (X_k)$ of fuzzy numbers is said to be $\Delta_{(v,r)}^s$ -bounded if the set $\{\Delta_{(v,r)}^s X_k : k \in N\}$ of fuzzy real numbers is bounded.

Let $\ell_\infty^F(\Delta_{(v,r)}^s)$ denote the set of all $\Delta_{(v,r)}^s$ -bounded sequences of fuzzy real numbers.

Similarly we can define the sets $c_0^F(\Delta_{v,r}^s)$, $c^F(\Delta_{v,r}^s)$ and $\ell_\infty^F(\Delta_{v,r}^s)$ of $\Delta_{v,r}^s$ -null, $\Delta_{v,r}^s$ -convergent and $\Delta_{v,r}^s$ -bounded sequences of fuzzy real numbers, where $(\Delta_{v,r}^s X_k) = (\Delta_{v,r}^{s-1} X_k - \Delta_{v,r}^{s-1} X_{k+r})$ and $\Delta_{v,r}^0 X_k = v_k X_k$ for all $k \in N$, which is equivalent to the following binomial representation:

$$\Delta_{v,r}^s X_k = \sum_{i=0}^s (-1)^i \binom{s}{i} v_{k+ri} X_{k+ri}.$$

Taking $s = 0$ and $v_k = 1$ for all $k \in N$ in the above definitions, we get the spaces c_0^F , c^F and ℓ_∞^F .

In general, the spaces $c_0^F(\Delta_{v,r}^s)$, $c^F(\Delta_{v,r}^s)$ and $\ell_\infty^F(\Delta_{v,r}^s)$ are not Banach spaces. In fact, it is not possible in general to find some fuzzy real number $X-Y$ such that $X=Y+(X-Y)$ (called the Hukuhara difference when it exists.)

Let $Sc_0^F(\Delta_{v,r}^s)$, $Sc^F(\Delta_{v,r}^s)$ and $S\ell_\infty^F(\Delta_{v,r}^s)$ be the subsets of $c_0^F(\Delta_{v,r}^s)$, $c^F(\Delta_{v,r}^s)$ and $\ell_\infty^F(\Delta_{v,r}^s)$ respectively, consisting of sequences of fuzzy real numbers that satisfy the Hukuhara difference. Such subsets exist as every real number is a fuzzy real number.

Theorem 1. *The spaces $Sc_0^F(\Delta_{v,r}^s)$, $Sc^F(\Delta_{v,r}^s)$ and $S\ell_\infty^F(\Delta_{v,r}^s)$ are Banach spaces under the norm:*

$$\|X\|' = \sup_k \|\Delta_{(v,r)}^s X_k\| \tag{2}$$

Proof. We prove the result only for the case $Sc^F(\Delta_{v,r}^s)$; for the other cases it will follow on applying similar arguments. It is easy to see that $\|\cdot\|'$ is a norm on $Sc^F(\Delta_{v,r}^s)$. To prove completeness, let (X^i) be a Cauchy sequence in $Sc^F(\Delta_{v,r}^s)$, where $X^i = (X_k^i) = (X_1^i, X_2^i, \dots)$ for each $i \in N$. Then for a given $\varepsilon > 0$, there exists a positive integer n_0 such that

$$\|X^i - X^j\|' = \sup_k \|\Delta_{(v,r)}^s X_k^i - \Delta_{(v,r)}^s X_k^j\| < \varepsilon \text{ for all } i, j \geq n_0.$$

It follows that

$$\|\Delta_{(v,r)}^s X_k^i - \Delta_{(v,r)}^s X_k^j\| < \varepsilon \text{ for all } i, j \geq n_0 \text{ and } k \in N.$$

This implies that $(\Delta_{(v,r)}^s X_k^i)$ is a Cauchy sequence in $L(R)$ for all $k \geq 1$. But $L(R)$ is complete, so $(\Delta_{(v,r)}^s X_k^i)$ is convergent in $L(R)$ for all $k \geq 1$.

For simplicity, let $\lim_{i \rightarrow \infty} \Delta_{(v,r)}^s X_k^i = \sum_{u=0}^s (-1)^u \binom{s}{u} v_{k-ru} X_{k-ru}^i = N_k$, for example for each $k \geq 1$. Considering $k = 1, 2, \dots, rs, \dots$, we can easily conclude that $\lim_{i \rightarrow \infty} X_k^i = X_k$ exists for each $k \geq 1$ (see (1)).

It remains to show that $X = (X_k) \in Sc^F(\Delta_{v,r}^s)$. Now we can find that

$$\lim_{j \rightarrow \infty} \|\Delta_{(v,r)}^s X_k^i - \Delta_{(v,r)}^s X_k^j\| < \varepsilon \text{ for all } i \geq n_0 \text{ and } k \in N.$$

Hence,

$$\|\Delta_{(v,r)}^s X_k^i - \Delta_{(v,r)}^s X_k\| < \varepsilon \text{ for all } i \geq n_0 \text{ and } k \in N.$$

This implies that

$$\|X^i - X\|' < \varepsilon \text{ for all } i \geq n_0$$

Since $Sc^F(\Delta_{v,r}^s)$ is a linear space, it follows that $X = (X_k) \in Sc^F(\Delta_{v,r}^s)$. This completes the proof.

Theorem 2. *The spaces $Sc_0^F(\Delta_{v,r}^s)$, $Sc^F(\Delta_{v,r}^s)$ and $S\ell_\infty^F(\Delta_{v,r}^s)$ are Banach spaces under the norm:*

$$\|X\|'' = \sum_{k=1}^{rs} \|X_k\| + \sup_k \|\Delta_{v,r}^s X_k\|$$

Proof. The proof follows by similar arguments as applied to proving Theorem 1.

Remark 1. For any sequence $X = (X_k)$, $X \in Z(\Delta_{v,r}^s)$ if and only if $X \in Z(\Delta_{(v,r)}^s)$, for $Z = c_0^F, c^F$ and ℓ_∞^F . Also, it is obvious that the norms $\|\cdot\|'$ and $\|\cdot\|''$ are equivalent.

Theorem 3. (i) *The spaces $Sc_0^F(\Delta_{v,r}^s)$, $Sc^F(\Delta_{v,r}^s)$ and $S\ell_\infty^F(\Delta_{v,r}^s)$ are isometric with the spaces Sc_0^F, Sc^F and $S\ell_\infty^F$.*

(ii) *The spaces $Sc_0^F(\Delta_{v,r}^s)$, $Sc^F(\Delta_{v,r}^s)$ and $S\ell_\infty^F(\Delta_{v,r}^s)$ are isometric with the spaces Sc_0^F, Sc^F and $S\ell_\infty^F$.*

Proof. (i) For $Z = c_0^F, c^F$ and ℓ_∞^F , let us define a mapping $f: SZ(\Delta_{v,r}^s) \rightarrow SZ$ as follows:

$$fX = Y = (\Delta_{(v,r)}^s X_k), \text{ for every } X \in SZ(\Delta_{(v,r)}^s) \quad (3)$$

Then

$$\begin{aligned} \|fX\|_F &= \|Y\|_F = \sup_k \|Y_k\| \\ &= \sup_k \|\Delta_{(v,r)}^s X_k\|, \text{ where } \|\cdot\|_F \text{ is a norm on } SZ, \text{ which can be} \end{aligned}$$

obtained from (2) by taking $s = 0$ and $v_k = 1$ for all $k \in N$.

$$= \|X\|', \text{ using (2).}$$

This completes the proof.

(ii) In view of Remark 1, we can also define a mapping similar to (3) on the spaces $Sc_0^F(\Delta_{v,r}^s)$, $Sc^F(\Delta_{v,r}^s)$ and $S\ell_\infty^F(\Delta_{v,r}^s)$. Thus, the proof follows.

REFERENCES

1. L. A. Zadeh, "Fuzzy sets", *Inform. Control*, **1965**, 8, 338-353.
2. M. Matloka, "Sequences of fuzzy numbers", *BUSEFAL*, **1986**, 28, 28-37.
3. S. Nanda, "On sequences of fuzzy numbers", *Fuzzy Sets Syst.*, **1989**, 33, 123-126.
4. C. Çakan and M. Şengönül, "The ordinary and almost convergence of sequences of fuzzy numbers", *Thai J. Math.*, **2004**, 2, 79-89.
5. H. Altınok, Y. Altın and M. Et, "Lacunary almost statistical convergence of fuzzy numbers", *Thai J. Math.*, **2004**, 2, 265-274.
6. E. Savaş, "A note on sequence of fuzzy numbers", *Inform. Sci.*, **2000**, 124, 297-300.
7. H. Kizmaz, "On certain sequence spaces", *Canad. Math. Bull.*, **1981**, 24, 169-176.
8. M. Et and R. Colak, "On generalized difference sequence spaces", *Soochow J. Math.*, **1995**, 21, 377-386.
9. B. C. Tripathy and A. Esi, "A new type of difference sequence spaces", *Int. J. Sci. Technol.*, **2006**, 1, 11-14.
10. B. C. Tripathy, A. Esi and B. K. Tripathy, "On a new type of generalized difference Cesàro sequence spaces", *Soochow J. Math.*, **2005**, 31, 333-340.
11. H. Dutta, "Characterization of certain matrix classes involving generalized difference summability spaces", *Appl. Sci.*, **2009**, 11, 60-67.
12. H. Dutta, "On some isometric spaces of c_0^F , c^F and ℓ_∞^F ", *Acta Univ. Apulensis Math. Inform.*, **2009**, 19, 107-112.
13. H. Dutta, "On some complete metric spaces of strongly summable sequences of fuzzy numbers", *Rend. Sem. Mat. Univ. Politec. Torino*, **2010**, 68, 29-36.
14. H. Dutta and T. Bilgin, "Strongly $(V^\lambda, A, \Delta_{(vm)}^n, p)$ -summable sequence spaces defined by an Orlicz function", *Appl. Math. Lett.*, **2011**, 24, 1057-1062.
15. M. Başarır, Ş. Konca and E. E. Kara, "Some generalized difference statistically convergent sequence spaces in 2-normed space", *J. Ineq. Appl.*, **2013**, 177 (doi:10.1186/1029-242X-2013-177).

Full Paper

Flexural performance of foam concrete containing pulverised bone as partial replacement of cement

Funso Falade¹, Efe Ikponmwosa^{1,*} and Christopher Fapohunda²

¹ Department of Civil and Environmental Engineering, University of Lagos, Lagos, Nigeria

² Department of Building, Caleb University, Imota, Lagos, Nigeria

* Corresponding author, e-mail: efe_ewaen@yahoo.com

Received: 27 March 2013 / Accepted: 27 January 2014/ Published: 29 January 2014

Abstract: This paper presents the results of a study conducted to investigate the flexural behaviour of foam concrete containing pulverised bone as partial replacement of cement. A total of sixty reinforced beams (150×150×750 mm) were used to investigate the flexural behaviour of the specimens. For reinforcement of the beams, hot-rolled, deformed 10-mm-diameter bars with yield and ultimate stresses of 478.10 N/mm² and 710.81 N/mm² respectively were used. The cement constituent of the mix was partly replaced with up to 20% of pulverised bone. The flexural parameters investigated are crack formation and its pattern, failure mode, ultimate load, theoretical and experimental ultimate moments, deflection and stiffness. From the results of this investigation, it is concluded that the provision of the design standard in relation to shear and flexural design of beams can be considered as adequate for the design of reinforced foam concrete. It is further concluded that the stiffness is not affected by the inclusion of pulverised bone in the mix at up to 15% cement replacement level, and neither is the deflection pattern of the uncracked sections of the specimens affected by the inclusion of pulverised bone. The bending moments of the specimens, however, decreased with increase in pulverised bone.

Keywords: foam concrete, cement, pulverised bone, flexural strength

INTRODUCTION

Foam concrete is a lightweight concrete that has proved suitable for lightly-loaded structural applications and as a weight-reducing measure in structures. It has also made possible the use of many industrial and agricultural waste products in its production with attendant environmental benefits [1-3]. A waste product suitable for use in foam concrete production, especially for low-cost construction, is pulverised bone obtained from cow bones generated from abattoirs [4]. Results of our previous investigation [4] conducted on paste and mortar have shown that pulverised bone is suitable as a partial replacement of cement because of its pozzolanic properties [5, 6]. Falade *et al.* [7] have demonstrated that using pulverised bone as a partial replacement of cement, at up to 20%

replacement level, in the production of foam concrete results in a lightweight concrete material with adequate strength (compressive and tensile) for structural applications in line with the recommendations for lightweight concrete [8, 9]. Furthermore, the use of pulverised bone was also found to be cost-effective when compared with normal concrete of comparable strength [10]. The objectives of the present study are to investigate into the flexural characteristic of foam concrete containing pulverised bone as a partial replacement of cement. The flexural parameters studied are crack formation and propagation, deflection, ultimate moment and stiffness.

MATERIALS AND METHODS

Materials

Ordinary Portland cement produced in accordance with British and Nigerian standards [11, 12] was used as the main binder. Cow bones from which pulverised bone was produced were obtained from Oko-Oba abattoir in Agege local government area of Lagos State. The bones were dried after they had been separated from all the muscles, flesh, tissues, intestines and fat. The dried bones were then pulverised with a grinder into powder and the fraction passing through BS sieve aperture opening of size 150 μm (0.15 mm) was packaged in bags and stored in a cool dry place. Sand from River Ogun at Ibafo town in Ogun State of Nigeria was used for this work. Particles passing through 3.35-mm sieve but retained on 0.150-mm sieve were used. Coarser aggregate might settle in a lightweight mix and lead to collapse of the foam during mixing. Lithofoam, a protein-based foaming agent supplied by Dr Lucas of West Germany, was used in this study. This is in line with the findings [13, 14] that protein-based foaming agents produce more stable, smaller and stronger bubble structure, resulting in foam concrete with higher strength when compared to foam concrete produced by other types of foaming agents. The dilution ratio for the surfactant was one part of surfactant to 25 parts of water. The water used was potable tap water. This is crucial when using a protein-based foaming agent because organic contamination can have an adverse effect on the quality of the foam, and hence of the concrete produced.

Mix Proportions

From available literature [15-17], foam concrete of structural value can be produced at densities between 1200-1900 kg/m^3 . The density being the design criterion in foamed concrete, a mix proportion that produces the target plastic density of 1600 kg/m^3 ($\pm 100 \text{ kg/m}^3$) was then developed. To achieve the desired design density and workability, trial mixes were carried out. The following mix design parameters were adopted: (i) a binder (cement and pulverised bone)/sand ratio of 1: 3, (ii) a water/binder ratio of 0.5, and (iii) a foaming agent dilution of 1:25. The mix constituent proportions are shown in Table 1.

Reinforced Concrete Beam Details and Instrumentation

In order to assess the flexural behaviour of the foam concrete, reinforced foam concrete beams were designed in accordance with British Standard [18], the current code of practice in use in Nigeria. Details of the beam are shown in Figure 1.

Table 1. Mix constituent proportions for foam concrete mixes

PB*	Binder (kg)		Sand (kg)	Water for base mix (kg)	Foam concentration	
	Cement	PB*			Mixing water (kg)	Foam agent (g)
0%	25.00	0.00	75	12.50	4.688	187.5
5%	23.75	1.25	75	12.50	4.688	187.5
10%	22.50	2.50	75	12.50	4.688	187.5
15%	21.25	3.75	75	12.50	4.688	187.5
20%	20.00	5.00	75	12.50	4.688	187.5

* PB = Pulverised bone

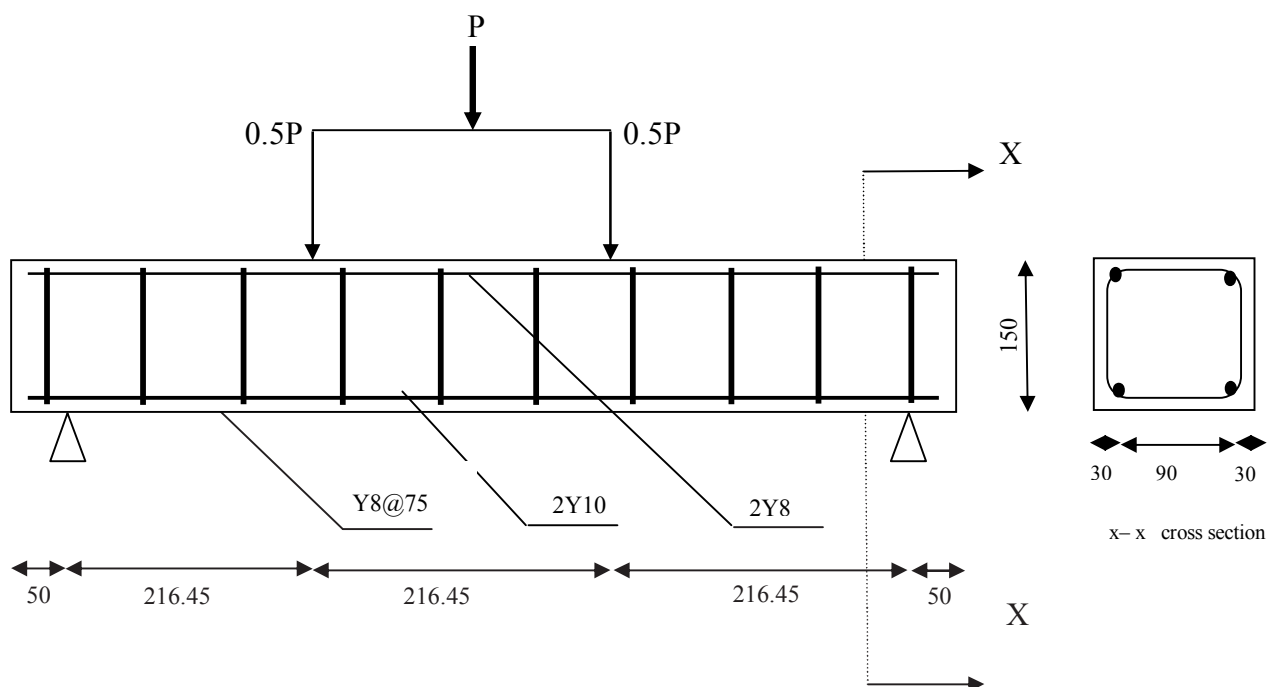


Figure 1. Details of reinforced foam concrete beam and loading arrangement. All dimensions are in millimetres. High yield steel is indicated by Y and the number following Y represents the diameter. The number before Y indicates the number of either tension or compression reinforcements while the symbol @ represents the spacing of links. The applied load is represented by P. Line X-X indicates the point of cross-section.

The beams (150×150×750 mm) were reinforced with minimum area of reinforcement (0.13% bh , b = breadth of beam, h = depth of beam) in accordance with British Standard [18]. The reinforcement for the beams consisted of two 10-mm-diameter hot-rolled, deformed bars with yield and ultimate stresses of 478.10 N/mm² and 710.81 N/mm² respectively. For shear reinforcement, 8-mm-diameter hot-rolled, deformed bars with yield and ultimate stresses of 475.42 N/mm² and 666.90 N/mm² respectively were used. The cover was 30 mm while the spacing for shear reinforcement was 75 mm to satisfy the requirement of British Standard [18], limiting the spacing for shear reinforcement to a value less than 0.75 of the effective depth (0.75 × 107 = 80.75 mm).

The replacement of cement with pulverised bone in the beams was varied from 0 to 20% at 5% increment (based on preliminary findings). Beams without pulverised bone served as control.

Beam specimens were produced and tested under the third point loading (Figure 2) in accordance with British Standard [19]. A dial gauge was placed under the beam at the mid-span to measure the deflection at regular interval of loading. The load at which the first visible crack was noticed was recorded; so was the load at which failure occurred. The test was terminated when a little increase in load led to a very large deflection. A total number of 60 beams were cast and tested at 28-day curing age [20].



Figure 2. Testing arrangement of beam specimens

RESULTS AND DISCUSSION

Crack Formation, Its Pattern and Failure Mode

For all the beams, both with and without pulverised bone, the typical crack patterns formation is shown in Figure 3. The crack usually started at the support followed by a tiny one adjacent to it. These cracks gradually widened, so that at failure another crack parallel to the previous one developed as well as a tiny vertical one at the centre.

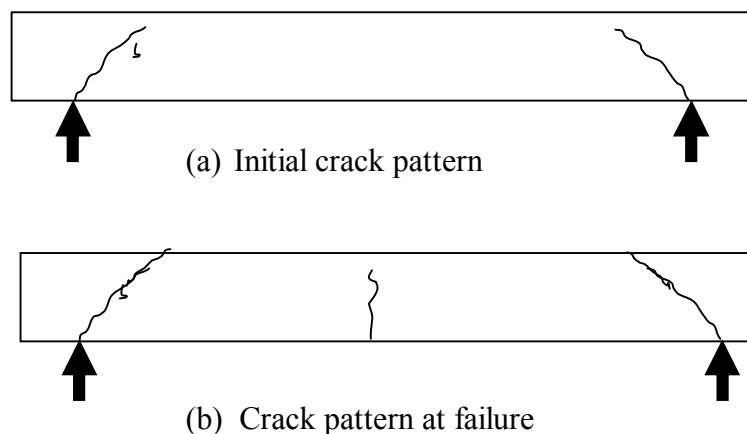


Figure 3. Crack development of beams

The angle of inclination of the cracks to the horizontal varied between 41.8-49° as the percentage of cement replacement with pulverised bone increased (Table 2), the average being 44.95°. In the design of links for beams with normal concrete, it is assumed [18] that the diagonal crack is generated at an angle of 45° to the tension reinforcement (i.e. to the horizontal) for normal concrete.

Table 2. Angle of inclination of the cracks to the horizontal

% PB*	Angle (degree) of crack from horizontal	Deviation from 45°	% Deviation
0	41.80 ± 0.20	- 3.20	- 7.11
5	42.00 ± 0.90	- 3.00	- 6.67
10	43.95 ± 0.22	- 1.05	- 2.23
15	46.97 ± 1.26	+1.97	+ 4.38
20	49.00 ± 0.78	+4.00	+ 8.89

* Pulverised bone

From the above values of angle of inclination in Table 2, the numerical variation was less than 10%. Thus, the equations developed for the calculation of area of shear reinforcement for beams of normal concrete (equation 1), according to British Standard [18], can be considered valid for reinforced foam concrete beam with and without pulverised bone. These equations, on the basis of shear stress value, are given as [18]:

$$\left. \begin{aligned}
 A_{sc} &= \frac{0.4s_v b}{0.95f_{yv}} \quad \text{or nominal links} && \text{(for } v < 0.5v_c) \\
 A_{sc} &\geq \frac{0.4s_v b}{0.95f_{yv}} && \text{(for } 0.5v_c < v < (v_c + 0.4)) \\
 A_{sc} &= \frac{0.4s_v b(v + v_c)}{0.95f_{yv}} && \text{(for } v_c + 0.4 < v < 0.8\sqrt{f_{cu}} \text{ or } 5\text{N/mm}^2)
 \end{aligned} \right\} (1)$$

where:

- A_{sc} = area of shear reinforcement
- s_v = spacing of shear reinforcement
- f_{yv} = characteristic strength of shear reinforcement
- b = breath of the beam section
- v = shear stress due to ultimate loads
- v_c = shear resistance of the concrete

The failure mode for all the specimens irrespective of the content of the pulverised bone was in the form of inclined cracks that developed at the edge of the support, extending to the direction of the loading point as the load was increased, thus resulting in the splitting of the beam. This can be seen in Figure 3. This mode of failure is described as the diagonal tension failure [2].

Effect of Pulverised Bone on Failure Load and Failure Moment

The theoretical bending moment was calculated for each of the beam specimens from equation (2), derived by assuming the idealisation of rectangular stress block and using an average stress of $0.67 f_{cu}$ (N/mm²) over 0.9 time of the neutral axis depth, i.e. the stress block contained in British Standard [18] as suggested by Regan and Arasteh [21]:

$$M_u = 0.156f_{cu}bd^2 \dots\dots\dots (2)$$

where:

- f_{cu} = compressive strength of specimen for each cement replacement level with pulverised bone (N/mm²)
- b = width of beam specimen (mm)
- d = effective depth (mm)

The experimental bending moment (M_{EXP}) was calculated by using the equation for the structural form that is compatible with the third point loading configuration as shown in Figure 4.

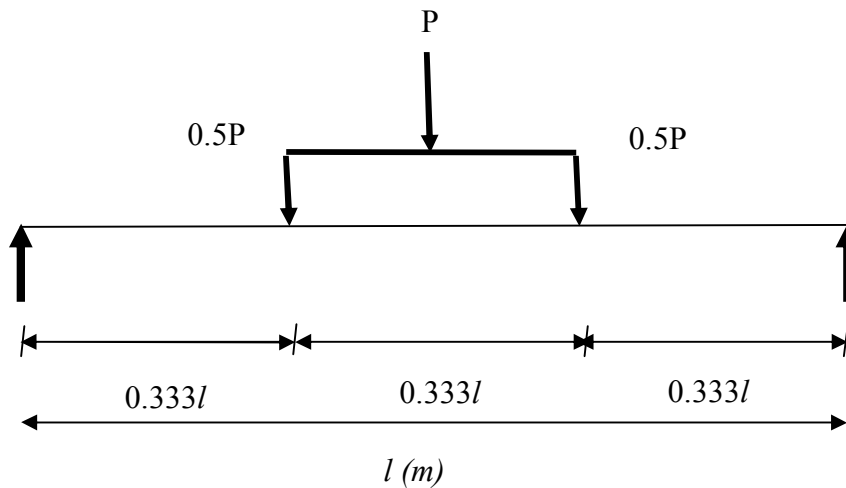


Figure 4. Structural configuration for third point loading (P = applied load, l = span of beam)

The bending moment equation [22] is:

$$M = 0.167Pl \dots\dots\dots (3)$$

where:

- M = maximum bending moment
- P = failure load (KN)
- L = span of beam specimen (m)

The failure load, the theoretical ultimate moment (M_{BS}) and the experimental ultimate moment (M_{EXP}) computed from equations (2) and (3) are shown in Table 3. It is noted, however, that in computing M_{EXP} , the service load was obtained by dividing the load at the first visible crack by 1.6. This presupposes that flexural failure by the load has already occurred at the first visible crack, and this load was thus used to calculate the experimental ultimate moment. From the Table, the following observations can be made.

Table 3. Comparison between experimental and theoretical bending moments

% PB	Load at first crack (KN)	Failure load (KN)	% Decrease in failure load	Service load (KN)	Theoretical (BS 8110) design moment (KN.m), M_{BS}	Experimental ultimate moment (KN.m), M_{EXP}	$\frac{M_{EXP}}{M_{BS}}$
0%	75.00 ± 0.50	92.50 ± 0.96	-	46.88	4.13	4.40	1.07
5%	70.00 ± 1.50	87.50 ± 1.32	5.4	43.75	3.88	4.10	1.06
10%	70.00 ± 0.87	85.00 ± 1.31	8.1	43.75	3.75	4.10	1.09
15%	65.00 ± 0.50	80.00 ± 0.87	13.5	40.63	3.55	3.81	1.07
20%	62.50 ± 0.50	72.50 ± 0.87	21.6	39.06	3.48	3.66	1.05

* PB = pulverised bone

Effect of pulverised bone on failure load

It is observed from Table 3 that the failure load decreases with increasing pulverised bone content. The load at which the first crack occurred follows the same trend. This can be attributed to a lowering of density with increase in pulverised bone content as a result of lower specific gravity of pulverised bone (2.22) in relation to that of cement (2.92). On average the cracking load is about 82% of the failure load (81.1%, 80.0%, 82.4%, 81.3% and 86.2% for 0%, 5%, 10%, 15% and 20% respectively of cement replacement with pulverised bone).

Effect of pulverised bone on ultimate moment

The effects of pulverised bone on the flexural strength can be seen in Table 3. The bending moments (both theoretical and experimental) decrease with increasing pulverised bone content, probably as a result of reduced density [7], with consequent reduction in compressive strength. The bending moments are calculated on the assumption that failure takes place at the onset of the first visible crack. The values of the experimental bending moments are consistently higher than those of the theoretical ones calculated using equation (2), although the difference can be considered insignificant (generally less than 10%), considering the fact that aerated concrete is a variable material. Thus equation (2) developed on the basis of rectangular stress idealisation can be considered to be valid for foam concrete with and without pulverised bone.

Effect of Reinforcement on Failure Load

The failure loads for the beam specimens are shown in Table 4. It can be seen that the addition of reinforcement significantly improves the flexural performance of the foam concrete at all replacement levels. The failure loads for reinforced beam specimens are multiples of those of unreinforced specimens. This is an indication that the inclusion of reinforcement inhibits the propagation of cracks in foam concrete and thus enhances its bending resistance.

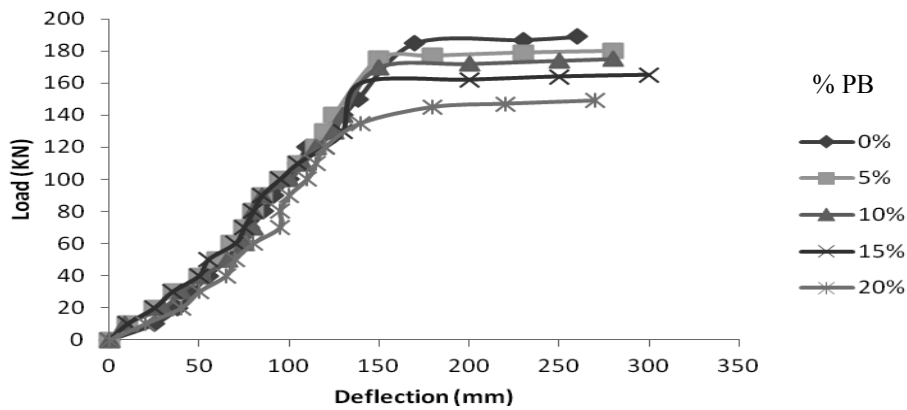
Effect of Pulverised Bone on Load Deflection

The mid-span load-deflection curves for the foam concrete with and without pulverised bone are presented in Figure 5. The curves are characterised by three distinctly different segments separated by three significant events that took place during the process of loading until failure. Using the 0% replacement (Figure 5b) as representative, these regions are AB, BC and CD. In the

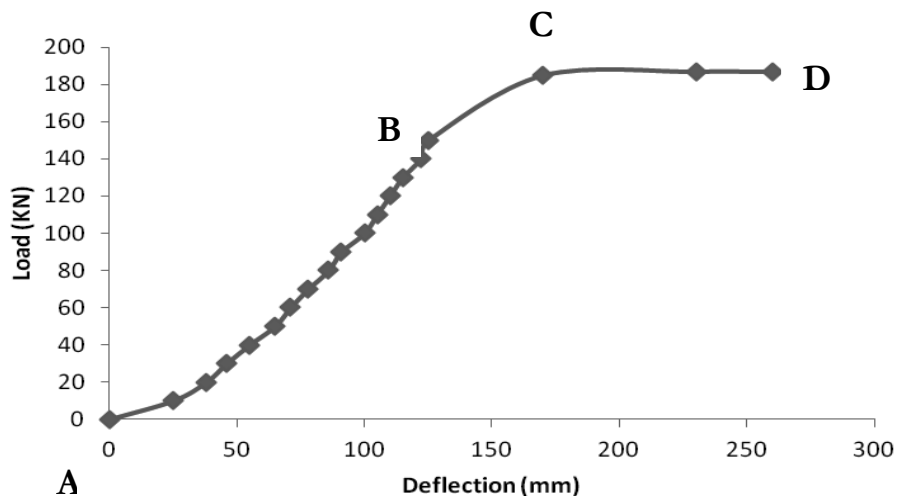
Table 4. Effect of reinforcement on failure load

% PB*	Failure load (KN) of beam without reinforcement, P_{WOR}	Failure load (KN) of beam with reinforcement, P_{WR}	P_{WR} / P_{WOR}
0%	15.0 ± 1.80	92.50 ± 1.96	6.17
5%	15.0 ± 0.87	87.50 ± 1.32	5.83
10%	12.5 ± 1.32	85.00 ± 1.31	6.80
15%	12.5 ± 0.00	80.00 ± 0.87	6.80
20%	10.0 ± 0.50	72.50 ± 0.87	7.25

* PB = pulverised bone



(a) Load deflection for all cement replacements with pulverised bone



(b) Load deflection for 0% replacement of cement with pulverised bone

Figure 5. Load-deflection curves for foam concrete

first region (AB), deflection can be considered to be directly proportional to the applied load until the first visible crack appears. This region terminates at the load at which the first visible crack occurs. The relationship between load and deflection of the material can be described as linear in this region. The second region (BC) represents that between the load at first crack and the load at failure. A relatively larger deflection results from load increase until complete failure. Also, the cracks become wider and the load deflection cannot be considered to be linear. The last is the failure region (CD) where sustained load results in a large deflection.

Table 5 compares the cracking load to the failure load for all the mixes. The cracking load decreases with increasing pulverised bone content. This can be attributed to a decrease in density and consequent decrease in compressive strength. The failure load also follows the same trend. The cracking load is 82% of the failure load on the average. The effect of pulverised bone on the deflection is presented in Table 6. It can be seen that the deflection at first crack of the foam concrete with 5-20% pulverised bone in relation to the control (0%) does not differ significantly. In other words, the addition of pulverised bone has no effect on the specimens up to initial cracking, although the same cannot be said of the behaviour after the appearance of first crack and at failure. At failure, the final deflection of the foam concrete with 15-20% pulverised bone becomes significant in relation to the control.

Table 5. Comparison between cracking and failure loads

% PB*	Cracking load (KN)	Failure load (KN)	% Cracking load in relation to failure load
0%	75.00 ± 0.00	92.50 ± 0.00	81.1
5%	70.00 ± 5.00	87.50 ± 5.00	80.0
10%	70.00 ± 5.00	85.00 ± 5.00	82.4
15%	65.00 ± 0.00	80.00 ± 0.00	81.3
20%	62.50 ± 0.00	72.50 ± 0.00	86.2

* PB = pulverised bone

Table 6. Effect of pulverised bone on deflection of foam concrete

% PB*	Deflection at crack (mm)	% Difference from control	Deflection at failure (mm)	% Difference from control
0	125 ± 0.00	-	260 ± 5.00	-
5	125 ± 5.00	0	280 ± 0.00	7.7
10	130 ± 5.00	4	280 ± 5.00	7.7
15	130 ± 0.00	4	300 ± 5.00	15.4
20	135 ± 0.00	8	300 ± 0.00	15.4

* PB = Pulverised bone

Stiffness

Sin [23] reported that the gradient of the load-deflection curve is an indication of beam stiffness. The stiffness computed from load-deflection curves in Figure 5 is shown in Table 7. Prior to cracking, the stiffness values are not affected significantly by the inclusion of pulverised bone up to 15% replacement, the difference being less than 10%. It only becomes significant at 20% replacement. However, after cracking, the stiffness is affected by inclusion of pulverised bone at all replacement levels. The loss of stiffness after cracking is a consequence of the reduction in cross-sectional area of the concrete. The stiffness of the control is not affected by cracking.

Table 7. Stiffness of foam concrete beam specimens

% PB *	Pre-crack stiffness	% Variation from control	Post-crack stiffness	% Variation from control
0%	1.09 ± 0.00	--	1.09 ± 0.01	--
5%	1.12 ± 0.01	+ 2.75	1.40 ± 0.02	28.40
10%	1.08 ± 0.00	- 0.91	1.50 ± 0.04	37.62
15%	1.00 ± 0.00	- 8.25	1.50 ± 0.02	37.62
20%	0.89 ± 0.02	- 18.35	2.00 ± 0.05	83.50

* PB = Pulverised bone

CONCLUSIONS

From the results of this investigation, the followings conclusions can be made:

- 1) The equation developed for the calculation of shear reinforcement for beams in normal concrete can be considered valid for reinforced foam concrete beam with and without pulverised bone.
- 2) Increase in pulverised bone does not have an effect on crack formation and propagation, and neither does it have any effect on the mode of failure.
- 3) Deflection of beam specimens increases as the quantity of pulverised bone in the mix increases.
- 4) Increase in the dosage of pulverised bone brings about the reduction in bending moment.
- 5) Equation (2), developed on the basis of rectangular stress idealisation for normal concrete, can be considered to be valid for foam concrete with and without pulverised bone.
- 6) The stiffness of foam concrete is not affected by the inclusion of pulverised bone up to 15% replacement level.
- 7) The use of reinforcement significantly improves the flexural performance of foam concrete.

ACKNOWLEDGEMENTS

We appreciate the Management of the University of Lagos providing a substantial fund for this research as well as creating a conducive environment for the execution of the work at the Structures and Concrete Laboratories in the Civil and Environmental Engineering Department.

REFERENCES

1. E. K. Nambiar and K. Ramamurthy, "Models for strength prediction of foam concrete", *Mater. Struct.*, **2008**, *41*, 247-254.
2. U. J. Alengaran, M. Z. Jumaat and H. Mahmud, "Structural behaviour of reinforced palm kernel shell foamed concrete beams", in "Challenges, Opportunities, and Solutions in Structural Engineering and Construction" (Ed. N. Ghafoori), CRC Press, Boca Raton, **2009**, Ch.41.
3. M. W. Hussin and K. Abdullah, "Properties of palm oil fuel ash cement based aerated concrete panel subjected to different curing regimes", *Malaysia J. Civil Eng.*, **2009**, *21*, 17-31.
4. F. Falade, E. Ikponmwoosa and C. Fapohunda, "Potential of pulverized bone as a pozzolanic material", *Int. J. Sci. Eng. Res.*, **2012**, *3*, 15-20.
5. R. L. Day, "Pozzolans for use in low-cost housing", Report to the International Development Centre, Ottawa Canada, **1990**.
6. M. S. Shetty, "Concrete Technology: Theory and Practice", Multicolour Edn., S. Chand and Company Ltd, New Delhi, **2009**, pp.45-50.
7. F. Falade, E. Ikponmwoosa and C. Fapohunda, "A study on the compressive and tensile strength of foamed concrete containing pulverized bone as a partial replacement of cement", *Univ. Pakistan J. Eng. Appl. Sci.*, **2013**, *13*, 82-93.
8. ACI Committee 213, "Guide for Structural Lightweight Aggregate Concrete", American Concrete Institute, Farmington Hills (MI), **2003**.
9. RILEM, "Functional Classification of Lightweight Concrete: Recommendations LC2", 2nd Edn., RILEM Publications, Bagnaux, **1978**.
10. F. Falade, E. Ikponmwoosa and C. Fapohunda, "Low-cost construction through the use of pulverized bone foam concrete (PB-FAC)", *Civil Environ. Res.*, **2013**, *3*, 107-113.
11. BS 12, "Specifications for Portland Cement", British Standards Institution, London, **1996**.
12. NIS 444, "Standard for Cement", Standard Organisation of Nigeria, Lagos, **2003**.
13. D. Aldridge, "Foamed concrete for highways bridge works", One-day Awareness Seminar on Foamed Concrete: Properties, Applications and Potential, **2000**, University of Dundee, Scotland, pp.33-41.
14. G. McGovem, "Manufacture and supply of ready-mix foamed concrete", One-day Awareness Seminar on Foamed Concrete: Properties, Applications and Potential, **2000**, University of Dundee, Scotland, pp.12-25.
15. K. C. Brady, G. R. A. Watts and M. R. Jones, "Specifications for Foamed Concrete—The Use of Foamed Concrete as Backfill", TRL Ltd., Wokingham, **2001**, pp.2-10.
16. M. R. Jones and A. McCarthy, "Preliminary views on the potential of foamed concrete as a structural material", *Magaz. Concrete Res.*, **2005**, *57*, 21-31.
17. Litebuilt, "Lightweight, foamed or cellular concrete technology", <http://www.litebuilt.com> (Accessed: January 2011).
18. BS 8110, "Structural Use of Concrete – Part 1: Code of Practice for Design and Construction", British Standards Institution, London, **1997**.
19. BS EN 12390 – 5, "Testing Hardened Concrete: Flexural Strength of Test Specimens", British Standards Institution, London, **2009**.
20. J. K. Wright and J. G. MacGregor, "Reinforced Concrete: Mechanics and Design", 5th Edn., Pearson Education International, Upper Saddle River (NJ), **2009**, pp.61-72.
21. P. E. Regan and A. R. Arasteh, "Lightweight aggregate foamed concrete", *Struct. Eng.*, **1990**, *68*, 168-173.

22. Constructional Steel Research, “Steel Designers Manual”, 4th Edition, ELBS and Granada Publishing, London, **1982**, p.35.
23. L. H. Sin. “Structural response of LWC beams in flexure”, *PhD Thesis*, **2007**, National University, Singapore.

© 2014 by Maejo University, San Sai, Chiang Mai, 50290 Thailand. Reproduction is permitted for noncommercial purposes.

Communication

An efficient Hantzsch synthesis of 1,4-dihydropyridines using *p*-toluenesulfonic acid under solvent-free condition

Masoud Nasr-Esfahani *, Morteza Montazerzohori and Razieh Raeatikia

Department of Chemistry, Yasouj University, Yasouj, Iran

* Corresponding author, e-mail: manas@mail.yu.ac.ir

Received: 28 July 2013 / Accepted: 23 February 2014 / Published: 3 March 2014

Abstract: An efficient Hantzsch synthesis of various substituted 1,4-dihydropyridines from an aldehyde, a β -dicarbonyl compound and ammonium acetate using *p*-toluenesulfonic acid in a solvent-free condition in the absence of any other co-catalyst is described. The process is simple and environmentally benign and the catalyst is commercially available and inexpensive. This method has the advantages of excellent yield (80–96%) and short reaction time (5-20 min.). Irradiation of a typical 1,4-dihydropyridine leads to the corresponding pyridine.

Keywords: Hantzsch synthesis, 1,4-dihydropyridines, *p*-toluenesulfonic acid, solvent-free synthesis

INTRODUCTION

In recent years, notable attention has been focused on the synthesis of 1,4-dihydropyridyl compounds due to their significant biological activities [1]. 1,4-Dihydropyridines (1,4-DHPs), as analogues of NADH coenzymes and other related derivatives, are widely used as calcium channel blockers for the treatment of cardiovascular disorder including hypertension, angina and cardiac arrhythmias [2]. Today, commercial representatives such as nifedipine (**1**), amlodipine (**2**), felodipine (**3**) and nicardipine (**4**) are some of the best selling drugs that are used in the treatment of hypertension (Figure 1).

1,4-Dihydropyridines are calcium antagonists [3], antitubercular agents [4] and neuropeptide Y Y1 receptor antagonists [5]. They possess neuroprotective [6], platelet antiaggregation [7] and antidiabetic activities [8]. These cases clearly demonstrate the remarkable potential of new 1,4-DHP derivatives as a source of valuable drug candidates.

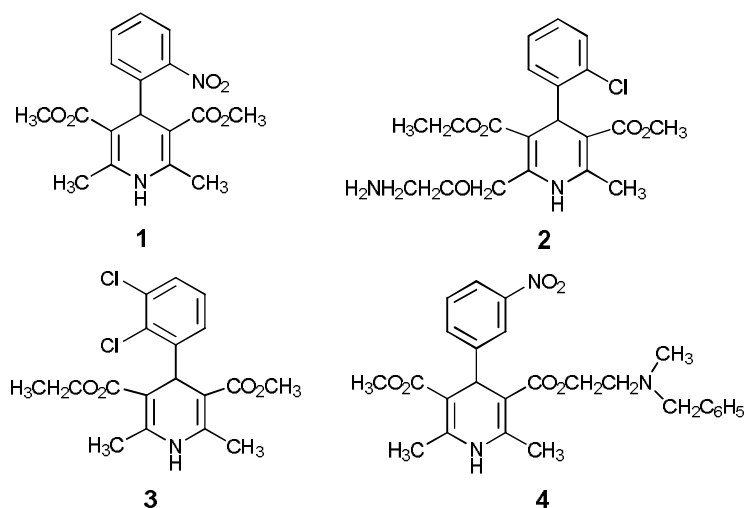


Figure 1. Some commercial 1,4-DHPs

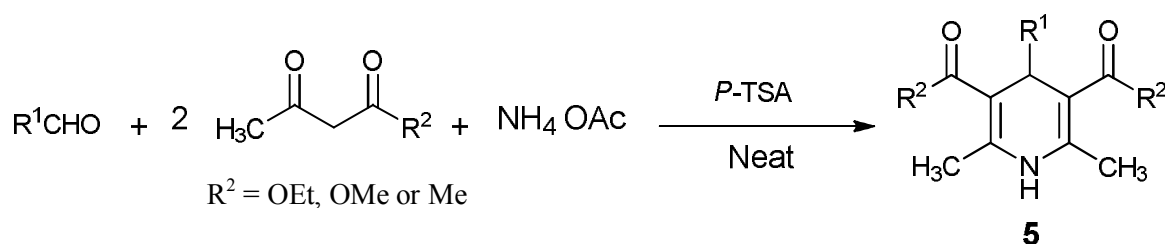
The classical synthesis of 1,4-DHPs by Hantzsch method [9] was developed as a one-pot condensation of an aldehyde with ethyl acetoacetate and ammonia either in acetic acid at room temperature or by refluxing in an alcohol for a long time [10]. However, the yields of the corresponding 1,4-DHPs obtained by the Hantzsch synthesis were generally low with harsh reaction conditions and long reaction times. A number of modified methods under improved conditions have been reported. In many of reported methods for the 1,4-DHP synthesis, solvent media such as ethanol, methanol and acetonitrile that may be harmful to the environment were used [11-13]. Also, several solvent-free procedures have been reported, but in spite of their potential utilities, many of those methods suffer from unsatisfactory yields, expensive and toxic reagents, and long reaction times [14]. Thus, the development of an efficient and versatile method for the preparation of Hantzsch reaction is an active ongoing research area and there is still a scope for further improvement towards milder reaction conditions, short reaction times and improved yields.

p-Toluenesulfonic acid (*p*-TSA) is a strong organic acid with about a million times stronger than benzoic acid [15] and is one of the few strong acids that are solid and hence conveniently weighed. Also, unlike some of the strong mineral acids, e.g. nitric acid, sulfuric acid and perchloric acid, *p*-TSA is non-oxidising. In synthetic point of view, countless useful transformations including Hantzsch condensation in a solution condition for the synthesis of polyhydroquinolines [16] have been developed using *p*-TSA as catalyst.

In the present study, we have found that *p*-TSA can be used for an efficient Hantzsch synthesis of a wide variety of 1,4-DHPs under solvent-free condition in the absence of any other organic or inorganic acids as auxiliary proton source. Furthermore, a photochemical reaction of a typical 1,4-DHP was also investigated. As expected, irradiation of the 1,4-DHP by UV light gave the corresponding polysubstituted pyridine.

DISCUSSION

In continuation of our programme on the chemistry of 1,4-dihydropyridines [17], herein we report an efficient one-pot procedure for the catalytic synthesis of 1,4-dihydropyridines from alkyl or aryl aldehydes, β -dicarbonyl compounds and ammonium acetate using *p*-TSA under solvent-free condition (Scheme 1).



Scheme 1. Catalytic synthesis of 1,4-dihydropyridines

Effect of Catalyst Concentration

The catalyst concentration was varied over a range of 5-25 mol% on the basis of the total volume of the reaction mixture. Table 2 shows the effect of catalyst concentration on the reaction between the benzaldehyde, ethyl acetoacetate and ammonium acetate. The yield of the corresponding 1,4-DHP increased with increasing catalyst concentration from 5 to 20 mol%. Further addition of catalyst had no noticeable effect on the yield. Thus, in all other reactions an amount of 20 mol% of *p*-TSA was used.

Table 1. Catalyst effect on the synthesis of diethyl 2,6-dimethyl-4-phenyl-1,4-dihydropyridines-3,5-dicarboxylate

Entry	Amount of <i>p</i> -TSA (g)	Mol% of <i>p</i> -TSA	Reaction time (min.)	Yield (%) ^a
1	0.0095	5	36	50
2	0.0190	10	25	60
3	0.0285	15	25	75
4	0.0380	20	15	90
5	0.0475	25	16	90

^a Isolated yield

Synthesis of 1,4-Dihydropyridines Catalysed by *p*-TSA

Using ammonium acetate

The results of the reactions of alkyl or aryl aldehydes, β -dicarbonyl (ethyl acetoacetate, methyl acetoacetate and acetyl acetone) and ammonium acetate in the presence of *p*-TSA at 80°C are shown in Table 2. Both aliphatic and aromatic aldehydes bearing either activating or deactivating groups react well with the β -dicarbonyls to yield the corresponding 1,4-DHPs. The reactions can be completed in 5-20 min. in high to excellent yields (80-96%). For larger scale synthesis, a typical reaction (Entry 1 of Table 2) was performed with ten times the amounts of reactants and catalyst used in the experimental section, from which a yield of 85% was obtained.

Using ammonia

To investigate the effect of the state of ammonia, aqueous ammonia was used in place of ammonium acetate in a few selected reactions under solvent-free condition or refluxing ethanol. As shown in Table 3, the reactions take longer to complete and give diminished yields in the presence of aqueous ammonia as compared with ammonium acetate. Further, between the solution and solvent-free conditions using ammonia, the latter gives a faster reaction and a higher yield.

Table 2. Results of synthesis of 1,4-dihydropyridines in the presence of *p*-TSA as per Scheme 1

Entry	R ¹	R ²	product	Reaction time (min.)	Yield (%) ^a	M.p.(°C) ^b	
						Found	Reported
1	C ₆ H ₅	OEt	5a	15	90	156-158	157-159 [14a]
2	2-NO ₂ C ₆ H ₄	OEt	5b	5	94	168-169	169-170 [18]
3	CH ₃	OEt	5c	10	85	127-129	128-130 [19]
4	2-ClC ₆ H ₄	OEt	5d	5	95	126-127	123-125 [20]
5	3-NO ₂ C ₆ H ₄	OEt	5e	10	96	161-163	162-164 [14a]
6	4-BrC ₆ H ₄	OEt	5f	15	95	159-161	160-162 [14a]
7	4-NO ₂ C ₆ H ₄	OEt	5g	10	90	128-129	130-132 [21]
8	4-CH ₃ OC ₆ H ₄	OEt	5h	20	96	160-162	158-160 [21]
9	2-CH ₃ OC ₆ H ₄	OEt	5i	15	95	142-143	141-143 [14b]
10	4-ClC ₆ H ₄	OEt	5j	10	90	143-145	144-146 [14a]
11	2-Thienyl	OEt	5k	10	92	171-173	172-174 [21]
12	2-Furyl	OEt	5l	5	95	161-163	160-162 [21]
13	C ₆ H ₅ CHCH ₃	OEt	5m	10	93	133-135	-
14	4-BrC ₆ H ₄	OMe	5n	10	90	195-197	-
15	(CH ₃) ₂ CHCH ₂	OMe	5o	15	80	121-123	122-124 [22]
16	3-NO ₂ C ₆ H ₄	OMe	5p	10	95	208-210	210-212 [22]
17	2,4-Cl ₂ C ₆ H ₃	OMe	5q	15	90	189-190	190-192 [22]
18	3-NO ₂ C ₆ H ₄	Me	5r	20	85	200-202	-
19	2-Furyl	Me	5s	20	80	174-176	-

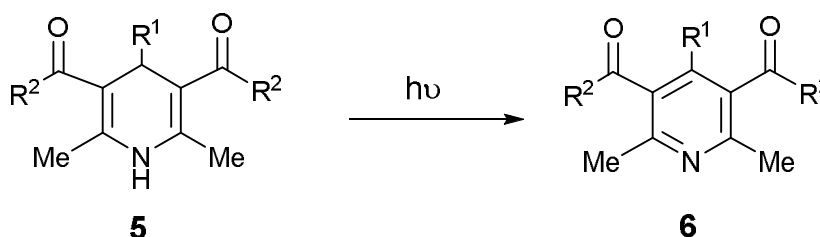
^a Yields refer to isolated and purified products.^b Characterised also by spectral data in comparison with literature report.**Table 3.** Effects of using ammonia on the synthesis of 1,4-DHPs in solution and solvent-free conditions

Entry	Product	NH ₃ (aq)		NH ₃ (aq)/EtOH	
		Reaction time (min.)	Yield (%) ^a	Reaction time (min.)	Yield (%) ^a
1	5a	20	65	35	45
2	5h	25	80	46	53
3	5j	35	75	80	43
4	5l	13	85	20	50

^a Isolated yield

Photochemical Reaction

1,4-DHPs may be oxidised under UV irradiation in the presence or absence of oxygen, leading to the corresponding pyridines [23]. For investigation of the photochemical reaction of 1,4-DHPs (Scheme 2), we chose the reaction of 2-chlorophenyl derivative (**5d**) as a typical sample. Spectroscopic and physical data of the photoproduct (**6**) show that it was aromatised to the corresponding pyridine. For example, comparison of the ultraviolet spectra of **5d** and **6** indicates a hypsochromic shift (blue shift) of the absorption of the photoproduct, which is characteristic of a pyridine ring (Figure 2). In the presence of sunlight, this reaction occurs more slowly [24]. This photochemical process is a useful synthetic step to produce the polysubstituted pyridines.



Scheme 2. Photochemical reaction of 1,4-DHPs (**6**: R¹ = 2-ClC₆H₄, R² = OEt)

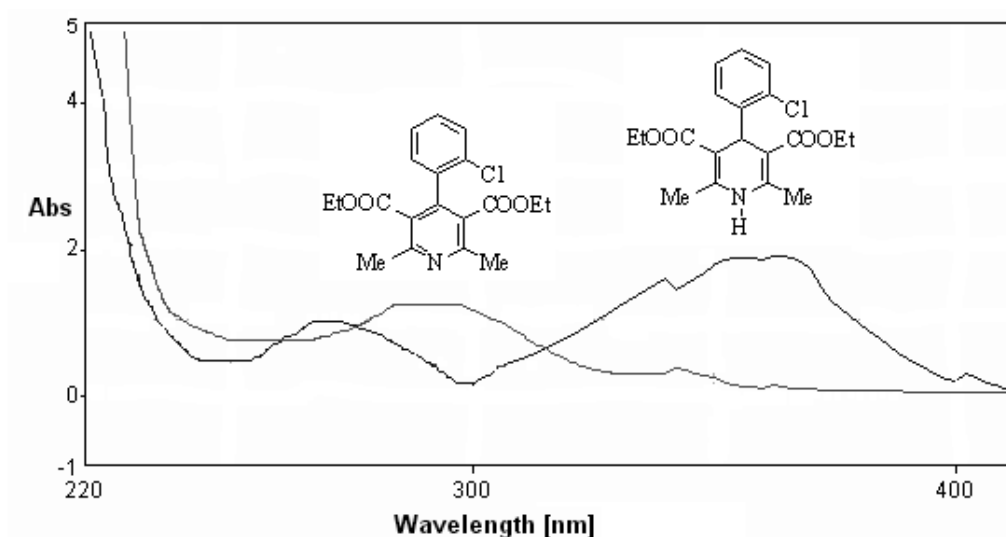


Figure 2. UV spectra of diethyl 2,6-dimethyl-4-(4-chlorophenyl)-1,4-dihydropyridine-3,5-dicarboxylate (**5d**) and its photoproduct (**6**)

CONCLUSIONS

A simple and efficient procedure for the Hantzsch synthesis of 1,4-dihydropyridines has been developed. Mild reaction conditions, absence of solvent, short reaction times, easy isolation of the products, good to excellent yields and large scale applicability are the main advantages. Irradiation of the product obtained by UV light gives the corresponding pyridine readily, a useful route to polysubstituted pyridines.

EXPERIMENTAL

Chemicals were purchased from Merck, Fluka and Aldrich chemical companies. All of the products were identified by comparison of their physical and spectral data with those of the authentic samples. Melting points were determined using a Barnstead Electrothermal (BI 9300) apparatus and were uncorrected. The progress of the reactions was monitored by thin layer chromatography (TLC) using silica gel plates and UV(254 nm) detection. IR spectra (KBr disc) were recorded on a JASCO IR-680 spectrophotometer. ¹H NMR spectra (in CDCl₃) were obtained by a Bruker-Arance AQS (300 MHz) or Bruker 400 Ultrasheid (400 MHz) spectrometers. A JASCO-V570 UV-visible spectrophotometer was used for recording ultraviolet spectra. Elemental analysis (CHNS) was performed using a LECO CHNS-932 elemental analyser.

General Procedure for Preparation of 1,4-Dihydropyridines

A mixture of alkyl or aryl aldehyde (1 mmol), β-dicarbonyl (2 mmol) and ammonium acetate (1.5 mmol) was heated at 80°C in the presence of *p*-TSA (0.0380 g, 20 mol%) under stirring for 5-20 min. The progress of the reaction was monitored by TLC. After completion of the reaction, the mixture was cooled to room temperature and then ethanol (5 mL) was added to the reaction mixture. The resulting solid product was filtered and recrystallised from ethanol to give a pure product in 80-96% yield based on the starting aldehyde.

For preparation using ammonia in place of ammonium acetate, it was similarly executed as follows. In a round-bottom flask the aldehyde (1 mmol), β-dicarbonyl (2 mmol), aqueous 25% (w/w) ammonia (0.5 mL), and *p*-TSA (0.0380 g, 20 mol%) in ethanol (5 mL) or without ethanol were mixed thoroughly. The flask was heated at 80 °C with concomitant stirring. After completion of the reaction, the mixture was cooled to room temperature and the resultant solid product was filtered and recrystallized from ethanol to give a pure product.

The physical and spectroscopic data of new compounds are as follows:

Diethyl 2,6-dimethyl-4-(1-phenylethyl)-1,4-dihydropyridine-3,5-dicarboxylate (5m)

M.p.131-132°; *R*_f 0.64 (n-hexane: ethyl acetate = 4:1); IR(cm⁻¹): 3330, 3122, 1675; NMR (δ): 1.18 (t, *J* = 7.2, 6H), 1.28 (t, *J* = 6.8, 3H), 2.202 (s, 6H), 2.75-2.84(m, 1H), 4.06 (q, *J* = 7.0 Hz, 4H), 4.28 (d, 1H, *J* = 4.8 Hz), 5.50 (s, 1H), 7.08-7.27 (m, 5H). Anal. Calcd. for C₂₁H₂₇NO₄: C, 70.56; H, 7.61; N, 3.92; O, 17.90; found: C, 70.50; H, 7.69; N, 3.85.

Dimethyl 2,6-dimethyl-4-(4-bromophenyl)-1,4-dihydropyridine-3,5-dicarboxylate (5n)

M.p.196-198°; *R*_f 0.625 (CCl₄: ethyl acetate = 3:1); IR(cm⁻¹): 3305, 3069, 2951, 1696, 1659, 1585; NMR(δ): 2.33 (s, 6H), 3.64 (s, 6H), 4.96 (s, 1H), 5.73(bs, 1H), 7.13-7.34 (dd, *J* = 8.4 and 17.4 Hz, 4H). Anal. Calcd. for C₁₇H₁₈BrNO₄: C, 53.70; H, 4.77; Br, 21.01; N, 3.68; O, 16.83; found: C, 53.63; H, 4.82; N, 3.64.

2,6-Dimethyl-3,5-diacetyl-4-(3-nitrophenyl)-1,4-dihydropyridine (5r)

M.p.200-203°; *R*_f 0.72 (CCl₄: ethyl acetate = 4:1); IR(cm⁻¹): 3316, 2951, 3069, 1670, 1525, 1589, 1472; NMR(δ): 2.38 (s, 6H), 2.28 (s, 6H), 5.29 (s, 1H), 6.033 (bs, 1H), 7.38-8.04 (m, 4H). Anal. Calcd. for C₁₇H₁₈N₂O₄: C, 64.96; H, 5.77; N, 8.91; O, 20.36; found: C, 64.90; H, 5.87; N, 8.84.

2,6-Dimethyl-3,5-diacetyl-4-(2-furyl)-1,4-dihydropyridine (5s)

M.p.174-176°; R_f 0.21 (n-hexane: ethyl acetate = 6:1); IR(cm^{-1}): 3275, 3027, 2926, 1650, 1598; NMR(δ): 2.36 (s, 6H), 2.33 (s, 6H), 5.5 (s, 1H), 7.2 (bs, 1H), 5.907-6.22 (m, 3H). Anal. Calcd. for $\text{C}_{15}\text{H}_{17}\text{NO}_3$: C, 69.48; H, 6.61; N, 5.40; O, 18.51; found: C, 69.57; H, 6.55; N, 5.50.

Irradiation Reaction

A solution containing **5d** (0.145 g, 0.4 mmol) in chloroform (20 mL) under air bubbling was stirred at room temperature and irradiated by UV light (400W high-pressure mercury lamp, $\lambda \geq 280$ nm) for 6 hr [23]. The reaction mixture was cooled in Duran glass by cold running water. The progress of the reaction was monitored by TLC. After completion of the reaction, evaporation of the solvent followed by chromatography on a silica-gel plate (eluent: CCl_4 /ethyl acetate = 5:1) afforded a pure product (**6**) (0.119 g, 82%): m.p.60-62° (lit.61-62° [25]); IR(cm^{-1}): 2920, 1720, 1617, 1480, 1172, 754; NMR(δ): 0.97 (t, 6H, $J = 7.1$ Hz), 2.62 (s, 6H), 4.07 (q, 4H, $J = 7.1$ Hz), 7.20-7.41 (m, 4H); UV(CH_3OH): λ_{max} 235 nm, $\epsilon = 19952$.

ACKNOWLEDGEMENT

The partial support of this work by Yasouj University is acknowledged.

REFERENCES

1. R. Shan, C. Velazquez and E. E. Knaus, "Syntheses, calcium channel agonist-antagonist modulation activities, and nitric oxide release studies of nitrooxyalkyl 1,4-dihydro-2,6-dimethyl-3-nitro-4-(2,1,3-benzoxadiazol-4-yl)pyridine-5-carboxylate racemates, enantiomers, and diastereomers", *J. Med. Chem.*, **2004**, *47*, 254-261.
2. J. C. Emmet (Ed.), "Comprehensive Medicinal Chemistry", Vol. 3, Pergamon Press, Oxford, **1990**, Ch.14.1.
3. S. Visentin, B. Rolando, A. D. Stilo, R. Fruttero, M. Novara, E. Carbone, C. Roussel, N. Vanthuyne and A. Gasco, "New 1,4-dihydropyridines endowed with NO-donor and calcium channel agonist properties", *J. Med. Chem.*, **2004**, *47*, 2688-2693.
4. P. S. Eharkar, B. Desai, H. Gaveria, B. Varu, R. Loriya, Y. Naliapara, A. Shah and V. M. Kulkarni, "Three-dimensional quantitative structure-activity relationship of 1,4-dihydropyridines as antitubercular agents", *J. Med. Chem.*, **2002**, *45*, 4858-4867.
5. G. S. Poindexter, M. A. Bruce, J. G. Breitenbucher, M. A. Higgins, S. Y. Sit, J. L. Romine, S. W. Martin, S. A. Ward, R. T. McGovern, W. Clarke, J. Russell and I. Antal-Zimanyi, "Dihydropyridine neuropeptide Y Y1 receptor antagonists 2: Bioisosteric urea replacements", *Bioorg. Med. Chem.*, **2004**, *12*, 507-521.
6. V. Klusa, "Cerebrocrast, neuroprotectant cognition enhancer", *Drugs Future*, **1995**, *20*, 135-138.
7. R. G. Bretzel, C. C. Bollen, E. Maeser and K. F. Federlin, "Nephroprotective effects of nitrendipine in hypertensive type I and type II diabetic patients", *Am. J. Kidney Dis.*, **1993**, *21*, 53-64.
8. A. K. Ogawa, C. A. Willoughby, R. Bergeron, K. P. Ellsworth, W. M. Geissler, R. W. Myer, J. Yao, G. Harris and K. T. Chapman, "Glucose-lowering in a db/db mouse model by dihydropyridine diacid glycogen phosphorylase inhibitors", *Bioorg. Med. Chem. Lett.*, **2003**, *13*, 3405-3408.

9. A. Hantzsch, "Über die synthese pyridinartiger verbindungen aus acetessigäther und aldehydammoniak", *Justus Liebigs Ann. Chem.*, **1882**, 215, 1-82.
10. B. Loev and K. M. Snader, "The Hantzsch reaction. I. Oxidative dealkylation of certain dihydropyridines", *J. Org. Chem.* **1965**, 30, 1914-1916.
11. G. Sabitha, G. S. K. K. Reddy, C. S. Reddy and J. S. Yadav, "A novel TMSI-mediated synthesis of Hantzsch 1,4-dihydropyridines at ambient temperature", *Tetrahedron Lett.*, **2003**, 44, 4129-4131.
12. M. A. Zolfigol and M. Safaiee, "Synthesis of 1,4-dihydropyridines under solvent-free conditions", *Synlett*, **2004**, 5, 827-828.
13. (a) M. A. Chari and K. Syamasundar, "Silica gel/NaHSO₄ catalyzed one-pot synthesis of Hantzsch 1,4-dihydropyridines at ambient temperature", *Catal. Commun.*, **2005**, 6, 624-626; (b) M. Arslan, C. Faydali, M. Zengin, M. Küçükislamoglu and H. Demirhan, "An efficient one-pot synthesis of 1,4-dihydropyridines using alumina sulfuric acid (ASA) catalyst", *Turk. J. Chem.*, **2009**, 33, 769-774; (c) F. M. Moghaddam, H. Saeidian, Z. Mirjafary and A. Sadeghi, "Rapid and efficient one-pot synthesis of 1,4-dihydropyridine and polyhydroquinoline derivatives through the Hantzsch four component condensation by zinc oxide", *J. Iran. Chem. Soc.*, **2009**, 6, 317-324.
14. (a) S. S. Mansoor, K. Aswin, K. Logaiya and S. P. N. Sudhan, "Melamine trisulfonic acid as an efficient catalyst for the synthesis of 2,6-dimethyl-4-substituted-1,4-dihydropyridine-3,5-diethyl/dimethylcarboxylate derivatives via Hantzsch reaction in solvent free condition", *J. King Saud Univ. -Sci.*, **2013**, 25, 191-199; (b) A. Debache, L. Chouguiat, R. Boulcina and B. Carboni, "A one-pot multi-component synthesis of dihydropyrimidinone/thione and dihydropyridine derivatives via Biginelli and Hantzsch condensations using *t*-BuOK as a catalyst under solvent-free conditions", *Open Org. Chem. J.*, **2012**, 6, 12-20; (c) M. Mahesh, V. Siddaiah, Y. K. Rao, Y.-M. Tzeng and C. Sridhar, "A simple and efficient one-pot synthesis of 1,4-dihydropyridines using heterogeneous catalyst under solvent-free conditions", *J. Mol. Catal. A - Chem.*, **2006**, 260, 179-180.
15. J. P. Guthrie, "Hydrolysis of esters of oxy acids: pK_a values for strong acids; Brønsted relationship for attack of water at methyl; free energies of hydrolysis of esters of oxy acids; and a linear relationship between free energy of hydrolysis and pK_a holding over a range of 20 pK units", *Can. J. Chem.*, **1978**, 56, 2342-2354.
16. S. R. Cherkupally and R. Mekala, "*p*-TSA catalyzed facile and efficient synthesis of polyhydroquinoline derivatives through Hantzsch multi-component condensation", *Chem. Pharm. Bull.*, **2008**, 56, 1002-1004.
17. (a) M. Nasr-Esfahani, M. Moghadam, S. Tangestaninejad and V. Mirkhani, "Biomimetic oxidation of Hantzsch 1,4-dihydropyridines with tetra-*n*-butylammonium periodate catalyzed by tetraphenylporphyrinatomanganese(III) chloride [Mn(TPP)Cl]", *Bioorg. Med. Chem. Lett.*, **2005**, 15, 3276-3278; (b) M. Nasr-Esfahani, M. Moghadam, S. Tangestaninejad, V. Mirkhani and A. R. Momeni, "Rapid and efficient oxidation of Hantzsch 1,4-dihydropyridines with sodium periodate catalyzed by manganese (III) Schiff base complexes", *Bioorg. Med. Chem.*, **2006**, 14, 2720-2724; (c) M. Montazerzohori, B. Karami, M. Nasr-Esfahani and S. A. Musavi, "Silver salts/ iodine monochloride as a new oxidation system for the oxidative aromatization of 1,4- dihydropyridines", *Heterocycl. Commun.*, **2007**, 13, 289-295; (d) M. Nasr-Esfahani, M. Moghadam and G. Valipour, "Rapid and efficient aromatization of

- Hantzsch 1,4-dihydropyridines with potassium peroxomonosulfate catalyzed by manganese(III) Schiff base complexes”, *J. Iran. Chem. Soc.*, **2008**, 5, 244-251.
18. S. X. Wang, Z. Y. Li, J. C. Zhang and J. T. Li, “The solvent-free synthesis of 1,4-dihydropyridines under ultrasound irradiation without catalyst”, *Ultrason. Sonochem.*, **2008**, 15, 677-680.
 19. M. Li, W. S. Guo, L. R. Wen, Y. F. Li and H. Z. Yang, “One-pot synthesis of Biginelli and Hantzsch products catalyzed by non-toxic ionic liquid (BMImSac) and structural determination of two products”, *J. Mol. Catal. A - Chem.*, **2006**, 258, 133-138.
 20. B. Loev, M. M. Goodman, K. M. Snader, R. Tedeschi and E. Macko, “Hantzsch-type dihydropyridine hypotensive agents”, *J. Med. Chem.*, **1974**, 17, 956-965.
 21. A. Debache, W. Ghalem, R. Boulcina, A. Belfaitah, S. Rhouati and B. Carboni, “An efficient one-step synthesis of 1,4-dihydropyridines via a triphenylphosphine-catalyzed three-component Hantzsch reaction under mild conditions”, *Tetrahedron Lett.*, **2009**, 50, 5248-5250.
 22. H. Salehi and Q. X. Guo, “Synthesis of substituted 1,4-dihydropyridines in water using phase-transfer catalyst under microwave irradiation”, *Synth. Commun.*, **2004**, 34, 4349-4357.
 23. (a) H. R. Memarian, M. Abdoli-Senejani and S. Tangestaninejad, “Photosensitized oxidation of unsymmetrical 1,4-dihydropyridines”, *J. Iran. Chem. Soc.*, **2006**, 3, 285-292; (b) H. R. Memarian, M. Abdoli-Senejani and D. Döpp, “Photoinduced aromatization of unsymmetrically substituted 1,4-dihydropyridines”, *J. Chin. Chem. Soc.*, **2007**, 54, 131-139.
 24. L. J. Ngez-Vergara, C. Sunkel, J. A. Squella, “Photodecomposition of a new 1,4-dihydropyridine: Furnidipine”, *J. Pharm. Sci.*, **1994**, 83, 502-507.
 25. K. Y. Ko and J. Y. Park, “Aromatization of Hantzsch 1,4-dihydropyridines with pyridinium dichromate”, *Bull. Korean Chem. Soc.*, **1995**, 16, 200-201.

© 2014 by Maejo University, San Sai, Chiang Mai, 50290 Thailand. Reproduction is permitted for noncommercial purposes.

Technical Note

An alternative synthesis of (\pm)-phenylephrine hydrochloride

Wipanoot Baison, Aphiwat Teerawutgulrag*, Pakawan Puangsombat and Nuansri Rakariyatham

Department of Chemistry, Faculty of Science, Chiang Mai University, Chiang Mai 50200, Thailand

* Corresponding author, e-mail: aphiwattee@yahoo.co.uk

Received: 4 July 2013 / Accepted: 5 March 2014 / Published: 6 March 2014

Abstract: This study presents alternative synthetic pathways and reagents for the preparation of racemic phenylephrine hydrochloride. Using *m*-hydroxybenzaldehyde as starting material, two separate pathways—epoxidation and bromohydrin formation—are presented. Both routes provide good yields (overall of 71% and 66% respectively) and can be performed at mild conditions.

Keywords: phenylephrine, phenylephrine hydrochloride, *m*-hydroxybenzaldehyde, alpha adrenergic receptor agonist

INTRODUCTION

Phenylephrine hydrochloride (PE) or 3-(1-hydroxy-2-(methylamino)ethyl)phenol hydrochloride (**1**: Figure 1) is an α_1 -adrenergic receptor agonist [1] used as a topical nasal decongestant and in eye drops to dilate the pupil. Recently, PE has been marketed in the optically active (*R*)-form as a substitute for pseudoephedrine, a precursor in the production of methamphetamine, a notorious narcotic drug [2]. Various methods for the synthesis of PE have been documented in the literature. Legerlotz [3-5] reported the classical industrial synthetic pathway. Racemic PE was resolved using tartaric acid in order to obtain the (*R*)-form [6].

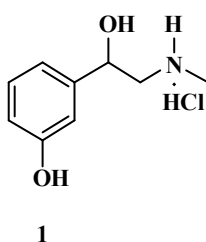
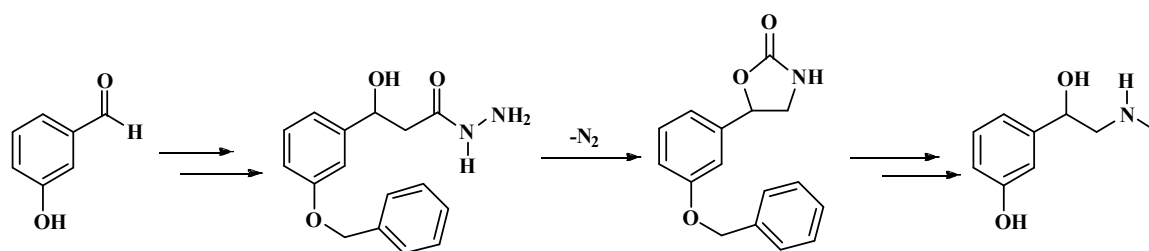
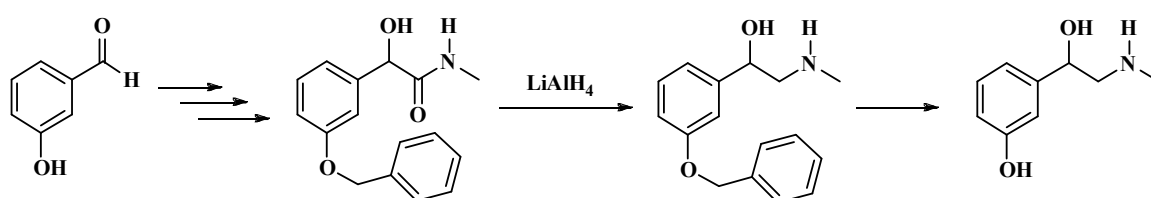


Figure 1. Phenylephrine hydrochloride

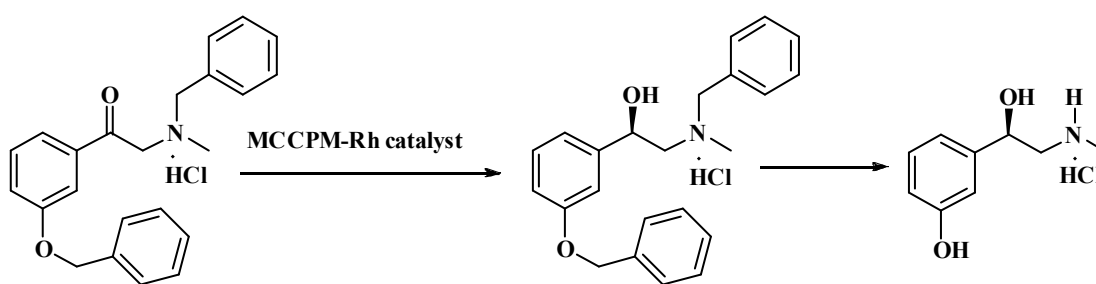
Nonchiral synthesis of PE was reported in 1951 by Bergmann and Sulzbacher [7], who used *m*-hydroxybenzaldehyde as starting material and a Curtius rearrangement of a beta-hydroxyl acid azide as the key step (Scheme 1). In 1961, Russell and Childress [8] used the same starting material for the synthesis of racemic PE, employing the reduction of mandelamide with lithium aluminium hydride as the key step (Scheme 2). Takeda *et al.* [9] reported an asymmetric synthesis of chiral PE using *(2R,4R)*-dicyclohexylphosphino-2-diphenylphosphinomethyl-1-*(N*-methycarbonyl)-pyrrolidine (MCCPM)-rhodium as chiral catalyst, producing *(R)*-PE as a product with 85% ee (Scheme 3).



Scheme 1. Synthesis of phenylephrine by Curtius rearrangement of beta-hydroxyl acid azide



Scheme 2. Synthesis of phenylephrine using reduction of mandelamide with lithium aluminium hydride as key step

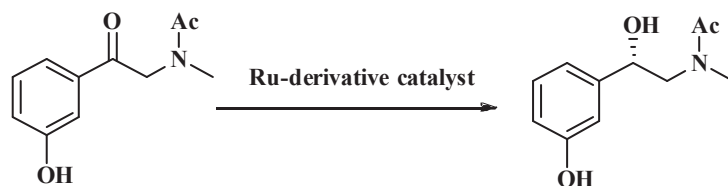


Scheme 3. Synthesis of *(R)*-PE using MCCPM-rhodium catalyst

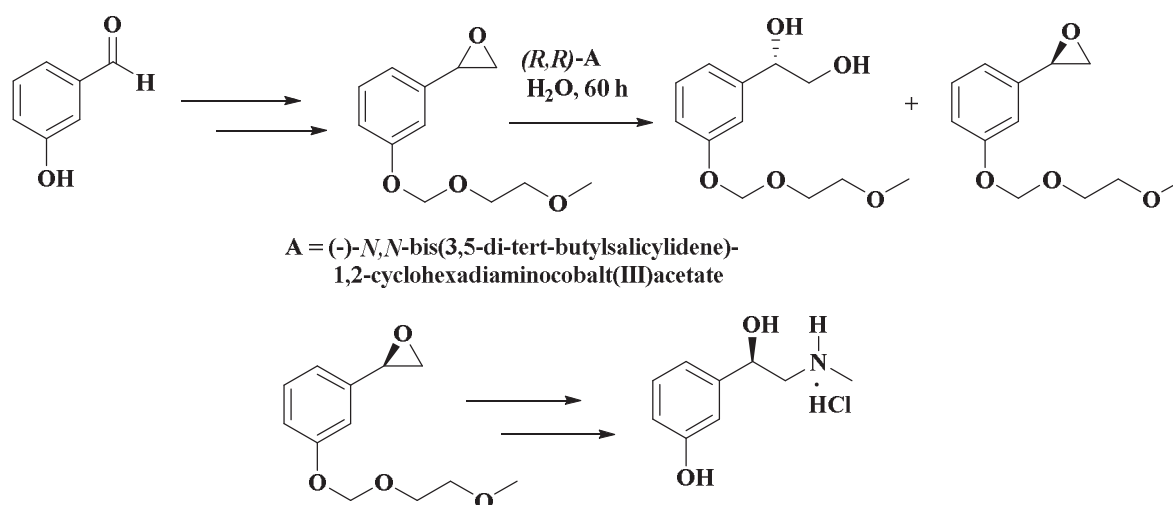
McGarrity and Zanotti-Gerosa [10] reported a feasibility study on a new route to *(R)*-PE based on ruthenium-derivative-catalysed asymmetric hydrogenation of an *N*-protected aminoketone precursor (Scheme 4). The direct and fast asymmetric reduction of *N*-protected aminoketone was highly enantioselective (>95% ee) but the *(S)*-PE was the main product in most conditions.

Gurjar *et al.* [11] studied the hydrolytic kinetic resolution of a styrene oxide derivative. They used *(R,R)*-SalenCo^{III}OAc complex to induce racemic styrene epoxide to *(R)*-form at 45% yield (97% ee) as shown in Scheme 5 [11]. In 2003, Pandey *et al.* [13] reported *(R)*-PE synthesis via Sharpless asymmetric dihydroxylation with 98% ee, yielding the desired product in seven steps

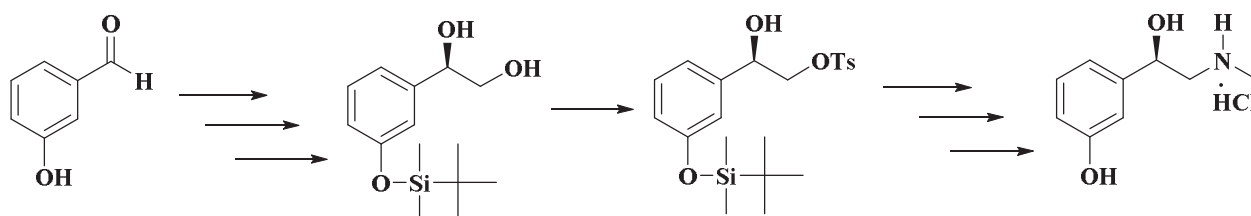
(Scheme 6). In this paper, we report a variation of the route and reagents for preparing PE in high yields using mild conditions.



Scheme 4. Asymmetric hydrogenation of *N*-protected aminoketone



Scheme 5. Synthesis of (*R*)-PE via hydrolytic kinetic resolution

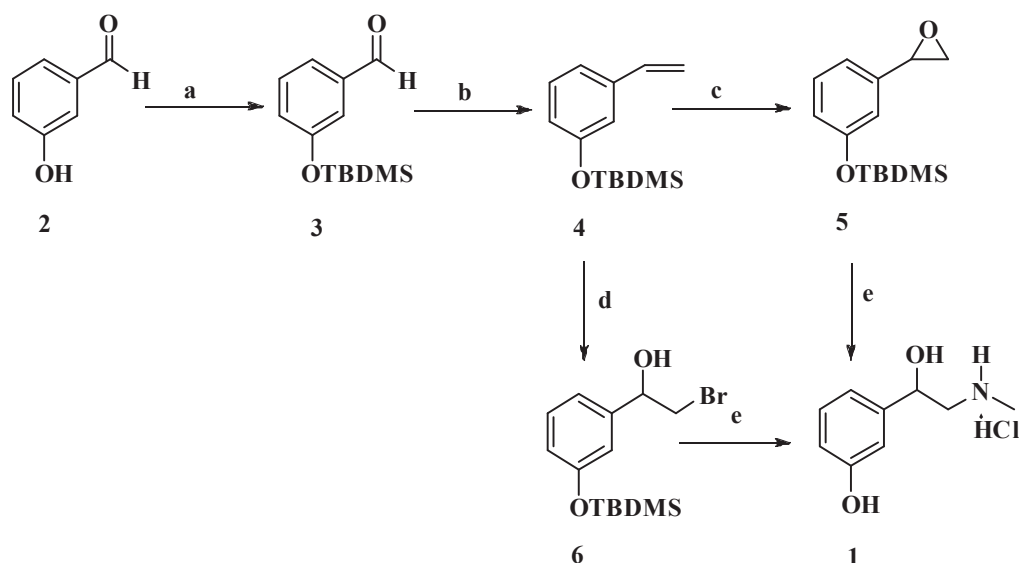


Scheme 6. Synthesis of (*R*)-PE via Sharpless asymmetric dihydroxylation

DISCUSSION

Synthesis of PE (**1**) was initiated from *m*-hydroxybenzaldehyde (**2**), as illustrated in Scheme 7. The protection of **2** with *t*-butyldimethylsilyl chloride (TBDMS-Cl) in the presence of imidazole produced the silyl compound **3** in quantitative yield. The Wittig olefination of **3** with methyltriphenylphosphonium iodide and *t*-BuOK in THF at ambient temperature furnished styrene **4** in 97% yield. After these steps, the synthesis could be performed using two pathways. The epoxidation of **4** with *m*-chloroperoxybenzoic acid (MCPBA) in CH₂Cl₂ at room temperature produced epoxide **5** in 81% yield, while treatment of **4** with *N*-bromosuccinimide (NBS) in the presence of H₂O and DMSO at room temperature produced bromohydrin **6** in 80% yield. The epoxide **5** and bromohydrin **6** was treated with methylamine in methanol at room temperature and

the TBDMS group deprotected with 6M hydrochloric acid solution at room temperature to produce **1** in 90% (from epoxide **5**) and 85% (from bromohydrin **6**). The overall yields of **1** via epoxide **5** and bromohydrin **6** were 71% and 66% respectively.



Scheme 7. Synthesis of PE (**1**). Reagents and condition: (a) TBDMS-Cl, imidazole, 0°; (b) $\text{CH}_3\text{P}^+\text{Ph}_3\text{I}^-$, *t*-BuOK, 0°; (c) MCPBA, RT; (d) NBS, H_2O , DMSO, 0°; (e) i. MeNH_2 , RT ii. HCl, RT

CONCLUSION

A practical and alternative method for the synthesis of racemic phenylephrine hydrochloride has been performed using mild conditions with good overall yields.

EXPERIMENTAL

m-Hydroxybenzaldehyde, TBDMS-Cl, MCPBA, imidazole, potassium *tert*-butoxide and methylamine were purchased from Aldrich. Methyltriphenylphosphonium iodide was prepared from triphenylphosphine and methyl iodide. *N*-Bromosuccinimide was recrystallised in water at 90° and dried in oven at 60° for 2 hr. All solvents were distilled prior to use. Thin-layer chromatography (TLC) was performed on silica 60 F_{264} plates and column chromatography was carried out on silica gel (0.063-0.20 mm).

^1H -NMR spectra were recorded on a 400-MHz or 500-MHz Bruker Avance using trimethylsilane as the internal standard in CDCl_3 or $\text{DMSO}-d_6$. ^{13}C -NMR spectra were recorded on a 100-MHz or 125-MHz Bruker Avance using trimethylsilane as the internal standard in CDCl_3 or $\text{DMSO}-d_6$. Mass spectra were recorded on ESI-Q-TOF-MS (Micromass, Manchester, UK). IR spectra were recorded on a FT-IR spectrometer (Tensor 27) as neat film or KBr disc. Melting point was determined on MEL-TEMP (Laboratory Devices Inc., USA) and used without correction.

3-(*tert*-Butyldimethylsilyloxy)benzaldehyde (**3**)

Imidazole (4.21 g, 61.8 mmol) and TBDMS-Cl (9.31 g, 61.7 mmol) was added to a stirred solution of *m*-hydroxybenzaldehyde (**2**) (5.04 g, 41.3 mmol) in dry dichloromethane (50 mL) at 0°. The mixture was then allowed to warm up to room temperature. After 24 hr, water (30 mL) was added and the organic layer was washed with brine (10 mL), dried (Na_2SO_4) and concentrated under

reduced pressure. The residue was purified on silica gel by eluting with EtOAc-hexane (1:4) to give compound **3** as a pale yellow liquid (10.13 g, quantitative yield): IR 2958, 2927, 2860, 1705, 1581, 1275, 840 cm^{-1} ; $^1\text{H-NMR}$ δ 9.94 (s, 1H), 7.46 (dt, $J = 7.5, 1.3$ Hz, 1H), 7.38 (t, $J = 7.8$ Hz, 1H), 7.33 (dd, $J = 2.3, 1.6$ Hz, 1H), 7.10 (m, 1H), 0.99 (s, 9H), 0.22 (s, 6H); $^{13}\text{C-NMR}$ δ 191.85, 156.27, 137.85, 129.95, 126.37, 123.43, 119.69, 25.52, 18.05, -4.58; HRMS calculated for $\text{C}_{13}\text{H}_{21}\text{O}_2\text{Si}$ $[\text{M}+\text{H}]^+$ 237.1311, found 237.1313.

tert-Butyldimethyl(3-vinylphenoxy)silane (4)

Potassium *tert*-butoxide (2.90 g, 25.9 mmol) was added to a stirred suspension of methyltriphenylphosphonium iodide (10.32 g, 25.5 mmol) in dry THF (50 mL) at 0°. The mixture was stirred at room temperature for 1 hr; then aldehyde **3** (5.01 g, 21.2 mmol) was added portionwise. The mixture was stirred for 2 hr at room temperature and diluted with water (40 mL). The aqueous layer was extracted with ethyl acetate (2×40 mL). The combined organic layer was washed with brine (10 mL), dried (Na_2SO_4) and concentrated under reduced pressure. The crude product was purified on silica gel by eluting with EtOAc-hexane (1:19) to furnish, after concentration, compound **4** (4.82 g, 97%) as a colourless liquid: IR 2957, 2930, 2858, 1578, 1485, 1279, 839 cm^{-1} ; $^1\text{H-NMR}$ δ 7.27 (t, $J = 7.8$ Hz, 1H), 7.11 (d, $J = 7.6$ Hz), 7.02 (s, 1H), 6.86 (d, $J = 8.0$ Hz, 1H), 6.77 (dd, $J = 17.5, 10.8$ Hz, 1H), 5.82 (d, $J = 17.6$ Hz, 1H), 5.32 (d, $J = 10.8$ Hz, 1H), 1.12 (s, 9H), 0.33 (s, 6H); $^{13}\text{C-NMR}$ δ 155.84, 139.06, 136.75, 129.36, 119.51, 119.49, 117.72, 113.78, 25.69, 18.17, -4.42; HRMS calculated for $\text{C}_{14}\text{H}_{23}\text{O}_2\text{Si}$ $[\text{M}+\text{H}]^+$ 235.1518, found 235.1512.

tert-Butyldimethyl(3-oxiranylphenoxy)silane (5)

MCPBA (1.01 g, 5.83 mmol) was added to a stirred solution of compound **4** (0.65 g, 2.76 mmol) in CH_2Cl_2 (15 mL) at room temperature. After 3 hr, the reaction mixture was washed with saturated sodium thiosulfate solution (5 mL) and saturated NaHCO_3 solution (5 mL). The organic layer was washed with brine (5 mL), dried (Na_2SO_4) and concentrated under reduced pressure. The residue was purified on silica gel by eluting with EtOAc-hexane (1:19) to produce, after concentration, compound **5** (0.56 g, 81%) as a colourless liquid: IR 3048, 2931, 2858, 1606, 1486, 1284, 957, 833 cm^{-1} ; $^1\text{H-NMR}$ δ 7.20 (t, $J = 8.0$ Hz, 1H), 6.90 (d, $J = 7.6$ Hz, 1H), 6.80 (d, $J = 7.3$ Hz, 2H), 3.79 (dd, $J = 4.0, 2.6$ Hz, 1H), 3.09 (dd, $J = 5.6, 4.1$ Hz, 1H), 2.74 (dd, $J = 5.6, 2.5$ Hz, 1H), 1.03 (s, 9H), 0.23 (s, 6H); $^{13}\text{C-NMR}$ δ 155.80, 139.24, 129.30, 119.64, 118.42, 116.74, 51.87, 50.82, 25.51, 17.99, -4.60; HRMS calculated for $\text{C}_{14}\text{H}_{23}\text{O}_2\text{Si}$ $[\text{M}+\text{H}]^+$ 251.1467, found 251.1465.

2-Bromo-1-(3-(tert-butyldimethylsilyloxy)phenyl)ethanol (6)

NBS (1.14 g, 6.43 mmol) and water (0.25 mL) were added to a stirred solution of compound **4** (0.52 g, 2.22 mmol) in DMSO (8 mL) at 0°C. After 45 min., ice-cooled water (10 mL) was added. The aqueous phase was extracted with ethyl acetate (2×10 mL). The combined organic layer was washed with brine (5 mL), dried (Na_2SO_4) and concentrated under reduced pressure. The residue was purified on silica gel by eluting with EtOAc-hexane (1:19) to produce, after concentration, compound **6** (0.59 g, 80%) as a colourless liquid: IR 3422, 2956, 2858, 1602, 1485, 1065, 1278, 835 cm^{-1} ; $^1\text{H-NMR}$ δ 7.22 (t, $J = 7.8$ Hz, 1H), 6.95 (d, $J = 7.6$ Hz, 1H), 6.88 (br, 1H), 6.80 (d, $J = 8.0$ Hz, 1H), 4.85 (d, $J = 8.3$ Hz, 1H), 3.61 (d, $J = 9.1$ Hz, 1H), 3.51 (t, $J = 9.7$ Hz, 1H), 2.77 (s, 1H), 1.00 (s, 9H), 0.21 (s, 6H); $^{13}\text{C-NMR}$ δ 155.85, 141.89, 129.59, 119.98, 118.79, 117.69, 73.51, 40.04, 25.62, 18.12, -4.45; HRMS calculated for $\text{C}_{14}\text{H}_{23}\text{O}_1\text{SiBr}$ $[\text{M}+\text{H}-\text{OH}]^+$ 315.0630, found 315.0346.

Phenylephrine hydrochloride (1)*Via epoxide compound 5*

A solution of **5** (0.51 g, 2.05 mmol) in dry methanol (5 mL) was saturated with methylamine gas and left stirred at room temperature for 2 hr. The solution was concentrated to give the crude mixture. Hydrochloric acid (6M, 0.50 mL) was added to the solution of the crude mixture in methanol (5 mL). The resulting solution was stirred at room temperature for 2 hr and then concentrated under reduced pressure. The residue was purified on silica gel by eluting with methanol:dichloromethane (1:19) to produce, after concentration, PE (**1**) (0.38 g, 90%) as a white solid: m.p.141-143° (Lit.141° [11]); IR 3419, 2963, 2798, 1593, 1462, 1274, 1083, 879 cm⁻¹; ¹H-NMR δ 9.56 (s, 1H), 8.99 (br, 1H), 7.15 (t, *J* = 7.8 Hz, 1H), 6.81 (br, 1H), 6.78 (d, *J* = 7.7 Hz, 1H), 6.70 (d, *J* = 8.0 Hz, 1H), 6.11 (s, 1H), 4.83 (d, *J* = 8.3 Hz, 1H), 3.05 (d, *J* = 12.5 Hz, 1H), 2.11 (t, *J* = 12.4 Hz, 1H), 2.53 (s, 3H); ¹³C-NMR δ 157.99, 143.71, 129.78, 116.74, 115.12, 113.22, 68.49, 55.37, 33.14; HRMS calculated for C₉H₁₄NO₂ [M+H]⁺ 168.0980, found 168.1019.

Via bromohydrin compound 6

A solution of bromohydrin **6** (0.53 g, 1.60 mmol) in dry methanol (5 mL) was processed under the same procedure as above to produce **1** (0.29 g, 85%).

ACKNOWLEDGEMENTS

We thank the Development and Promotion of Science and Technology Talents Project (DPST), the Graduate School and the Department of Chemistry, Chiang Mai University for their financial support.

REFERENCES

1. H. J. Roth, A. Kleemann and T. Beisswenger, "Pharmaceutical Chemistry, Volume 1: Drug Synthesis", Halstead Press/Ellis Horwood Ltd., Chischester, **1988**, p. 44.
2. D. Reynolds, "Federal legislation leads to new drugs", **2007**, <http://www.dnronline.com/> (Accessed: February 2007).
3. H. Legerlotz, "Optically active monohydroxyphenylalkylamines", *German Patent DE 543529* (**1929**).
4. H. Legerlotz, "Monohydric amino alcohols and their derivatives", *German Patent DE 566578* (**1932**).
5. H. Legerlotz, "Optically active amino alcohols", *German Patent DE 585164* (**1933**).
6. F. D. Klingler, "Asymmetric hydrogenation of prochiral amino ketones to amino alcohols for pharmaceutical use", *Acc. Chem. Res.*, **2007**, *40*, 1367-1376.
7. E. D. Bergamann and M. Sulzbacher, "A new synthesis of 1-(*m*- and *p*-hydroxyphenyl)-2-methylaminoethanol (*m*- and *p*-sympathol)", *J. Org. Chem.*, **1951**, *16*, 84-89.
8. P. B. Russel and S. J. Childress, "New route to phenylephrine", *J. Pharm. Sci.*, **1961**, *50*, 713-714.
9. H. Takeda, T. Tachinami and M. Aburatuni, "Practical Asymmetric synthesis of (*R*)-(-)-phenylephrine hydrochloride catalyzed by (2*R*, 4*R*)-MCCPM-rhodium complex", *Tett. Lett.*, **1989**, *30*, 367-370.

10. J. F. McGarrity and A. Zanotti-Gerosa, “A feasibility study on the synthesis of phenylephrine via ruthenium-catalyzed homogeneous asymmetric hydrogenation”, *Tetrahedron Asym.*, **2010**, 21, 2479-2486.
11. M. K. Gurjar, L. M. Krishna, B. V. N. B. S. Sarma and M. S. Chorghade, “A practical synthesis of (*R*)-(-)-phenylephrine hydrochloride”, *Org. Process Res. Develop.*, **1998**, 2, 422-424.
12. R. K. Pandey, P. K. Upadhyay and P. Kumar, “Enantioselective synthesis of (*R*)-phenylephrine hydrochloride”, *Tetrahedron Lett.*, **2003**, 44, 6245-6246.

© 2014 by Maejo University, San Sai, Chiang Mai, 50290 Thailand. Reproduction is permitted for noncommercial purposes.

Full Paper

Wave run-up on sandbag slopes

Thamnoon Rasmeemasuang^{1,*}, Wanich Chuenjai¹ and Winyu Rattanapitikon²

¹ Department of Civil Engineering, Burapha University, Chonburi, Thailand

² Sirindhorn International Institute of Technology, Thammasat University, Pathumthani, Thailand

* Corresponding author, e-mail: thamnoon@buu.ac.th

Received: 15 April 2013 / Accepted: 12 March 2014 / Published: 17 March 2014

Abstract: On occasions, sandbag revetments are temporarily applied to armour sandy beaches from erosion. Nevertheless, an empirical formula to determine the wave run-up height on sandbag slopes has not been available heretofore. In this study a wave run-up formula which considers the roughness of slope surfaces is proposed for the case of sandbag slopes. A series of laboratory experiments on the wave run-up on smooth slopes and sandbag slopes were conducted in a regular-wave flume, leading to the finding of empirical parameters for the formula. The proposed empirical formula is applicable to wave steepness ranging from 0.01 to 0.14 and to the thickness of placed sandbags relative to the wave height ranging from 0.17 to 3.0. The study shows that the wave run-up height computed by the formula for the sandbag slopes is 26-40% lower than that computed by the formula for the smooth slopes.

Keywords: wave run-up, coastal protection, sandbag revetment, wave steepness, surf similarity parameter

INTRODUCTION

As ocean waves approach a coast, the majority of wave energy is dissipated across the surf zone by wave breaking. However, a portion of that energy is converted to potential energy in the form of run-up on the foreshore of the beach [1]. The wave run-up (R) is the vertical distance from the still water level to the maximum level of wave uprush on beaches or coastal structures such as breakwaters or seawalls [2], as depicted in Figure 1. The wave run-up is one of the most important parameters for many coastal engineering works. It is one of the factors in determining the height of the coastal structures [3] and is the upper extent of coastal sediment transport, which is very significant for coastal geo-morphological processes, i.e. coastal erosion and accretion [4]. Moreover, the run-up defines the inundated area due to storm surges or tsunamis. An accurate

prediction of the wave run-up is therefore necessary for effective coastal zone management and coastal disaster warning [5].

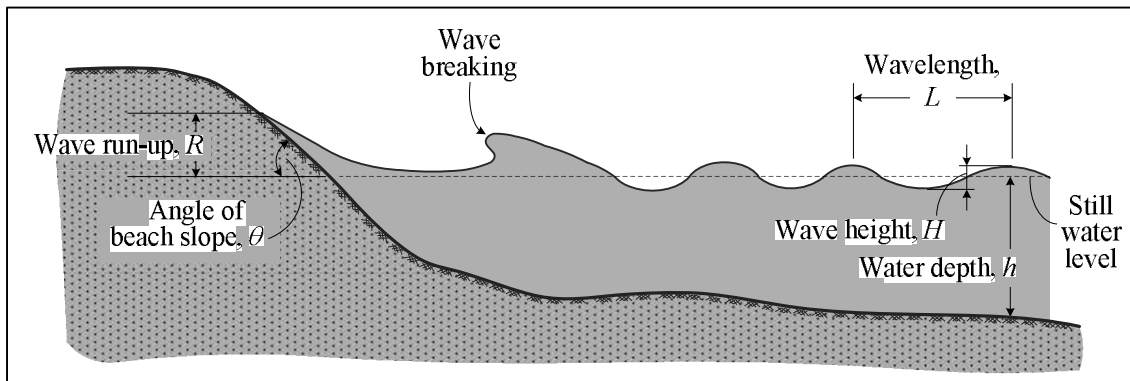


Figure 1. Definition of wave run-up

Previous studies on the wave run-up over sloping structures were mainly performed in laboratories. Hunt [1] carried out experiments on regular wave run-up on impervious, smooth slopes and proposed an empirical formula for predicting wave run-up height. Based on the experimental results, it was found that the wave run-up height normalised by deepwater wave height (R / H_o) is a function of the deepwater surf similarity parameter (ξ_o). Battjes and Roos [6] conducted similar laboratory experiments and obtained the results consistent with Hunt's. Besides studies of the regular waves, there were several studies of irregular waves. For instance, Ahrens [7] developed a method to estimate irregular wave run-up on smooth slopes based on results of several laboratory studies. Polynomial equations involving wave steepness were presented for computing representative wave run-up heights. Mase [3] performed an extensive series of laboratory tests on random wave run-up on smooth, gentle slopes and empirically determined a formula for predicting representative run-up heights. The formula was proposed as a power function of surf similarity.

In addition to the studies on wave run-up on smooth inclined planes, the behaviour of wave run-up on non-smooth slopes was also investigated. Van der Meer and Stam [8] conducted experiments on random wave run-up on rock slopes ranging from 1:1.15 to 1:4. There were four tested cross sections varying in thicknesses of the armour layer and the filter layer. Two relationships between relative wave run-up and surf similarity parameter were proposed. For a small surf similarity parameter (smaller than about 1.5), a linear relationship was taken, whereas for a larger surf similarity parameter (larger than about 1.5), the relationship was described simply by a power function, which resembles Mase's form [3]. Shankar and Jayaratne [9] carried out a series of hydraulic model tests to investigate the influences of roughness, layer thickness and porosity on the wave run-up on impermeable and permeable breakwaters. The surfaces of the breakwater models were made rough with gravels and welded wire meshes. Neelamani and Sandhya [10] investigated the wave run-up on plane, dentate and serrated seawalls that were fabricated using aluminum boxes zigzaggedly fixed on steel sheets. It was found that the sloping serrated seawall was capable of dissipating the wave energy better than the plane and dentate seawalls.

Apart from the smooth and non-smooth sloping structures mentioned above, sandbag revetments are occasionally found as a temporary measure to protect the coast from erosion. They are placed, as shown in Figure 2, on an existing slope, embankment or sea dike to protect the land from waves and strong currents [2]. One of the advantages of sandbag revetment is that, unlike rock

revetment, it still provides an easy access way for people to walk across to the beach and the sea. During the past decades, a few studies (e.g. [11-13]) were performed on the application of sandbags. However, they are largely related to typical aspects in terms of structural design and construction. Studies on wave run-up on sandbag slopes have been very limited. Kobayashi and Jacobs [11] adopted an empirical formula of Ahrens and McCartney [14] for predicting wave run-up on sandbag slopes. Only the surf similarity parameter with two empirical coefficients is used in the formula, and it may not be applicable for general cases because the thickness of sandbags is not taken into account in the formula. Heretofore, there have been no formulas accounting for the effect of sandbag thickness on the wave run-up.



Figure 2. Example of sandbag revetment at northern Pattaya beach, Chonburi province (photo taken on February 7, 2013)

The objective of the present study is to develop an empirical formula, in which the roughness of the slope surface is taken into account, for the wave run-up on sandbag slopes. The empirical parameters in the formula are obtained from the results of laboratory experiments on wave run-up on smooth slopes and sandbag slopes conducted in a wave flume. The accuracy of the formula is also discussed.

EXPERIMENTAL SET-UP

Experiments on wave run-up on sloping structures were conducted in a wave flume of 600 mm (width) \times 800 mm (depth) \times 16 m (length) as shown in Figure 3. The water depth was 350 mm uniformly throughout the test. Waves were generated by a regular wave generator capable of generating waves with steepness ranging from 0.01 to 0.14. A wave absorber was installed behind the wave generator to dissipate the waves at the backside of the flap plate. The assumption that the wave frequency corresponds to the frequency of the wave generator was applied in the study, although reflected waves might still occur in spite of the wave absorber, and the actual wave frequency (or period) might differ slightly from the frequency (or period) of the wave generator. The wave height and wave run-up were measured with two point gauges.

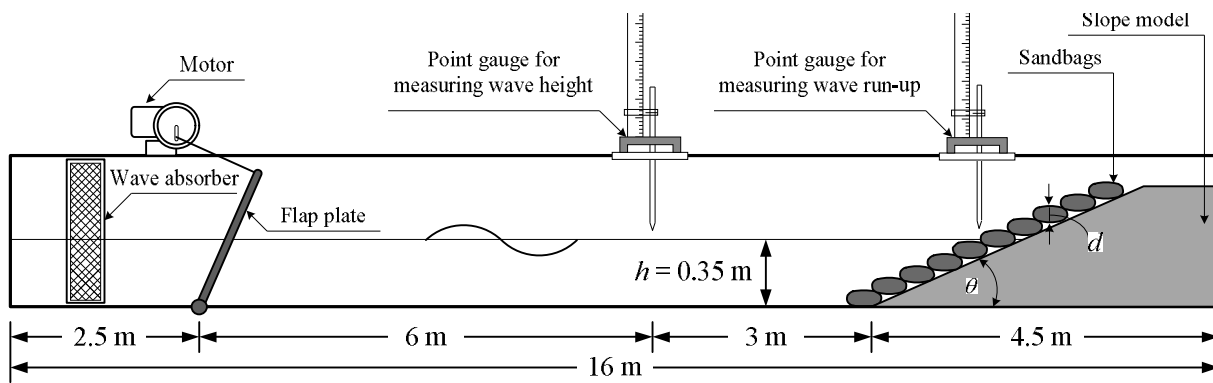


Figure 3. Experimental set-up (wave flume)

Two types of slope surface, i.e. smooth surface and sandbag surface, were used in the study. The smooth-surfaced slope was built with a 2.55-m-long stainless steel plate, whilst for the sandbag surface, linen bags filled with sand were arranged on the slope model. In order to study the effects of thickness of the placed sandbags on wave run-up, bags with five different widths (50, 75, 100, 125 and 150 mm) were used. The heights of the placed sandbags corresponding to their widths were 22.5, 28.5, 44.0, 52.5 and 61.0 mm respectively. The slope angles were 15°, 17.5°, 20°, 22.5° and 25°. All experimental conditions are summarised in Table 1.

Table 1. Experimental conditions

Parameter	Smooth slope	Sandbag slope
Water depth, h (mm)	350	
Frequency of wave generation (Hz)	0.83, 1.00, 1.17, 1.33, 1.50, 1.67	
Corresponding wave period, T (s)	1.20, 1.00, 0.86, 0.75, 0.67, 0.60	
Stroke of crank disk (mm)	80, 100, 120, 140, 160, 180, 200	
Wave height at the toe of the structure, H (mm)	20–140	
Wave steepness, H/L	0.01–0.14	
Slope angle, θ	15°, 17.5°, 20°, 22.5°, 25°	
Thickness of the placed sandbag, d (mm)	-	22.5, 28.5, 44, 52.5, 61
Number of test cases	210	1,050

When a wave generator generates waves propagating to and on the beach, the beach will cause wave reflection. The reflected waves will propagate back to the generator and reflect back at the generator. These reflections may cause a complex wave pattern in front of the beach and consequently may cause an incident wave to significantly differ from a target one. Three operations were performed to reduce the effect of the reflections:

- 1) A burst of a small number of waves was generated and the generator stopped between bursts to allow the reflected waves to die down. The wave height in each case was measured after the initial unsteady wave transients had died down. The measurements

were performed for about 5 minutes or prior to the changing of wave pattern due to the wave reflection. The wave height and wave run-up were measured ten times each. The values of wave height and wave run-up used in the analysis represent an average from each case.

- 2) The experiments were carried out under limited wave and beach conditions. As the wave reflection on a plane beach varies with the surf similarity parameter (ξ), the experiments were performed under small ξ (small slope and large wave steepness) conditions. From preliminary tests on plane beaches, it was found that the influence of wave reflection is significant when $\xi > 3$.
- 3) To avoid the occurrence of wave rundown and wave reflection in front of the slope, the incident wave height was measured at 3 m seaward from the toe of the slope, and the measurement was applied as the incident wave height at the toe of the slope.

FORMULA DEVELOPMENT

The measured run-up heights (R) acquired were used to develop a new run-up height formula. In total, 210 test cases for smooth slope conditions and 1,050 test cases for sandbag slope conditions were used in the development. Analysis and discussion of each condition are presented as follows.

Smooth Slope Conditions

According to the dimensional analysis [15], a wave run-up height R on a slope is expressed as:

$$\frac{R}{H} = f_1 \left(\frac{H}{L}, \tan \theta, \frac{h}{H}, \frac{d}{H}, \frac{\sqrt{K}}{H} \right) \quad (1)$$

where R is the wave run-up height, H is the wave height at the structure toe, L is the wavelength, $\tan \theta$ is the beach or structure slope, h is the water depth at the toe of the slope, d is the roughness height, and \sqrt{K} is the permeability of the structural material with the unit of square metre, which is related to the intrinsic permeability (k) with the unit of metre per second ($K = kv/g$, where ν is the kinematic viscosity of water and g is the acceleration of gravity).

For the wave run-up on smooth and impermeable slopes, the possible related parameters are H/L , $\tan \theta$ and h/H . As most of the existing formulas for computing R/H are proposed in terms of H/L and $\tan \theta$ (excluding h/H), the parameter H/L seems to be more significant than the term h/H . Moreover, Saville [16] found that the effect of h/H is negligible when h/H is larger than 3.0. In the present experiment the h/H values in most of the data are less than 3.0; therefore, the term h/H is not considered in this study. Thus, for a smooth and impermeable slope, Equation 1 becomes:

$$\frac{R}{H} = f_2 \left(\frac{H}{L}, \tan \theta \right) \quad (2)$$

Based on some existing formulas (e.g. the formulas of Hunt [1] and Mase [3]), a common parameter that is usually used to describe R on a smooth slope is the surf similarity parameter. Therefore, the function in Equation 2 can be simplified as:

$$\frac{R}{H} = f_3\left(\frac{\tan\theta}{\sqrt{H/L}}\right) = f_3(\xi) \quad (3)$$

where $\xi = \tan\theta/\sqrt{H/L}$ is the surf similarity parameter or the Iribarren Number [17]. In this study the wave length (L) was calculated based on the small amplitude wave theory.

Only the measured data of the wave run-up on smooth slopes are used in this case. The experiments cover a range of wave steepness from 0.01 to 0.14 ($0.01 \leq H/L \leq 0.14$) and slope angle from 15° to 25° ($15^\circ \leq \theta \leq 25^\circ$). The relationship between the measured R/H and ξ (in the log-log scale) is shown in Figure 4, which shows that the relationship can be fitted with a power function which is a straight line on a logarithmic graph. The equation of the fitted line can be written in a general form as:

$$\frac{R}{H} = a\xi^b \quad (4)$$

where a and b are the coefficients. From the regression analysis of $\log(R/H)$ and $\log(\xi)$, the values of a and b are 0.98 and 0.94 respectively. The best-fitted line is shown as the solid line in Figure 4. Thus, the formula for wave run-up on a smooth, impermeable slope is expressed as:

$$\frac{R}{H} = 0.98\xi^{0.94} \quad (5)$$

Figure 5 shows a comparison of observed and calculated relative run-up heights. Both the measured and the calculated values agree well, with a correlation coefficient (C.C.) of 0.90 between both values and a standard deviation (S.D.) of 0.51. It is obviously seen that the deviation increases as the relative run-up height increases. In the tests the relative run-up height was larger (e.g. $R/H > 2.0$) as the wave steepness got smaller (e.g. $H/L < 0.03$) and the surf similarity parameter got larger (e.g. $\xi > 2.5$). In a similar manner, the scatter of the prediction and the observation under the condition of small wave steepness and high surf similarity parameter is also found in other studies (e.g. [3, 7, 8]).

An attempt was made to relate R with the deep-water wave parameters (i.e. R/H_o versus ξ_o), as in the formula of Hunt [1]. The result is $R/H_o = 0.94\xi_o$, which is very close to the formula of Hunt (i.e. $R/H_o = \xi_o$). However, this formula is not used in this study because it gives less accuracy than that of Equation 5.

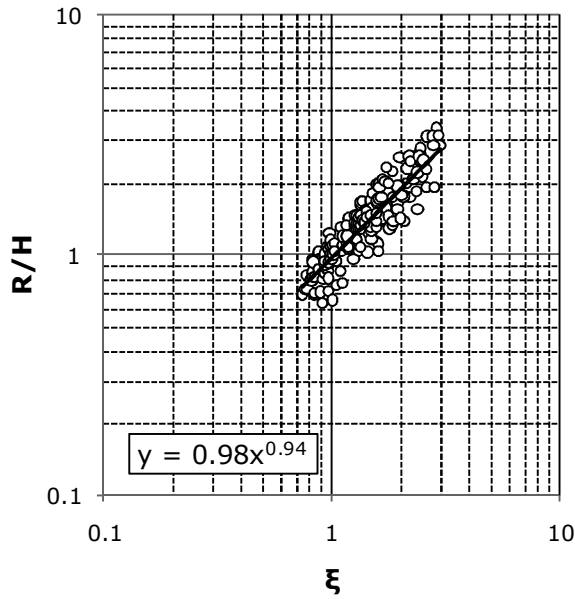


Figure 4. Relationship between relative run-up height (R/H) and surf similarity parameter (ξ) for the case of smooth slopes

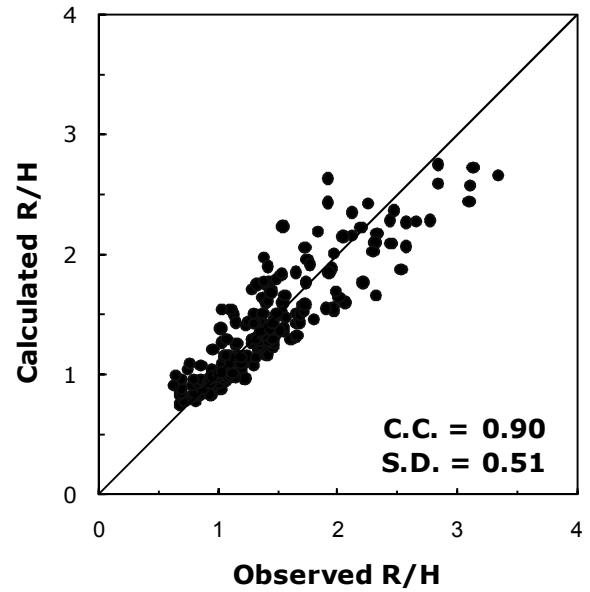


Figure 5. Comparison of observations and predictions of relative run-up height for the case of smooth slopes

Sandbag Slope Conditions

For wave run-up on sandbags, the possible related parameters are H/L , $\tan \theta$, d/H and $\sqrt{K/H}$. The effect of structure permeability is usually introduced when the barrier is rock or concrete units. However, sandbags (used in the present study) are also used as barrier in flood control. This means that the permeability of sandbags should be very small. Therefore, the effect of $\sqrt{K/H}$ is not considered in this study. A wave run-up formula considering the roughness height was proposed as Equation 6:

$$\frac{R}{H} = a_1 \xi^b \left[1 - a_2 \left(\frac{d}{H} \right)^c \right] \tag{6}$$

where a_1 and b are parameters from the case of the aforementioned smooth slopes, and are equal to 0.98 and 0.94 respectively, while a_2 and c are empirical parameters for the term of relative roughness height (d/H). In this study the heights of the placed sandbags shown in Table 1 are applied for the roughness height (d). It is noted that Equation 6 can be applied for the case of smooth slopes as well by putting the value of d as zero. (Then Equation 6 will revert to Equation 5.)

Equation 6 can be rearranged as:

$$1 - \frac{R/H}{a_1 \xi^b} = \Psi = a_2 \left(\frac{d}{H} \right)^c \tag{7}$$

The measured data on the wave run-up on sandbag slopes are used in this case. The experiments covered a range of wave steepness from 0.01 to 0.14 ($0.01 \leq H/L \leq 0.14$), slope angle from 15° to 25° ($15^\circ \leq \theta \leq 25^\circ$), and relative roughness height from 0.17 to 3.0 ($0.17 \leq d/H \leq 3.0$). To find out the values of the empirical parameters (a_2 and c), the relationship between the measured Ψ and

d/H is plotted (Figure 6), and then the values of a_2 and c are determined by the least square method. Thus, the formula for the wave run-up height on sandbag slopes in this study becomes:

$$\frac{R}{H} = 0.98\xi^{0.94} \left[1 - 0.34 \left(\frac{d}{H} \right)^{0.15} \right] \quad (8)$$

From the experimental results, it is obvious that the roughness of the slope face influences the height of wave run-up. On sandbag slopes, the wave run-up values are lower than those on the smooth slopes. Furthermore, at the same beach slope, the value decreases as the thickness of the placed sandbags increases. It is evident that the energy of the wave rushing up the slope is dissipated proportionately as the roughness height of the slope increases.

Figure 7 shows a comparison of the observed relative run-up values and those calculated by Equation 8. The calculated results agree well with the observed values, with a correlation coefficient of 0.86 between both values and a standard deviation of 0.35. From the experimental results, the term $\left[1 - 0.34(d/H)^{0.15} \right]$ ranges from 0.60 to 0.74, which can be interpreted that the relative run-up height calculated by Equation 8 is 26-40% smaller than that calculated by Equation 5.

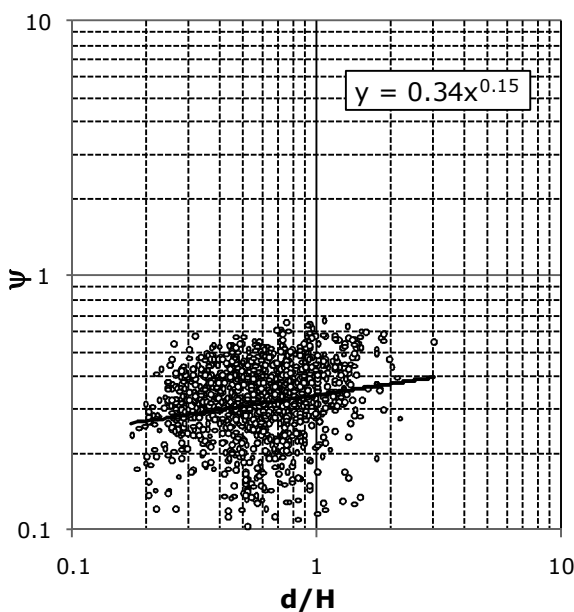


Figure 6. Relationship between relative roughness height (d/H) and value of Ψ in Equation 7 for the case of sandbag slopes

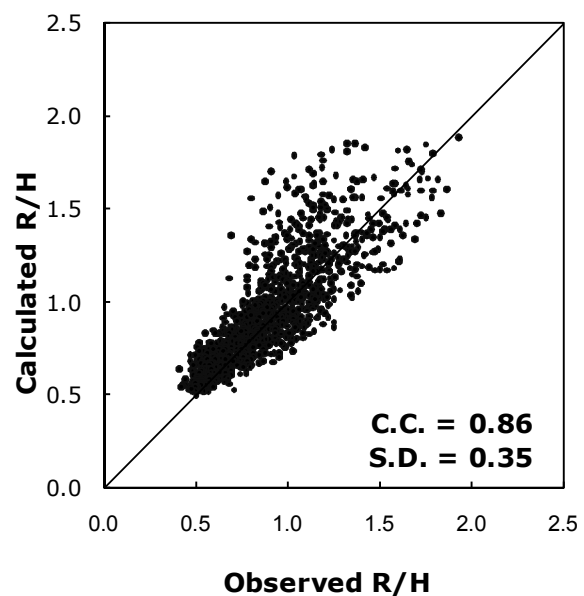


Figure 7. Comparison of observed and predicted relative run-up heights for the case of sandbag slopes

Figure 8 shows a comparison of the surf similarity (ξ) and relative wave run-up computed by Equation 8. From Figure 8, at the same ξ the wave run-up heights on sandbag slopes are considerably lower than those on smooth slopes. The roughness of the slope surfaces enhances friction that resists the onrush of water, with consequent decrease in the wave run-up. For the case of sandbag slopes, the wave run-up heights are about 26% and 40% lower for $d/H = 0.3$ and 3.0 respectively than those on smooth slopes. Therefore, in the design of sandbag revetments the wave run-up formula that considers the roughness (thickness of placed sandbags) would be more accurate

in determining the height of the structures. Accordingly, the economy of construction materials would be achieved.

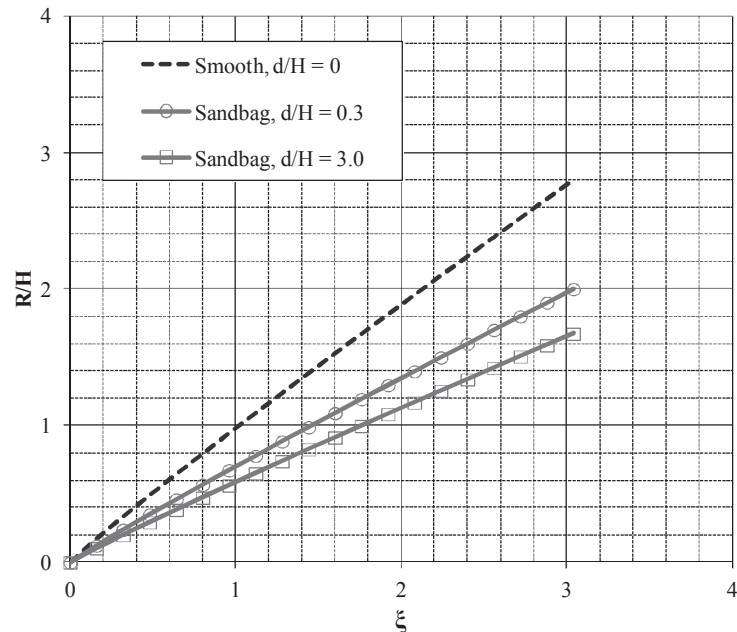


Figure 8. Relationship between surf similarity parameter (ξ) and relative wave run-up (R/H) computed by Equation 8

CONCLUSIONS

Studies on wave run-up on sandbag slopes have been very limited. There has been no formula accounting for the effect of sandbag thickness on wave run-up. This study develops an empirical formula in which the roughness of slope surfaces is taken into account for wave run-up on sandbag slopes. The development of the formula consists of two stages. Firstly, the measured experimental data of wave run-up on smooth slopes were analysed to identify a basic form of the wave run-up. After that, based on the measured data of the run-up on sandbag slopes, the term of the roughness effect was derived and included into the basic formula, which gives good agreement with the measured data. The proposed empirical formula is applicable to the wave steepness ranging from 0.01 to 0.14 and the thickness of placed sandbags relative to the wave height ranging from 0.17 to 3.0.

ACKNOWLEDGEMENTS

This research was supported by the Faculty of Engineering, Burapha University (Contract no. 12/2555).

REFERENCES

1. I. A. Hunt, Jr., "Design of seawalls and breakwaters", *J. Waterways Harbors Div.*, **1959**, 85, 123-152.
2. U.S. Army Corps of Engineers, "Coastal Engineering Manual", U.S. Army Engineer Research and Development Center, Washington, D.C., **2002**, Part II, Chapter 4.
3. H. Mase, "Random wave run-up height on gentle slope", *J. Waterway Port Coastal Ocean Eng.*, **1989**, 115, 649-661.

4. J. P. Ahrens and W. N. Seelig, "Wave runup on beaches", Proceedings of 25th Coastal Engineering Conference, **1996**, Orlando (FL), USA, pp.981-993.
5. S. J. Na, K. D. Do and K. D. Suh, "Forecast of wave run-up on coastal structure using offshore wave forecast data", *Coastal Eng.*, **2011**, 58, 739-748.
6. J. A. Battjes and A. Roos, "Characteristics of flow in run-up of periodic waves", Report No. 75-3 (Ch. 45), Faculty of Engineering and Geosciences, Delft University of Technology, Delft (Netherlands), **1975**.
7. J. P. Ahrens, "Irregular Wave Run-up on Smooth Slopes", U.S. Army Coastal Engineering Research Center, Springfield (VA), **1981**.
8. J. W. van der Meer and C. J. M. Stam, "Wave runup on smooth and rock slopes of coastal structures", *J. Waterway Port Coastal Ocean Eng.*, **1992**, 118, 534-550.
9. N. J. Shankar and M. P. R. Jayaratne, "Wave run-up and overtopping on smooth and rough slopes of coastal structures", *Ocean Eng.*, **2003**, 30, 221-238.
10. S. Neelamani and N. Sandhya, "Wave reflection, run-up, run-down and pressures on plane, dentated and serrated seawalls", *Coastal Eng. J.*, **2004**, 46, 141-170.
11. N. Kobayashi and B. K. Jacobs, "Stability of armor units on composite slopes", *J. Waterway Port Coastal Ocean Eng.*, **1985**, 111, 880-894.
12. P. E. Gadd, "Sandbag slope protection: Design, construction, and performance", in "Arctic Coastal Processes and Slope Protection Design" (Ed. A. C. T. Chen and C. B. Leidersdorf), American Society of Civil Engineers, New York, **1988**, pp.145-165.
13. W. P. Hornsey, J. T. Carley, I. R. Coghlan and R. J. Cox, "Geotextile sand container shoreline protection systems: Design and application", *Geotextil. Geomembr.*, **2011**, 29, 425-439.
14. J. P. Ahrens and B. L. McCartney, "Wave period effect on the stability of riprap", Proceedings of Conference on Civil Engineering in the Oceans/III, Vol. 2, **1975**, Newark (DE), USA, pp.1019-1034.
15. Y. Tsuchiya, Y. Kawata and T. Yashita, "Effects of roughness and permeability on wave run-up", Proceedings of 25th Japanese Conference on Coastal Engineering, **1978**, Yokohama, Japan, pp.160-164 (in Japanese).
16. T. Saville, Jr., "Wave run-up on shore structures", *J. Waterways Harbors Div.*, **1956**, 82, 1-14.
17. J. A. Battjes, "Surf similarity", Proceedings of 14th Coastal Engineering Conference, **1974**, Copenhagen, Denmark, pp.466-480.

© 2014 by Maejo University, San Sai, Chiang Mai, 50290 Thailand. Reproduction is permitted for noncommercial purposes.

Maejo International Journal of Science and Technology

ISSN 1905-7873

Available online at www.mijst.mju.ac.th

Full Paper

An adaptive radial basis function neural network (RBFNN) control of energy storage system for output tracking of a permanent magnet wind generator

Abu H. M. A. Rahim

Department of Electrical Engineering, King Fahd University of Petroleum and Minerals, Dhahran, Saudi Arabia

Email: ahrahim@kfupm.edu.sa

Received: 10 April 2013 / Accepted: 18 March 2014 / Published: 24 March 2014

Abstract: The converters of a permanent magnet synchronous generator have to be properly controlled to achieve maximum transfer of energy from wind. To achieve this goal, this article employs an energy storage device consisting of an energy capacitor interfaced through a voltage source converter which is operated through a smart adaptive radial basis function neural network (RBFNN) controller. The proposed adaptive strategy employs online neural network training as opposed to conventional procedure requiring offline training of a large data-set. The RBFNN controller was tested for various contingencies in the wind generator system. The adaptive online controller is observed to provide excellent damping profile following low grid voltage conditions as well as for other large disturbances. The controlled converter DC capacitor voltage helps maintain a smooth flow of real and reactive power in the system.

Keywords: adaptive control, energy storage control, radial basis function neural network, permanent magnet synchronous generator, wind turbine

INTRODUCTION

Variable-speed wind turbines based on permanent magnet synchronous generator (PMSG) are found to be attractive in large wind farms because of their advantages in terms of high efficiency of energy production, simple structure, low maintenance, etc. The full-rated converter in the PMSG separates the synchronous generator from the grid, and hence helps easy fault ride-through [1, 2]. However, with increased wind penetration and random wind speed fluctuations, the change in output

power can cause grid frequency variations [3]. Maintenance of DC link voltage in the converter system within precise limits is essential for maximum power transfer [4].

Control of the converters of a PMSG for frequency and voltage control has been widely reported in the literature. Two configurations have been considered: the generator-side converter working like a rectifier with the grid-side converter having fully controllable pulse-width-modulated (PWM) system, and the other having full PWM control of both generator-side and grid-side converters [5, 6]. Control of the generator-side converter for maximum power transfer was employed by Rim *et al.* [4], while Haque *et al.* [1] and Muyeen *et al.* [7] used grid-side converters for this purpose. Generator-side and grid-side converters for maximum power transfer and reactive control respectively were reported by Singh *et al.* [8]. Energy storage devices, along with flexible AC transmission system (FACTS), can supply both real (P) and reactive (Q) power and hence can make the converters operate at or near unity power factor. Sharma and Singh [9] and Bhende *et al.* [10] used battery energy storage, along with static compensator (STATCOM), for voltage and frequency control of a PMSG system. A simple proportional-integral-derivative (PID) controller in a STATCOM was shown to improve the stability of a permanent magnet wind generator [11]. Uehere *et al.* [3], Bhende *et al.* [10] and Conroy and Watson [12] demonstrated that coordinated converter control, pitch control, braking resistor and dump load can improve the wind system performance.

With the advancement in intelligent techniques, different families of neural networks have seen a recent rise in application to wind energy control under differing schemes. The use of artificial neural networks for rotor position estimation of a PMSG generator was reported by Batzel and Lee [13]. Lopes [14] employed neural networks for dynamic security assessment of a power system with wind in-feed. Pitch control of a PMSG system was reported using sliding mode control and neural network [15]. Neural network methods employing both back-propagation and radial basis function networks generally depend on training the network with a large set of input-output data. These networks may not perform well under randomly varying wind speed conditions or for the arbitrary nature of disturbances which they are not trained for. For control design, the neural network weights should be computed and updated adaptively according to the system conditions.

This article proposes a novel adaptive radial basis function neural network (RBFNN) control strategy for a permanent magnet wind generator system. The capacitor energy storage system compensates for both real and reactive power requirements of the wind system following any contingency. The weights of the neural network are adapted online from the measurements of the generator outputs. Simulation studies indicate that the adaptive RBFNN control provides excellent damping characteristics even for severe short circuits at the grid bus.

NOMENCLATURE

V_w	Wind speed
β	Pitch angle
λ	Tip-speed ratio
$d-q$	Direct and quadrature axes
R_a	Stator resistance
x_d, x_q	d-q axes synchronous reactance
V_s	Generator stator voltage

V_t	Inverter terminal voltage
V_c, C	DC capacitor voltage and capacitance in the converter
V_{dc}, C_{st}	DC capacitor voltage and capacitance in the storage device
m_1, m_2	Modulation indices of converters
α_1, α_2	Phase angles of the converters
ω_b, ω	Base angular speed, rotor angular speed
H, D	Inertia constant and damping coefficient
H_g, H_t	Inertia constant of generator and turbine
K_s, θ_s	Stiffness constant, torsion angle
D_b, D_g	Damping coefficient of turbine and generator
V_{st}, I_{st}	Voltage and current of VSC in the storage device
R_{st}, L_{st}	Resistance and inductance of VSC
P_{mech}, P_{elec}	Mechanical power input, electrical power output
pu (p.u.)	Per unit

PMSG SYSTEM MODEL

The grid-connected permanent magnet generator system considered in this work is shown in Figure 1. Variable frequency voltage generated by the machine is rectified and inverted to grid frequency through fully controlled back-to-back converters located between the generator terminals and the transmission line. A local load and an energy storage unit are connected at the grid side of the inverter. The relationships between the stator voltage, current and flux, expressed in per unit system, are written as [16, 17]:

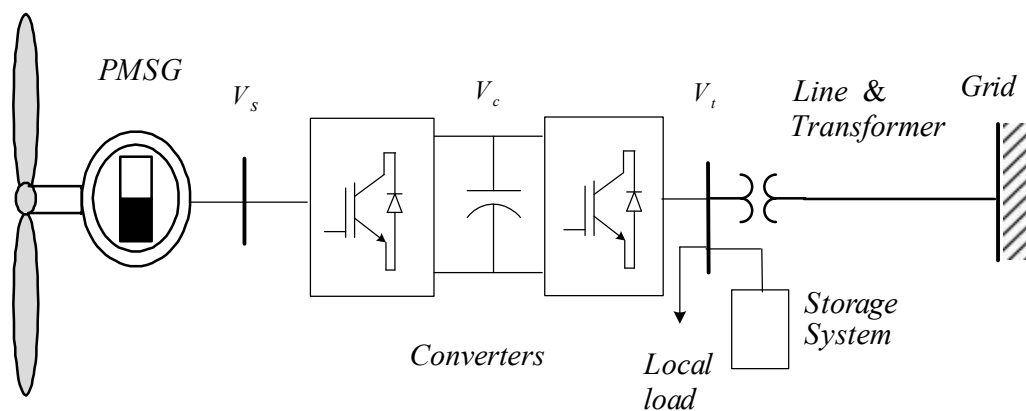


Figure 1. Permanent magnet synchronous generator connected to the grid bus

$$-R_a I_{sd} - \omega \psi_q + \frac{1}{\omega_o} \frac{d}{dt} (\psi_d) = V_{sd} \tag{1}$$

$$-R_a I_{sq} + \omega \psi_d + \frac{1}{\omega_o} \frac{d}{dt} (\psi_q) = V_{sq}$$

$$\psi_d = -x_d I_{sd} + \psi_{res} \tag{2}$$

$$\psi_q = -x_q I_{sq}$$

where V_s , I_s , and ψ are stator voltage, current and flux of the PMSG respectively; subscripts d and q represent direct and quadrature axes components of the quantities; R_a , x_d and x_q are stator resistance and synchronous reactances respectively; ψ_{res} is the flux from the permanent magnets; ω and ω_0 are generator angular frequency and base angular frequency respectively.

The electromechanical equations of motion of the generator and turbine rotor are written in terms of their respective angular speeds (ω , ω_t) as:

$$\begin{aligned} \dot{\omega} &= \frac{1}{2H_g} (K_s \theta_s - P_{elec} - D_g (\omega - 1)) \\ \dot{\omega}_t &= \frac{1}{2H_t} (P_{mech} - K_s \theta_s - D_t (\omega_t - 1)) \\ \dot{\theta}_s &= \omega_0 (\omega_t - \omega) \end{aligned} \tag{3}$$

where H and D are, respectively, inertia constants and damping coefficients of turbine and generator; K_s and θ_s represent, respectively, stiffness coefficient and torsion angle of the shaft connecting the two masses. The expressions for mechanical input power P_{mech} , which is the wind turbine output, and electrical power output P_{elec} are:

$$\begin{aligned} P_{mech} &= \frac{1}{2} \alpha A_b C_{pw} (\gamma, \beta) V_\omega^3 \\ P_{elec} &= \psi_{res} I_{sq} + (x_q - x_d) I_{sd} I_{sq} \end{aligned} \tag{4}$$

where α , A_b , C_{pw} , γ and β are density of air, turbine blade swept area, power coefficient, tip-speed ratio and turbine pitch angle respectively.

The normalised differential equation relating the inverter current (I_i) to the internal voltage (V_i) and terminal voltage (V_t) can be broken up in terms of d-q quantities as:

$$\begin{aligned} \frac{dI_{id}}{dt} &= \frac{\omega_0}{x_i} [V_{id} - V_{td} - R_i I_{id} + \omega x_i I_{iq}] \\ \frac{dI_{iq}}{dt} &= \frac{\omega_0}{x_i} [V_{iq} - V_{tq} - R_i I_{iq} - \omega x_i I_{id}] \end{aligned} \tag{5}$$

where subscripts d and q refer to direct and quadrature axes components of the inverter voltage and current; R_i and x_i are inverter resistance and reactance respectively. The generator stator voltage (V_s) and inverter internal voltage (V_i) are related to the DC capacitor voltage (V_c), converter and inverter modulation indices (m_1 , m_2) and phase angles (α_1 , α_2) through:

$$\begin{aligned} V_s &= m_1 V_c \angle \alpha_1 \\ V_i &= m_2 V_c \angle \alpha_2 \end{aligned} \tag{6}$$

The equation of the DC link capacitor located between the two converters is derived from the condition that the power supplied by the rectifier equals the power input to the inverter, and is expressed as:

$$\frac{dV_c}{dt} = \frac{1}{C} [m_1 I_{sd} \cos \alpha_1 + m_1 I_{sq} \sin \alpha_1 - m_2 I_{id} \cos \alpha_2 - m_2 I_{iq} \sin \alpha_2] \quad (7)$$

A full list of symbols is included in the nomenclature section.

ENERGY STORAGE CONTROLLER MODEL

The circuit configuration of the energy storage device is shown in Figure 2. It contains a storage capacitor which is interfaced to the wind generator system through a voltage source converter (VSC) and a buck-boost converter operated through switches S_1 and S_2 [18]. By controlling the delay angle of the switches in the converter, the direction of power flow can be reversed. The modulation index of the VSC allows control of the internal voltage given by the relation $V_{st} = mV_{dc} \angle \psi + \theta_m$. Here, θ_m is the angle of the inverter terminal voltage V_i at the point of connection of the storage device. A combination of modulation index and phase angle (m, ψ) control allows control of real and reactive power injection to the wind system. Applying Kirchhoff's voltage law, the dynamic relationship for d - q components of VSC output currents can be written as:

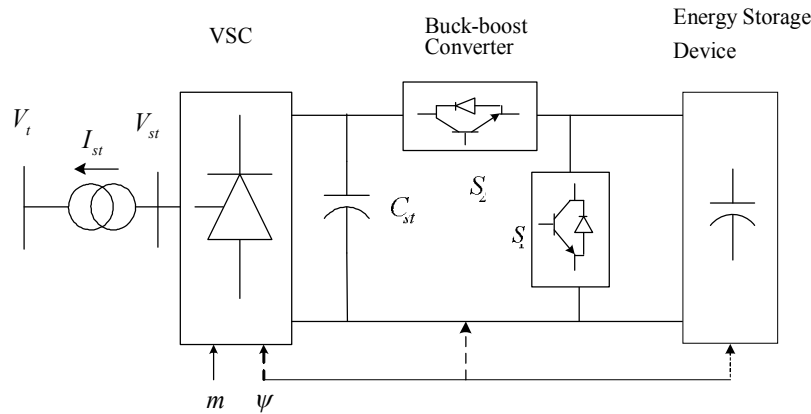


Figure 2. Capacitor energy storage control system

$$\begin{aligned} \frac{dI_{std}}{dt} &= \frac{\omega_0}{L_{st}} [-R_{st} i_{std} + \omega L_{st} I_{stq} + mV_{dc} \cos(\psi + \theta_m) - V_{td}] \\ \frac{dI_{stq}}{dt} &= \frac{\omega_0}{L_{st}} [-\omega L_{st} I_{std} + R_{st} I_{stq} + mV_{dc} \sin(\psi + \theta_m) - V_{tq}] \end{aligned} \quad (8)$$

where I_{std} and I_{stq} are, respectively, the direct and quadrature axes components of STATCOM current I_{st} ; V_{td} and V_{tq} are the d-q components respectively of terminal voltage V_i ; V_{dc} represents the voltage across the DC capacitor C_{st} ; R_{st} and L_{st} are the effective resistance and inductance of the VSC respectively. The voltage equation for DC link capacitor in the storage system, obtained by following the same procedure as in (8), is written as:

$$\frac{dV_{dc}}{dt} = \frac{-m}{C_{st}} [I_{std} \cos(\psi + \theta_m) + I_{stq} \sin(\psi + \theta_m)] + \frac{I_{ces}}{C_{st}} \quad (9)$$

The current from the storage capacitor (I_{ces}) is related to capacitance and its voltage (V_{ces}) by a simple relationship:

$$\frac{dV_{ces}}{dt} = \frac{I_{ces}}{C_{es}} \quad (10)$$

Combining the dynamic equations (1), (3), (5), (7), (8), (9) and (10), and eliminating the non-state variables through appropriate relationships, the composite state model for the PMSG system, along with the storage control device, is expressed as:

$$\begin{aligned} \dot{x} &= f[x, u] \\ y &= g[x, u] \end{aligned} \quad (11)$$

The control vector (u) is composed of m and ψ of the energy storage device and y represents the vector of chosen outputs.

ADAPTIVE RBFNN CONTROLLER

The main concept of the proposed control design is to maintain the wind generator output to pre-specified values following wind speed change, low voltage conditions or other arbitrary disturbances in the system. The controls in the storage system are activated by neural network controllers to compensate for P and Q imbalance in the wind system. In the usual neural network applications the offline training of large amounts of input-output data is required to generate a weighting matrix. These weights may not predict the output accurately in randomly or arbitrarily changing system conditions. For satisfactory control estimates, the training should be done online and the weight updates should be made as time progresses [19].

The configuration of the adaptive neural network controller proposed in this study is shown in Figure 3. The controller consists of a core radial basis function network (RBFN), an adaptation system for the RBFN and a proportional stabilising controller. The adaptation system consists of a linear estimate of the system matrices, an adaptation algorithm and a weight update policy. A proportional stabilising controller is incorporated in the strategy to ensure that the RBFN controller initialisation is stable while the weighting updates are initiated. Both the RBFN and the stabilising controller are activated by an error signal between the reference input (r) and the actual output (y). The output from the adapted neural network, along with the stabilising controller, is then fed to the wind generator system. As the training proceeds, the RBFN takes over the stabilising proportional controller [20, 21].

The structure of the RBFNN is shown in Figure 4. The neurons in the radial basis networks usually have three layers: the input, the hidden and the output layers. At any time, step k , the output of the hidden layer, can be expressed through [22]:

$$V(k) = W(k)^T \Psi(k) \quad (12)$$

where W is the weight matrix and Ψ is a set of basis functions, the j^{th} kernel of which is usually chosen to be the Gaussian function:

$$\psi_j(k) = \exp\left(-\|r(k) - c_j\|^2 / \sigma_j^2\right) \quad (13)$$

where c_j is the centre of the j^{th} neuron and σ_j represents the width of the layer.

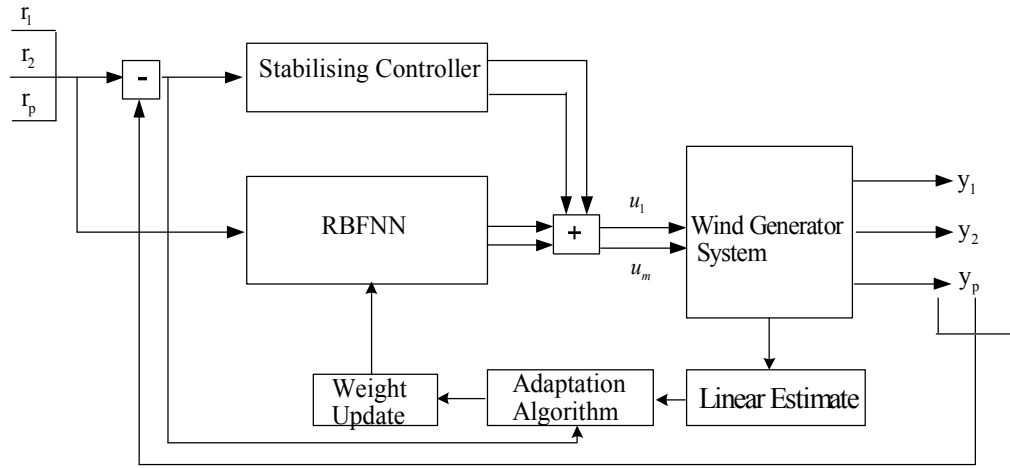


Figure 3. RBFN-based adaptive controller for wind generator system

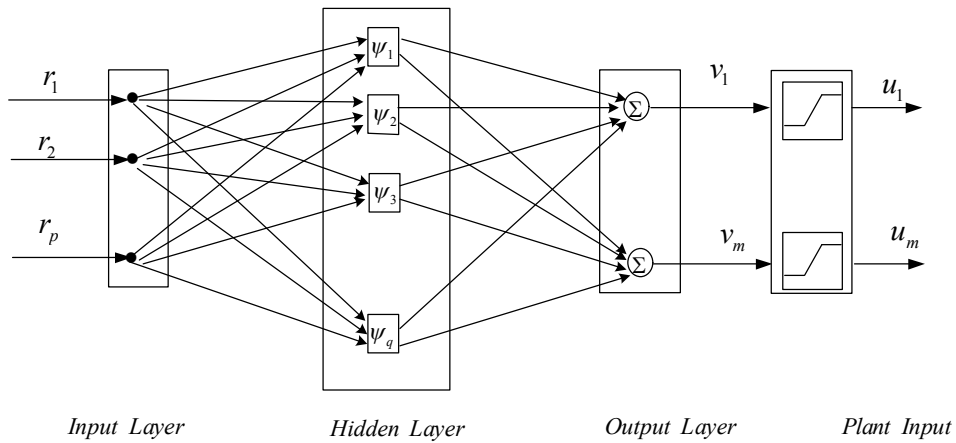


Figure 4. RBFNN structure

Considering the saturation to be a tangent sigmoid function, the j^{th} component of input (u) to the plant can be expressed as:

$$u_j(k) = \alpha_1 \frac{e^{\beta v_j(t)} - 1}{e^{\beta v_j(t)} + 1} = \alpha_1 \frac{e^{\beta w_j^T \phi(k)} - 1}{e^{\beta w_j^T \phi(k)} + 1} \quad (14)$$

Here $u_{max} = u_{min} = \alpha_1$, and β is slope of the sigmoid function. The error function (e) is defined as:

$$e(k) = r(k) - y(k) \quad (15)$$

The weighting matrix is obtained by minimising the mean square error (E), which is the product of the transpose of error (e^T) and error e at any time step k :

$$E = e^T(k) e(k) \quad (16)$$

The update law for the elements of the weighting matrix $W(k)$, using the gradient descent technique, is written as:

$$w_j(k+1) = w_j(k) - \eta \frac{\partial E}{\partial w_j} \quad (17)$$

After linearisation of the system of equations (11), its discrete form can be written in terms of A, B, C, D matrices as:

$$\begin{aligned} x(k+1) &= Ax(k) + Bu(k) \\ y(k) &= Cx(k) + Du(k) \end{aligned} \tag{18}$$

Substituting output y from (18) gives the expression for the gradient as:

$$\frac{\partial E}{\partial w_j} = -2e^T(k) \frac{\partial}{\partial w_j} [Cx(k) + Du(k)] \tag{19}$$

Using the chain rule and substituting the state equation from (18), it can be shown that:

$$\frac{\partial E}{\partial w_j} = -2e^T(k) \left[\frac{\partial CBu(k-1)}{\partial w_j} + \frac{\partial Du(k)}{\partial u_j} \right] \tag{20}$$

The recursive formula for the update of the weights is then:

$$\begin{aligned} w_j(k+1) &= w_j(k) + 2\eta \sum_{l=1}^p e_l(k) \\ &\left\{ \phi_{lj} \alpha_1 \frac{2\beta_1(k-1)e^{\beta_1 w_j^T(k-1)}}{(e^{\beta_1 w_j^T(k-1)} + 1)^2} + D_{lj} \alpha_1 \frac{2\beta_1(k)e^{\beta_1 w_j^T(k)}}{(e^{\beta_1 w_j^T(k)} + 1)^2} \right\} \end{aligned} \tag{21}$$

In the above equation, p is the number of output and ϕ_{lj} is the lj^{th} element of $(CB + \lambda_l)$ matrix. The quantity λ_l is selected so as to overcome zero entries of matrix CB at the start of the training process [23]. Quantity η is the learning rate of the radial basis function network. A step-by-step process is tabulated in Algorithm 1.

Algorithm 1. Adaptive RBFNN control algorithm

- Obtain a linear estimate of the PMSG model using offline identification or linearisation of the non-linear model.
 - Initialise stabilising controller with a gain small enough to ensure a stable initialisation.
 - Initialise RBFNN with random synaptic weights having small values.
 - Initialise a small learning rate η .
 - Select α depending upon the constraints required on the control inputs.
 - Based on (22), the weights are updated as the PMSG outputs are acquired at each sampling instance.
 - If the learning rate is small enough for the weights to converge, the PMSG outputs follow the reference trajectory.
-

TESTING THE CONTROLLER

The adaptive RBFNN controller design was implemented on the permanent magnet generator system considered in Figure 1. The control inputs are the modulation index and phase angles of the storage system converters, while the outputs to be tracked are the generator speed and terminal voltage. The generator is considered to be delivering 0.95 per unit (pu) power under steady condition at an average wind speed of 12 m/sec. The damping of the turbine-generator rotor is considered to be zero for a worst-case scenario. The system parameters are included in the

Appendix. Only those disturbances which give rise to oscillatory or unstable responses are reported in this article.

Figure 5 shows the synchronous generator speed variation when it is subjected to a 20% input torque pulse on the shaft for 300 milliseconds (ms). The torque unbalance gives an oscillatory response in the generator because of zero damping. Although the converter and DC capacitor system isolate the two synchronous systems, the generator and the grid, part of the large oscillations in the generator will get past the converters into the grid. From the response shown in the Figure, it can be seen that the adaptive online RBFN controller results in larger overshoots compared to the uncontrolled case at the beginning of the adaptive training process. This is due to near-zero initialisation of the RBF weights. As time progresses the network gets trained and the oscillations die out quickly.

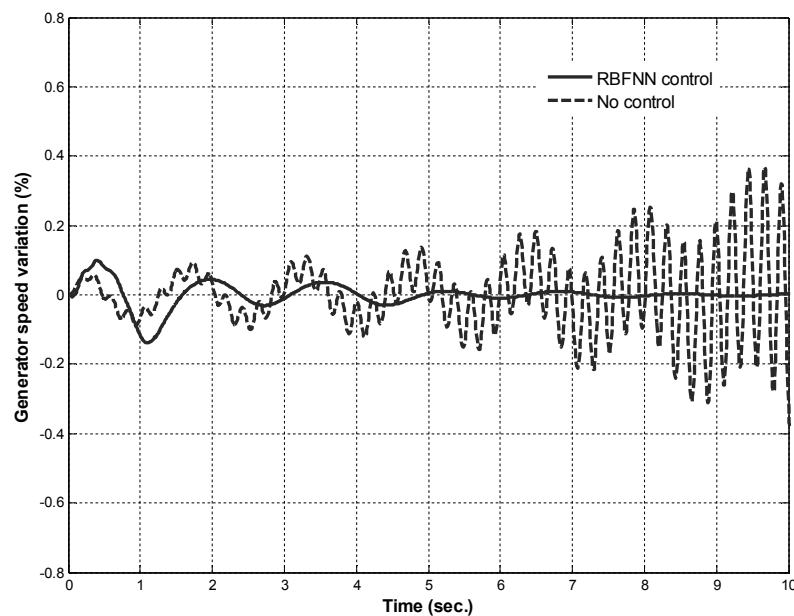


Figure 5. Speed variation of permanent magnet synchronous generator following a 20% input torque pulse for 300 ms with and without proposed RBFNN control

Figure 6 shows a comparison of the speed of the synchronous generator with the reference value when RBFNN control is applied. Figure 7 shows that the sum of squared error converges very fast. Figure 8 shows that in the early part of the transients, when the network has not been properly trained, the generator stator current momentarily increases by about 25%. However, it quickly returns to the normal level as the neural network gets trained. Maintenance of a constant level of the DC-link capacitor voltage is essential for maximising the power transfer through the converters. It can be observed from Figure 9 that the DC link voltage recovery is very fast with the adaptive neural network control. Variations of the control variables (m and ψ), given in Figure 10, show that the control effort falls to a reasonably smaller value quickly after a slightly large excursion at the start of the training process.

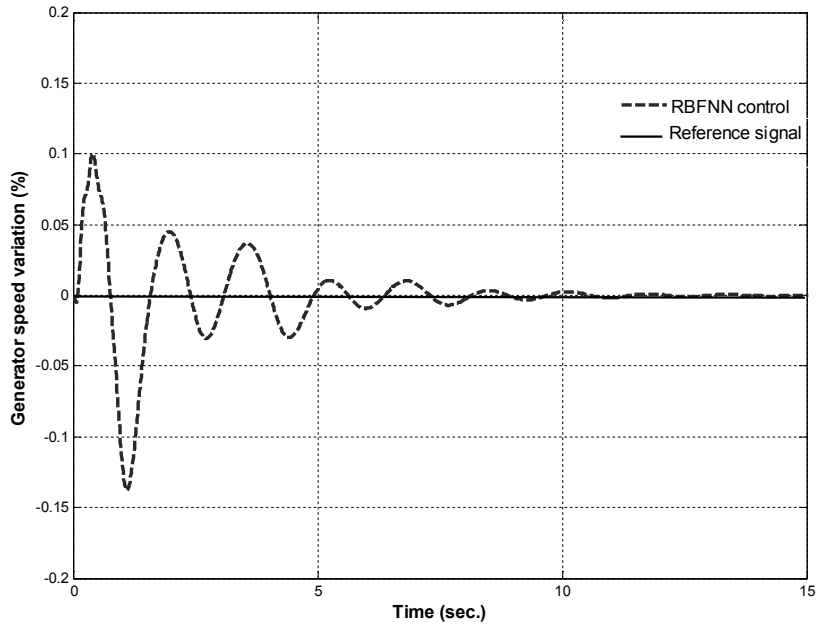


Figure 6. Variation of controlled generator speed from reference value

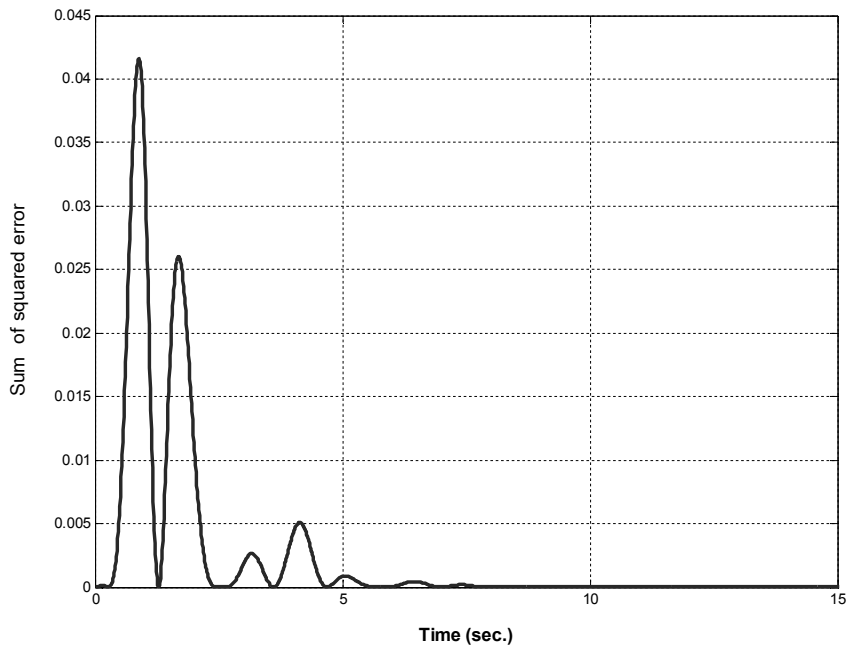


Figure 7. Sum of squared error for 20% input torque pulse

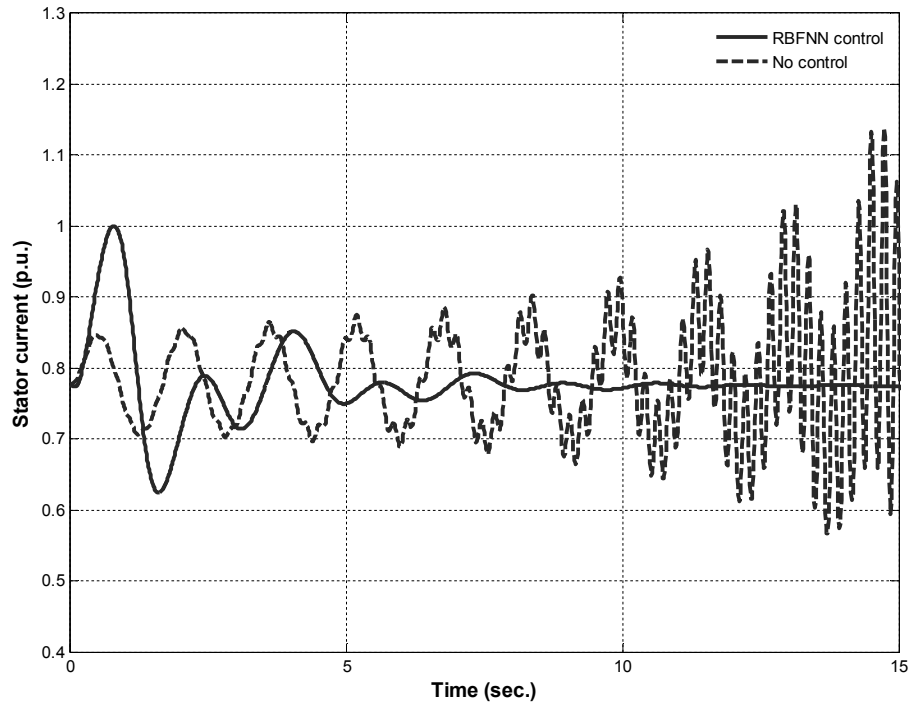


Figure 8. Generator stator current variation with and without adaptive RBFNN control

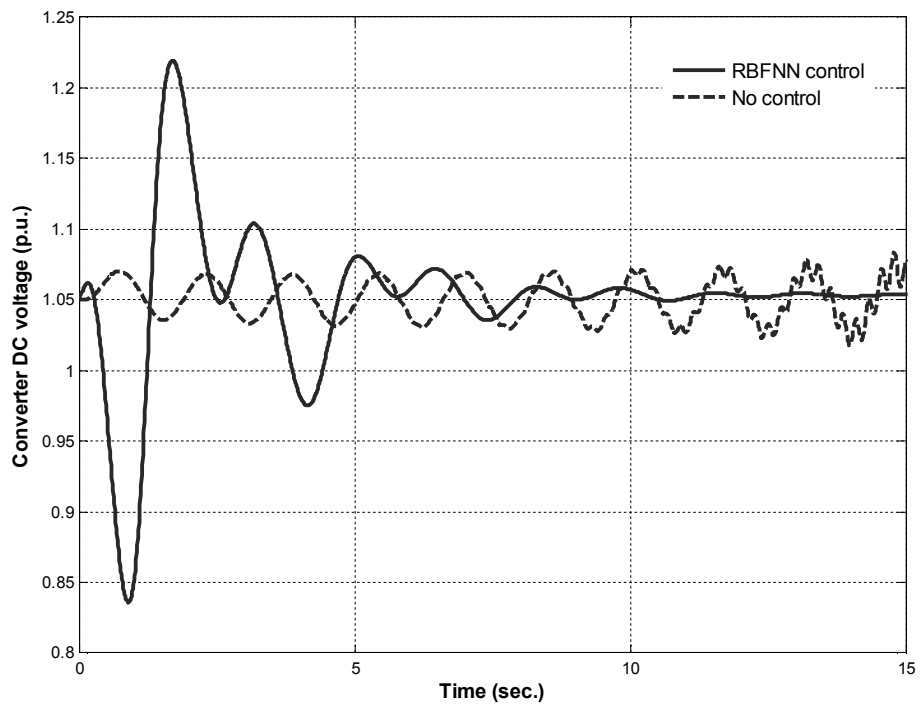


Figure 9. Converter DC-link voltage variation following a 20% input torque pulse

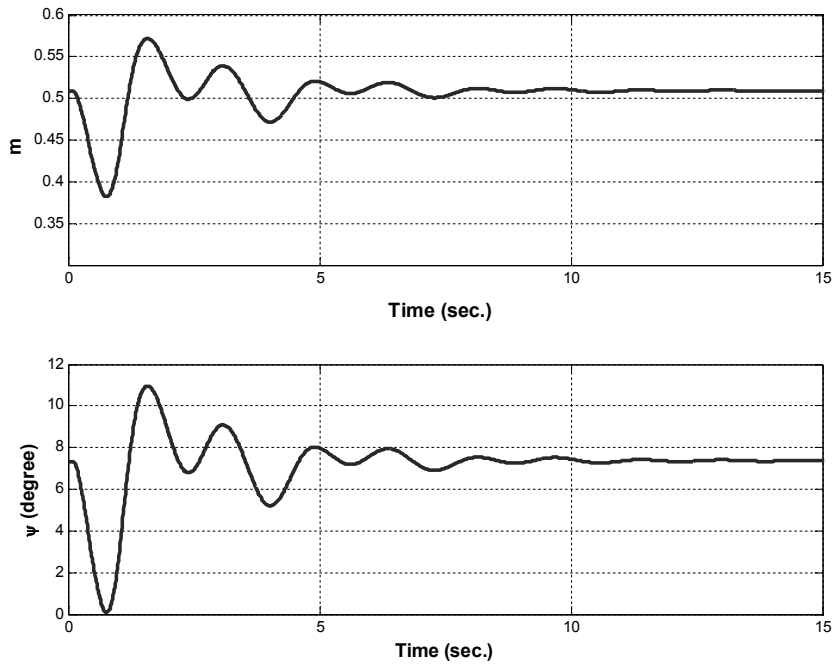


Figure 10. Modulation index (top figure) and phase angle controls (bottom figure) generated for 20% torque pulse case

Figure 11 shows a comparison of the generator speed variation response obtained from the following two strategies: a) the proposed adaptive RBFNN control, and b) decoupled P-Q strategy of supercapacitor control as reported in the literature [18]. The decoupled supercapacitor control of the PMSG involves a relatively complex controller, whose parameters are designed through an optimisation procedure. The major advantage of the proposed RBFNN controller over the earlier reported work is that the former can be implemented online and its performance is robust.

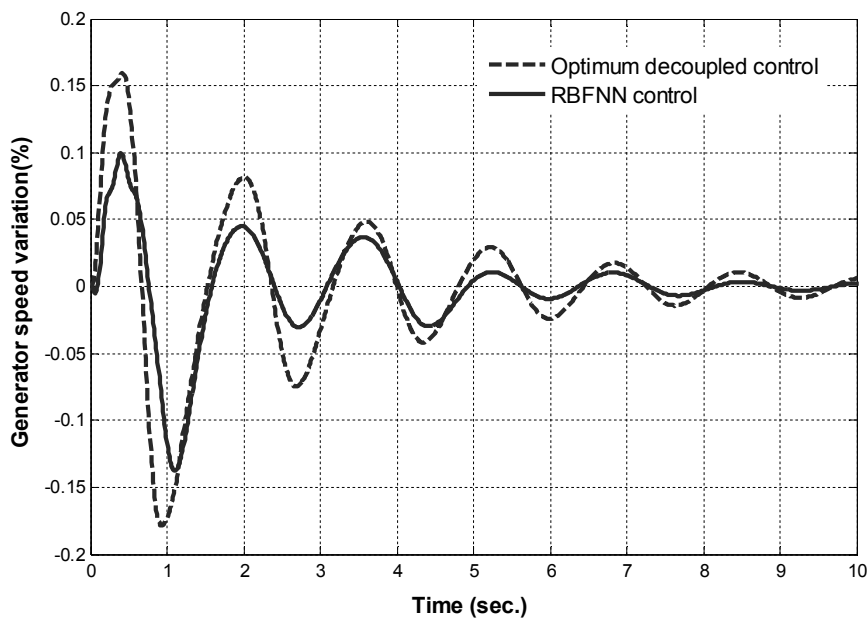


Figure11. Comparison of generator speed variation obtained from proposed RBFNN control with optimum de-coupled P-Q strategy reported in the literature

The robustness of the RBFNN controller was tested at very low voltage conditions on the grid bus. Figures 12-13 show variations in the turbine speed and converter DC voltage respectively, following a 200-ms three-phase fault on the grid. The system response without any additional control results in growing oscillation. The RBFNN strategy controls the oscillation effectively and restores normal operation in less than 10 sec. The initial generator current and converter voltage show large peaks because of random initialisation of the weights. However, as time progresses the weights get trained and the system response reaches steady value smoothly.

Figure 14 shows the variation in wind turbine speed and the generator terminal voltage following repetitive disturbances by input torque pulse. As can be observed, the initial transients in the subsequent disturbance are not as pronounced under the RBFNN control since the weight initialisation is no longer needed.

From a number of simulation studies, it is observed that the proposed adaptive RBFNN restores even the dynamically unstable system to normal operation very quickly. The amount of control required to achieve this has been observed to be reasonably small. The adaptive strategy is simple to implement as it involves only a few steps of computation.

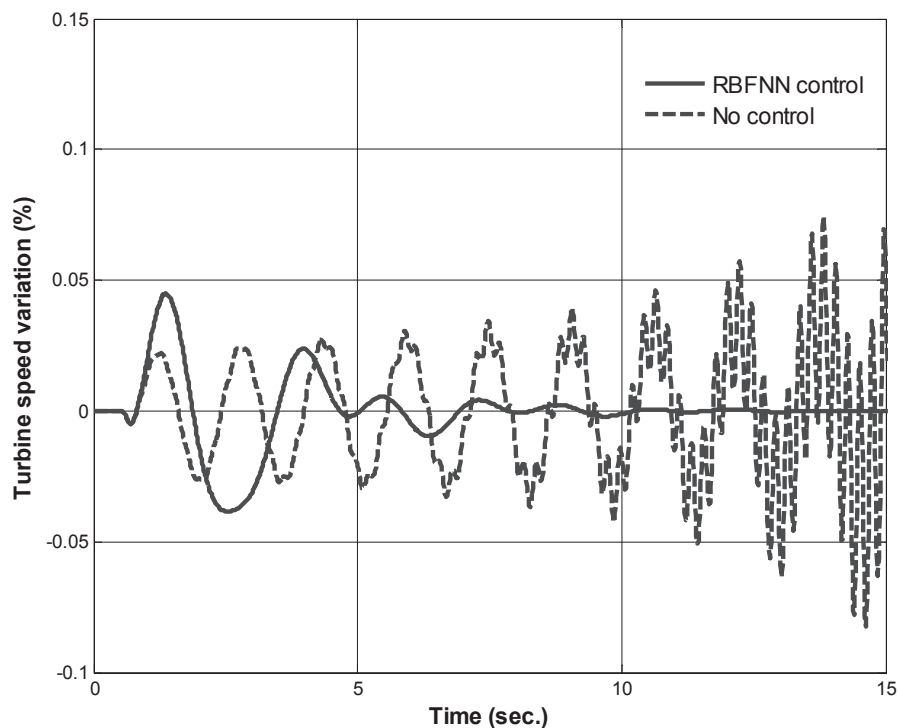


Figure 12. Wind turbine speed variation following a 200-ms three-phase fault at the grid bus with and without adaptive controller

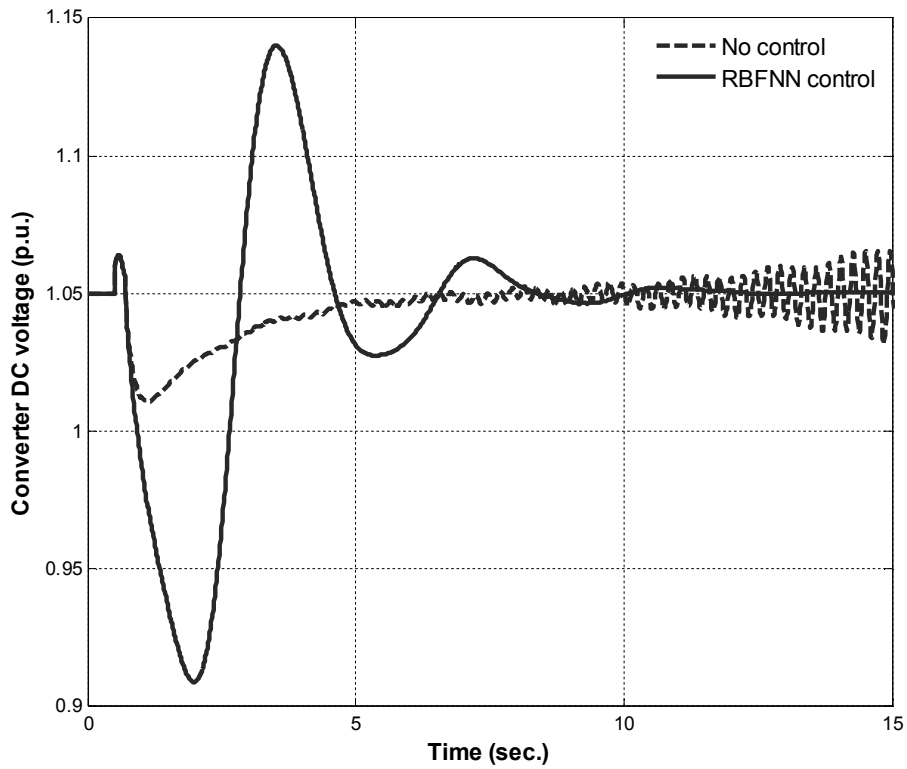


Figure 13. Converter DC voltage variation following a 200-ms grid fault corresponding to Fig. 12

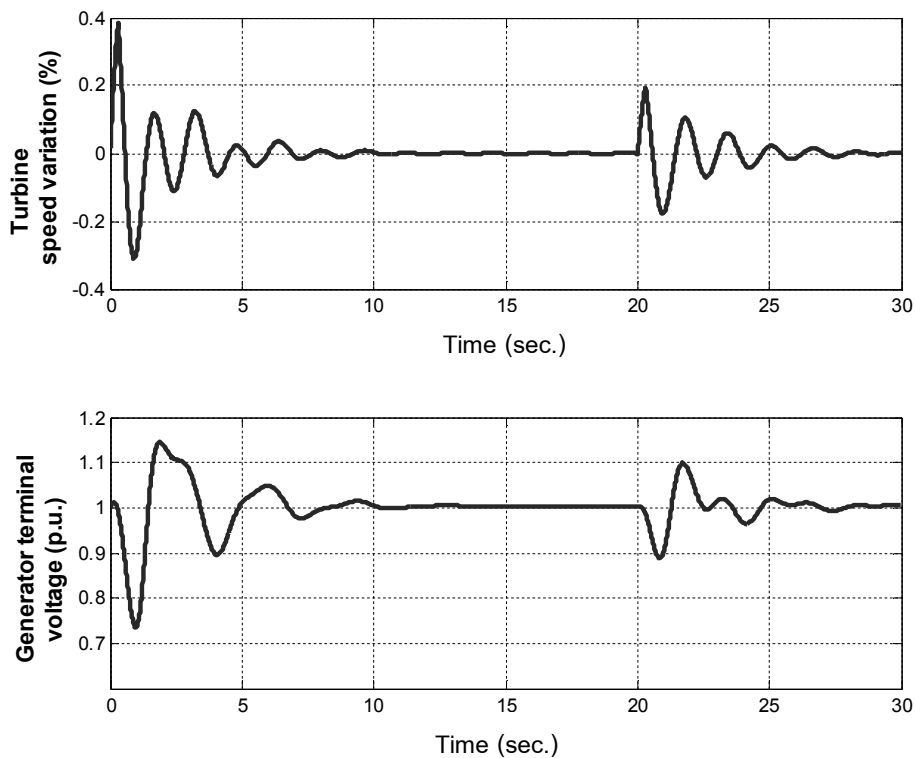


Figure 14. Wind turbine speed variation and generator terminal voltage under RBFNN control when subjected to repetitive disturbances

CONCLUSIONS

A novel online adaptive control strategy for an energy storage device has been proposed using artificial neural network. The strategy employs selected system outputs to predict the control and also updates the network weights online. No offline training is involved in the process. The objective of the strategy is to restore the permanent magnet wind generator to pre-specified levels of output following arbitrary disturbances in the system. This has been achieved by compensating for the wind generator P and Q imbalance through the energy storage device. The radial basis function considered has fast convergence characteristics. The proposed adaptive neural network control strategy is much superior to the classical neural controls, which employ fixed weights.

ACKNOWLEDGEMENTS

This work was conducted under KFUPM Research Group Project #RG1202-1&1202-2. The author wishes to acknowledge the support of King Fahd University of Petroleum and Minerals. Syed Z. Rizvi, lecturer of electrical engineering, is specially acknowledged for his contribution in the computational part.

REFERENCES

1. M. E. Haque, M. Negnevitsky and K. M. Muttaqi, "A novel control strategy for a variable-speed wind turbine with permanent-magnet synchronous generators", *IEEE Trans. Ind. Appl.*, **2010**, *46*, 331-339.
2. S. Zhang, K. J. Tseng, D. M. Vilathgamuwa, T. D. Nguyen and X. Y. Wang, "Design of a robust grid interface system for PMSG-based wind turbine generators", *IEEE Trans. Ind. Electron.*, **2011**, *58*, 316-328.
3. A. Uehara, A. Pratap, T. Goya, T. Senjyu, A. Yona, N. Urasaki and T. Funabashi, "A coordinated control method to smooth wind power fluctuations of a PMSG-based WECS", *IEEE Trans. Energy Convers.*, **2011**, *26*, 550-558.
4. K. H. Kim, Y. C. Jeung, D. C. Lee and H. G. Kim, "LVRT scheme of PMSG wind power systems based on feedback linearization", *IEEE Trans. Power Electron.*, **2012**, *27*, 2376-2384.
5. S. Kato and M. Michihira, "A comparative study on power generation characteristics of permanent magnet synchronous generators", Proceedings of International Power Electronics Conference, **2010**, Sapporo, Japan, pp.1499-1505.
6. S. Li, T. A. Haskew and L. Xu, "Conventional and novel control designs for direct driven PMSG wind turbines", *Electr. Power Syst. Res.*, **2010**, *80*, 328-338.
7. S. M. Mueen, R. Takahashi, T. Murata, J. Tamura, M. H. Ali, Y. Matsumura, A. Kuwayama and T. Matsumoto, "Low voltage ride through capability enhancement of wind turbine generator system during network disturbance", *IET Renew. Power Gener.*, **2009**, *3*, 65-74.
8. M. Singh, V. Khadkikar and A. Chandra, "Grid synchronisation with harmonics and reactive power compensation capability of a permanent magnet synchronous generator-based variable speed wind energy conversion system", *IET Power Electron.*, **2011**, *4*, 122-130.
9. S. Sharma and B. Singh, "Control of permanent magnet synchronous generator-based stand-alone wind energy conversion system", *IET Power Electron.*, **2012**, *5*, 1519-1526.
10. C. N. Bhende, S. Mishra and S. G. Malla, "Permanent magnet synchronous generator-based standalone wind energy supply system", *IEEE Trans. Sust. Energy*, **2011**, *2*, 361-373.

11. L. Wang and D. N. Truong, "Dynamic stability improvement of four parallel-operated PMSG-based offshore wind turbine generators fed to a power system using a STATCOM", *IEEE Trans. Power Del.*, **2013**, 28, 111-119.
12. J. Conroy and R. Watson, "Aggregate modelling of wind farms containing full-converter wind turbine generators with permanent magnet synchronous machines: Transient stability studies", *IET Renew. Power Gener.*, **2009**, 3, 39-52.
13. T. D. Batzel and K. Y. Lee, "High resolution rotor angle estimation for permanent magnet synchronous machines with Hall effect position sensors using neural networks", *Int. J. Eng. Intelli. Syst. Elect. Eng. Comm.*, **2000**, 8, 59-65.
14. J. A. P. Lopes, "Application of artificial neural networks to dynamic security assessment of electric power systems", *Int. J. Eng. Intelli. Syst. Elect. Eng. Comm.*, **1999**, 7, 19-28.
15. W. M. Lin, C. M. Hong, T. C. Ou and T. M. Chiu, "Hybrid intelligent control of PMSG wind generation system using pitch angle control with RBFN", *Energy Convers. Manage.*, **2011**, 52, 1244-1251.
16. S. Miyabukuro, M. Takiguchi, R. Takahashi, T. Murata, J. Tamura and T. Tsuchiya, "Modeling and simulation of wind turbine-fed interior permanent magnet synchronous generator", Proceedings of 18th International Conference on Electrical Machines, **2008**, Vilamoura, Portugal, pp.1-6.
17. A. O. D. Tommaso, R. Miceli, G. R. Galluzzo and M. Trapanese, "Efficiency maximization of permanent magnet synchronous generators coupled to wind turbines", Proceedings of IEEE Power Electronics Specialist Conference, **2007**, Orlando (FL), USA, pp.1267-1272.
18. A. H. M. A. Rahim, "Modeling and control of a PMSG wind system with STATCOM capacitor energy storage device", Proceedings of 12th IASTED Conference on Modelling and Simulation, **2012**, Banff, Canada, pp.249-254.
19. S. Kamalasan and A. A. Ghandakly, "A neural network parallel adaptive controller for dynamic system control", *IEEE Trans. Instr. Measur.*, **2007**, 56, 1786-1796.
20. M. T. Hagan, H. B. Demuth and O. D. Jesus, "An introduction to the use of neural networks in control systems", *Int. J. Robust Nonlinear Contr.*, **2002**, 12, 959-985.
21. J. Sarangapani, "Neural Network Control of Nonlinear Discrete-Time Systems", CRC Press, Boca Raton (FL), **2006**, Ch.3.
22. S. Huang, K. K. Tan, T. H. Lee and A. S. Putra, "Adaptive control of mechanical systems using neural networks", *IEEE Trans. Syst. Man Cyber. Part C*, **2007**, 37, 897-903.
23. H. N. Al-Duwaish and S. Z. Rizvi, "A robust controller for non-linear MIMO systems using radial basis function neural network", *Proc. IMechE Part I: J. Syst. Contr. Eng.*, **2011**, 225, 667-682.

APPENDIX

System Data (in per unit, except stated otherwise)

PMSG quantities: 1.5 MVA, 690 V, 40-pole, $f_b = 11.5$ Hz, $R_a = 0.01$, $X_d = 1$, $X_q = 0.7$, $H_g = 0.5$ s, $H_t = 3$ s, $K_s = 0.3$, Residual flux = 0.9

Converter parameters: $R_i = 0.05$, $X_i = 0.1$, $C = 1$; Storage capacitor and VSC: 250 kW, $R_{st} = 0.01$, $L_{st} = 0.15$, $C_{dc} = 1$

Local load and line: $P = 200$ kW, $Q = 400$ kVAR (including capacitor); $R_{line} = 0.1$, $X_{line} = 0.2$

© 2014 by Maejo University, San Sai, Chiang Mai, 50290 Thailand. Reproduction is permitted for non-commercial purposes.

Review

Factors affecting release of ethanol vapour in active modified atmosphere packaging systems for horticultural products

Weerawate Utto

Faculty of Agriculture, Ubon Ratchathani University, Ubon Ratchathani, Thailand

E-mail: agweerut@mail2.ubu.ac.th; tel. +66-45-353-500; fax +66-45-288-373

Received: 14 August 2013 / Accepted: 17 April 2014 / Published: 21 April 2014

Abstract: The active modified atmosphere packaging (active MAP) system, which provides interactive postharvest control, using ethanol vapour controlled release, is one of the current interests in the development of active packaging for horticultural products. A number of published research work have discussed the relationship between the effectiveness of ethanol vapour and its concentration in the package headspace, including its effect on postharvest decay and physiological controls. This is of importance because a controlled release system should release and maintain ethanol vapour at effective concentrations during the desired storage period. A balance among the mass transfer processes of ethanol vapour in the package results in ethanol vapour accumulation in the package headspace. Key factors affecting these processes include ethanol loading, packaging material, packaged product and storage environment (temperature and relative humidity). This article reviews their influences and discusses future work required to better understand their influences on ethanol vapour release and accumulations in active MAP.

Keywords: modified atmosphere packaging, ethanol vapour controlled release, active packaging, horticultural products

INTRODUCTION

A current and increasing trend in the development of active packaging systems for horticultural and food products is the employment of controlled release of gas-phase antimicrobial agents, e.g. ethanol [1-3], essential oils [4, 5], 2-nonanone [6] and hexanal [7-9]. Although these volatiles have generally-recognised-as-safe (GRAS) status, only ethanol vapour has been utilised industrially. Examples of ethanol vapour controlled release systems are Antimold Mild[®] and Negamold[®] sachets commercialised by the Freund Industrial Co. (Japan). Ethanol vapour controlled release systems are reportedly incorporated into modified atmosphere packaging (MAP) systems for

horticultural products, such as grape [1, 10, 11], tomato [12, 13], fresh-cut apple [14], sweet cherry [2] and fresh-cut papaya [15]. MAP containing active systems such as controlled release and O₂ scavenging can be designated 'active MAP' [16]. The application of an ethanol vapour controlled release system imparts antimicrobial activity and delay changes of postharvest quality by inhibiting ethylene synthesis and action [12], minimising discolouration and senescence [10, 13], thereby enhancing aroma [1, 2, 15, 17].

The release and accumulation of ethanol vapour at effective levels in the package headspace is the main purpose for which the ethanol controlled release system is designed, and these can technically be affected by a number of factors, including ethanol loading in the controlled release system, packaging film and storage environment. The aim of this review is to provide understanding of key factors and their influences on ethanol vapour release and accumulation in the active MAP.

CONFIGURATIONS OF ETHANOL VAPOUR CONTROLLED RELEASE SYSTEMS

Ethanol vapour controlled release systems that have been reported are developed in two key configurations: sachet and paper pad (Table 1). Sachet refers to a small packet containing a carrier which is pre-equilibrated with ethanol. The carriers contained in the sachet are usually porous adsorbents with a high specific surface area, such as those based on silica, which ensures that sufficient amounts of agents are available to be delivered within the desired time frame. Paper-based materials such as filter paper and newspaper are also utilised as carriers (Table 1). The ethanol-containing carriers developed for Antimold Mild[®] are reportedly called ethanol powder, due to their small and fine structures. This sachet material governs the release rate of ethanol vapour from the sachet to the package headspace. The material of Antimold Mild[®] is a paper/ethyl vinyl acetate copolymer for regulating ethanol vapour release [11, 18]. The paper-pad release system utilises paper as an ethanol carrier, which is technically soaked with ethanol liquid (Table 1). Unlike sachets, the paper pads are exposed to the environment with no physical barrier to limit ethanol vapour release. The ethanol left on the pad, compared to the sachet, should decrease at a faster rate.

Both controlled release configurations are extensively used in active MAP due to their convenience, as they can be added to the packages along with the product and conveniently removed from the packages and discarded at the end of the storage period. However, the use of sachets may pose a low probability that the packaging material properties will be compromised, especially the physical/mechanical properties. There are concerns among consumers about sachets inside packages in regard to the misuse of sachets such as fear of ingestion, spillage of sachet content into food causing adulteration of the food product, and 'foreign component' in the package [19].

FACTORS AFFECTING ETHANOL-VAPOUR RELEASE AND ACCUMULATION IN PACKAGE HEADSPACE

The release of ethanol vapour and its subsequent accumulation in the package headspace at an effective concentration level is desirable for controlling postharvest decay and physiological changes. The phenomenon can be affected by factors involving mass transfer processes in the sachet, the packaged horticultural product and the type of package. Figure 1 diagrammatically illustrates a concept model of the key mass transfer processes for release and accumulation of ethanol vapour in active MAP. The diagram is adapted from the model package reported by Bai et

Table 1. Examples of ethanol-vapour controlled release systems and their reported applications for horticultural products

Ethanol-vapour controlled release system			Horticultural product	Reference
Configuration	Carrier	Trade name		
Sachet	Ethanol powder	Antimold-Mild ^{® 1}	Broccoli	[18]
Sachet	Ethanol powder	Antimold-Mild [®]	Cherry	[2]
Sachet	Ethanol powder	Antimold-Mild [®]	Apple	[14]
Pad	Paper	-	Grape	[1]
Sachet	Filter paper	-	Papaya	[15]
-	Paper wick ²	-	Mango	[20]
Sachet	Ethanol powder	Antimold-Mild [®]	Broccoli	[21]
Sachet	Ethanol powder	Antimold-Mild [®]	Grape	[11]
Sachet	Ethanol powder	Antimold-Mild [®]	Broccoli	[22]
Pad	Filter paper	-	Chinese Bayberry	[23]
Pad	Newspaper sheet	-	Grape	[24]

¹ Commercialised by Freund Industrial Co. Ltd, Japan

² Immersed in ethanol

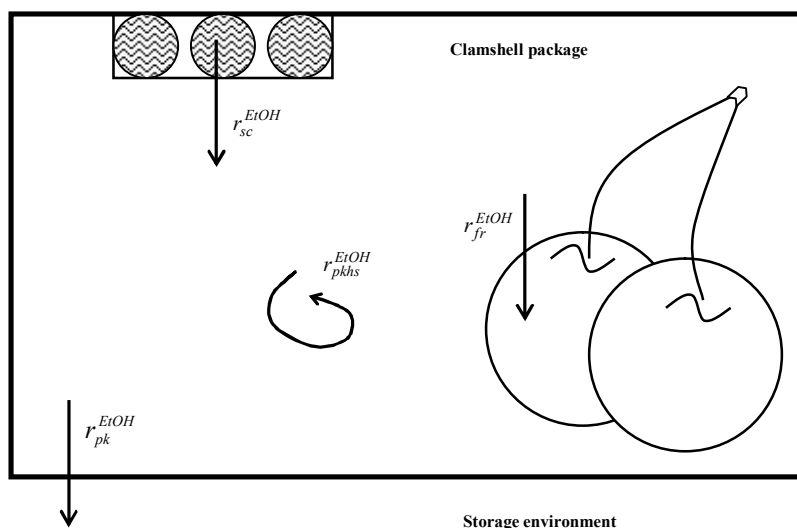


Figure 1. Conceptualisation of key mass transfer processes of release of ethanol vapour in a model clamshell package with enclosed sachet and sweet cherries simplified as one-dimensional transport (adapted from Bai et al. [2]). The Antimold Mild[®] was attached to the top lid of the clamshell and sweet cherries were packaged into the clamshell.

al. [2]: an incorporation of Antimold Mild[®] sachet into a clamshell package containing intact sweet cherry. Ethanol vapour is carried on a porous adsorbent and is continuously desorbed from it into the sachet atmosphere (simplified as one-dimensional mass transport) before crossing the sachet film into the package headspace (r_{sc}^{EtOH}). Ethanol vapour can both pass through the packaging material from the internal headspace to the storage environment (r_{pk}^{EtOH}) and interact with the product (r_{fr}^{EtOH}). The dynamic balance of the rates of these processes determines the net rate of accumulation of ethanol vapour in the package headspace (r_{pkhs}^{EtOH}). The key factors involved in the mass transfer processes (Figure 1) are reviewed and presented as follows.

Load of Ethanol on Carrier

Different loads of ethanol on carriers has different release and accumulation effects in the package headspace. Suzuki et al. [18] reported a linear relationship between the mass of ethanol on the carrier (3-12 g ethanol powder) and the peak concentration and accumulation pattern of ethanol vapour delivered from Antimold Mild[®] into the headspace of perforated PE bags containing broccoli branchlets at 20°C for 5 days. The peak release and quasi steady-state of ethanol concentration was reported for the 12g-sachet (Figure 2-I). Similarly, Smith et al. [25] reported higher peaks of ethanol vapour released from the Ethicap[®] type E₄ (4 g ethanol powder), compared to type E₁ (1 g ethanol powder) in the headspace of a high ethanol vapour barrier pouch at 25°C for 16 days (Figure 2-II; data on the 7th day of E₄+a_w 0.85 was not reported). In the study of Thompson seedless grape, Lurie et al. [1] reported that paper impregnated with ethanol with a loading ratio of 8 ml_{EtOH}/kg_{fruit} could apparently generate a higher initial peak and quasi steady-state concentration than a loading ratio of 4 ml_{EtOH}/kg_{fruit} (Figure 2-III). In a study on Red Globe table grape, Candir et al. [11] reported highest ethanol concentration measured in the headspace of a non-perforated bag (ZOEpac) containing Antimold Mild[®] with 8 g ethanol powder, in comparison to Antimold Mild[®] with 6 g and 3 g ethanol powder (Figure 2-IV). Recently Utto et al. [15] reported that the kinetic release rate and level of ethanol vapour concentration at 10°C are dependent on the ethanol load (0.5, 1.0 and 1.5g) on the filter paper.

The information noted above indicates that the higher the ethanol loading is on the carrier, the higher the release peak becomes and, most likely also, the higher the quasi steady-state concentration in package headspace results. This is explained by the differences in the system capacity of the sachet, which is in proportion to the mass of ethanol adsorbed. The extent of change in the ethanol vapour concentration is a function of the reciprocal of the system capacity [26], and therefore the slowest change in the vapour concentration in the sachet headspace, which is in equilibrium with ethanol adsorbed on the carrier, would occur in the system with the highest loading of ethanol. This causes the slowest change of concentration gradient across the sachet after the onset of release, thus resulting in the highest initial peak concentration and a slow depletion of ethanol vapour from the package headspace leads to a high quasi steady-state concentration. It can be noted that in Figure 2 the quasi steady-state concentrations of ethanol vapour developed in the long term storage, i.e. 2-4 months, become comparable regardless of ethanol loading.

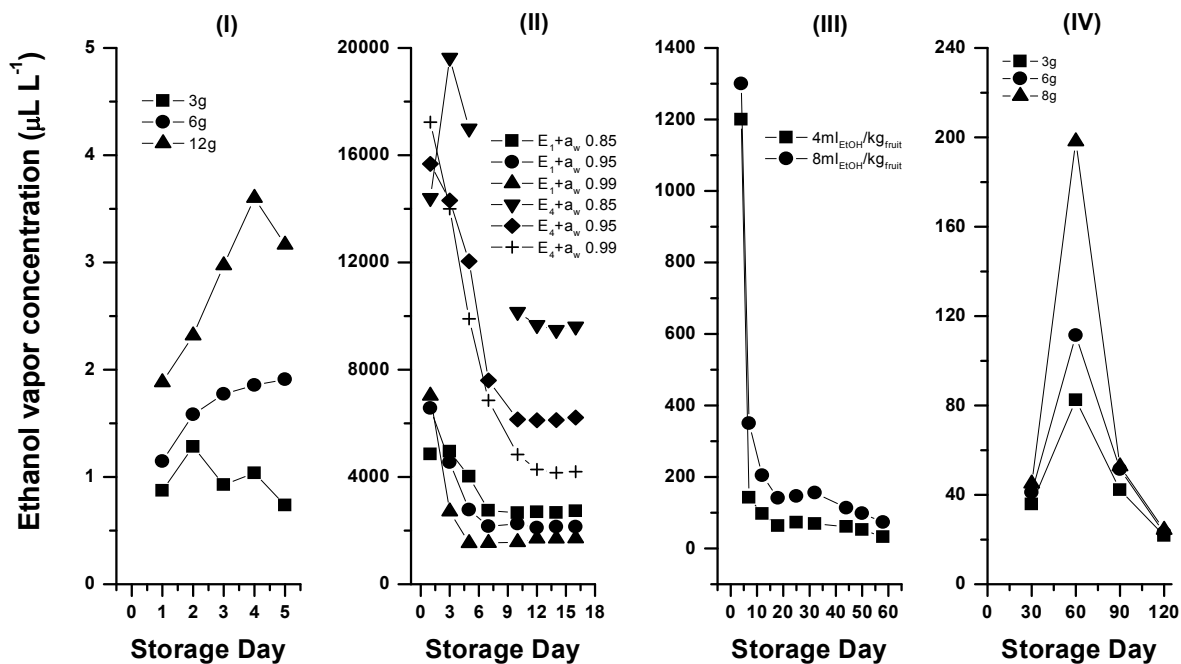


Figure 2. Changes in ethanol vapour concentration in the atmosphere of bags containing: (I) broccoli branchlets and varying mass of ethanol powder (3, 6 and 12 g) [17]; (II) a_w-adjusted potato dextrose agar plates and Ethicap[®] (type E₁: 1g ethanol powder and type E₄: 4g ethanol powder) [25]; (III) Thomson seedless grape and paper pad containing ethanol with 4 and 8 ml_{EtOH}/kg_{fruit} loading ratios [1]; (IV) Red Globe table grape and Antimold Mild[®] with varying mass of ethanol powder (3, 6 and 8 g) [11]

Packaging Material

Ethanol vapour released into the package headspace will permeate through the packaging material in accordance with the ethanol vapour concentration gradient between package headspace and environment. A high-barrier plastic film can accordingly minimise ethanol vapour permeation through the film, and a high vapour concentration can be achieved (Figure 2-II). Ethanol vapour released shows varied concentrations, and often there are high initial concentration peaks (Figure 2). Under such concentrations, the permeability to ethanol vapour of non-perforated films are likely to be concentration-dependent [27-29]. Miyauchi et al. [30] reported the concentration-dependent characteristic of ethanol-vapour permeability in polypropylene (PP), polyvinylidene chloride (PVC) and a multi-layer film (comprised of nitrocellulose, polyethylene terephthalate (PET) and aluminium layers). During the initial release, high vapour concentration can increase film permeability to ethanol vapour. High permeant concentrations tend to interact with film, thus leading to changes in its polymeric structure, which may increase free volume and facilitate permeation of the permeance through the film [27-29]. The rate of ethanol vapour permeation from the headspace to the immediate environment should then be increased, with consequent reduction in the concentration level of ethanol vapour accumulated in the package headspace. This may affect the efficiency of microbial or physiological control by ethanol vapour.

In addition to the non-perforated films, there are reports on using perforated films for packaging [11, 18]. Perforations physically facilitate and stimulate the permeation of gas and vapour through the film, thus effectively increasing film permeability. Ethanol vapour concentration in the

perforated package headspace subsequently becomes lower than that in the non-perforated one. Candir et al. [11] reported lower concentrations (36-44 L L⁻¹) in the headspace of perforated LDPE, compared to those of non-perforated bags (84-198 L L⁻¹). The lower ethanol vapour concentration accumulated in the perforated bags, however, may provide a benefit to the design of active MAP in relation to consumers' aroma perception of fermented ethanol vapour. High ethanol vapour concentrations may be considered 'foreign' and it may cause consumers to reject the product. Bai et al. [2] reported that the odour of ethanol vapour at 9-26 L L⁻¹ could be perceived after opening the clamshells containing cherry with an ethanol-vapour controlled release sachet. Although lowering ethanol vapour concentration in the package headspace may be achieved by the perforated film, it is important that the lowered concentration in the headspace has to be within the level at which ethanol vapour is effective for antimicrobial and/or physiological control.

Storage Environment (Temperature and Humidity)

An increase in storage temperature reportedly stimulates the release or desorption of adsorbed particles from the carrier, resulting in a high concentration accumulated in the package headspace. Bai et al. [2] reported that concentration peaks of ethanol vapour at 1°, 10° and 20 °C were approximately 12, 23 and 27 L L⁻¹ respectively, which is consistent with the findings of Candir et al. [11]. A high concentration of ethanol vapour in the package headspace at high storage temperature can provide better control of microbial proliferation, especially during postharvest handling when temperature fluctuations (likely temperature increase) are not uncommon [31-33].

Packaging film permeability is also well known for its temperature dependence [34]. Miyauchi et al. [30], for example, reported that there is a clear relationship between storage temperature (29-40 °C) and film permeability to ethanol vapour. Increasing temperature may be considered an additional effect on the high concentration accumulated at the release peak. High temperature can increase film permeability to ethanol vapour, thus stimulating the rate of ethanol vapour permeation from the headspace to the immediate environment and lowering the ethanol vapour concentration in the package headspace.

In addition to storage temperature, relative humidity reportedly can affect the ethanol vapour release rate. Smith et al. [35] reported that a high relative humidity can affect the equilibrium condition by stimulating the release of ethanol from Antimold Mild . The effect of relative humidity on the release process is assumed to be due to the competition for active adsorption sites through the displacement of adsorbed molecules by water vapour [25]. Given a reasonable porosity and water vapour permeability of controlled-release sachet material, high relative humidity developed in modified atmosphere packages containing fresh-cut horticultural products can be utilised for stimulating ethanol vapour release from the sachet, thus potentially providing better control of microbial proliferation under the high humidity developed in the package headspace.

However, if the sachet material is a hydrophobic plastic film, for example LDPE film, which is a good water vapour barrier, the high humidity accumulated in the package headspace will have a minimal effect on the release of ethanol vapour from the sachet [15]. High humidity accumulated in the package headspace of modified-atmosphere packages can, however, stimulate fungal decay and overcome the antifungal activity of the released ethanol vapour. In a study of Red Globe grape [11], Antimold[®] 80 (with 8g ethanol powder) placed in a non-perforated LDPE box liner reportedly did not give an effective antifungal activity compared to that in a perforated (6-mm holes) LDPE liner due to the high relative humidity accumulated in the non-perforated liner. Similar findings on the effect of high humidity on antifungal activity of ethanol vapour were reported in other grape

cultivars including ‘Superior’ [36], ‘Reliance’ and ‘Saturn’ [37]. It was remarked that the humidity level accumulated in the package headspace has to be controlled in order to maintain the antifungal activity of ethanol vapour released from the sachet.

Packaged Product

The interaction between ethanol vapour and the packaged product can evidently lower the concentration of ethanol vapour in the package headspace [2]. Similar evidence was reported for other volatile compounds including hexanal, nonanal and hexyl acetate [38, 39]. Whilst there are no reported studies for ethanol vapour, interactions between hexanal vapour and fresh-cut apple [40] and intact tomato [41] are reportedly concentration- and temperature-dependent. Given similar characteristics, interactions between ethanol vapour and products hypothetically should increase under a high storage temperature and ethanol vapour concentration, and these should rapidly decrease the concentration in the headspace. This assumption is supported by the study of Bai et al. [2], who reported that there was a sharp decrease in headspace concentration of ethanol vapour from ca. 27 to 13 L L⁻¹ at 20°C within 48 hr while the reduction time frame of ethanol vapour concentration at 10°C was 240 hr.

Interactions between ethanol vapour and the products may stimulate metabolism such as the respiration rates of tomato [42] and potato [43], and the biological conversion of ethanol vapour to acetaldehyde, which causes browning in grape [1]. Stimulation of respiration rate may cause high O₂ consumption and CO₂ production, which may affect the modified atmosphere developed in the package headspace as a result of the balance between respiration rate and rate of permeation of O₂ and CO₂ through the packaging film [44, 45]. However, ethanol vapour released in active MAP reportedly has no effect on the modified-atmosphere condition in packages containing sweet cherry [2], grape [1] and fresh-cut papaya [15] (Table 2). Similarly, Serrano et al. [46] reported that antifungal volatiles (eugenol, thymol and menthol) released from saturated gauze did not alter the levels of O₂ and CO₂ in plastic bags containing sweet cherry.

Such minimal effects of the vapour of ethanol or other volatiles released from the essential oils may be attributed to the developed modified-atmosphere conditions, which slow down metabolic processes in horticultural products [47] and consequently limit their interactions with the volatiles. In the study on intact tomato [7], continuous hexanal vapour treatment (40-70 L L⁻¹) reportedly increased respiration rate up to 50% during a 7-day storage at 20°C. In their subsequent work [41], however, the effect of hexanal vapour treatment on the respiration rate became minimal under a modified-atmosphere condition (10% O₂ and 5% CO₂ (v/v)). However, a significant effect of the antifungal eucalyptol volatile on the modified atmosphere was evident, as seen in the study of Serrano et al. [46]. This volatile was reported to increase the oxidative metabolism of cherry, thus causing a large change in the modified-atmosphere condition (ca. 7% O₂ and 3.5% CO₂) compared to that developed under eugenol, thymol and menthol volatiles (11-12% O₂ and 2-3% CO₂). Such information suggests that the design of active MAP has to take into account the change in modified-atmosphere condition by the volatile released.

Table 2. Modified atmosphere conditions developed in package headspace in which vapour of ethanol and other volatiles accumulated

Product	Storage temperature (°C)	Package	Controlled release system		Modified atmosphere condition ^a	Reference
			Active vapour	Steady-state concentration ($\mu\text{L}\cdot\text{L}^{-1}$)		
Grape	0	(1) Xtend [®] plastic liner (2) Polyethylene	Ethanol	(1) 32-350 (2) 70-640 ^b	(1) 8% CO ₂ and 12% O ₂ (2) 2% CO ₂ and 15-18% O ₂	[1]
Sweet cherry	10	Polystyrene clamshell	Ethanol	14-18	<2.6% CO ₂ and 19.4-21% O ₂	[2]
Papaya	10	LDPE bag	Ethanol	0.01-0.06	5% CO ₂ and 9% O ₂	[15]
Grape	0	Nonperforated LDPE (ZOEpac)	Ethanol	84-198	2-3% CO ₂ and 13-14% O ₂	[11]
Sweet cherry	1	Oriented polypropylene (OPP) bag	Eugenol, Thymol, Menthol	Not reported	2-3% CO ₂ and 11-12% O ₂	[46]

^a Reportedly not significantly different between bags with and without controlled release sachet

^b On the last storage day of 7-week storage trial, an upsurge of ethanol vapour from ca. 640 to ca. 900 $\mu\text{L}\cdot\text{L}^{-1}$ was reported.

CONCLUSIONS

This review provides information on key factors, viz. ethanol loading, packaging material, packaged product and storage environment (temperature and relative humidity), affecting the release of ethanol vapour in active MAP. The conceptual model representing the key mass transfer processes of the packaging system assists understanding of how these factors influence the processes. The design of active MAP to achieve effective ethanol concentration is complicated by interactions among packaging components, which are mainly the controlled release system, the packaging film and the product, thus resulting in changes of ethanol vapour concentration. This concentration importantly should be at a level at which it does not cause negative sensory responses from consumers whilst still providing effective control on the packaged product.

More studies should be conducted in order to understand the effects of simultaneous changes made to multiple factors influencing ethanol vapour release since most work reported has only manipulated a single factor. The understanding would assist packaging technologists and engineers to properly design components of active MAP to suit the packaging requirements of products and the shelf life desired. Mathematical models appropriately developed and validated could be utilised to optimise packaging designs through information obtained from the simulations. At the present time there are no available mathematical models reported for the design of ethanol-vapour release in active MAP.

REFERENCES

1. S. Lurie, E. Pesis, O. Gadiyeva, O. Feygenberg, R. Ben-Arie, T. Kaplunov, Y. Zutahy and A. Lichter, "Modified ethanol atmosphere to control decay of table grapes during storage", *Postharv. Biol. Technol.*, **2006**, 42, 222-227.

2. J. Bai, A. Plotto, R. Spotts and N. Rattanapanone, "Ethanol vapor and saprophytic yeast treatments reduce decay and maintain quality of intact and fresh-cut sweet cherries", *Postharv. Biol. Technol.*, **2011**, 62, 204-212.
3. D. Ustun, E. Candir, A. E. Ozdemir, O. Kamiloglu, E. M. Soylu and R. Dilbaz, "Effects of modified atmosphere packaging and ethanol vapor treatment on the chemical composition of 'Red Globe' table grapes during storage", *Postharv. Biol. Technol.*, **2012**, 68, 8-15.
4. N. Matan, H. Rimkeeree, A. J. Mawson, P. Chompreeda, V. Haruthaithanasan and M. Parker, "Antimicrobial activity of cinnamon and clove oils under modified atmosphere conditions", *Int. J. Food Microbiol.*, **2006**, 107, 180-185.
5. R. Lanciotti, A. Gianotti, F. Patrignani, N. Belletti, M. E. Guerzoni and F. Gardini, "Use of natural aroma compounds to improve shelf-life and safety of minimally processed fruits", *Trends Food Sci. Technol.*, **2004**, 15, 201-208.
6. E. Almenar, R. Catala, P. Hernandez-Munoz and R. Gavara, "Optimization of an active package for wild strawberries based on the release of 2-nonanone", *LWT-Food Sci. Technol.*, **2009**, 42, 587-593.
7. W. Utto, A. J. Mawson and J. E. Bronlund, "Hexanal reduces infection of tomatoes by *Botrytis cinerea* whilst maintaining quality", *Postharv. Biol. Technol.*, **2008**, 47, 434-437.
8. P. Thavong, D. D. Archbold, T. Pankasemsuk and R. Koslanund, "Hexanal vapours suppress spore germination, mycelial growth, and fungal-derived cell wall degrading enzymes of postharvest pathogens of longan fruit". *Chiangmai J. Sci.*, **2011**, 38, 139-150.
9. R. A. Spotts, P. L. Sholberg, P. Randall, M. Serdani and P. M. Chen, "Effects of 1-MCP and hexanal on decay of d'Anjou pear fruit in long-term cold storage", *Postharv. Biol. Technol.*, **2007**, 44, 101-106.
10. E. Pesis, "The role of the anaerobic metabolites, acetaldehyde and ethanol, in fruit ripening, enhancement of fruit quality and fruit deterioration", *Postharv. Biol. Technol.*, **2005**, 37, 1-19.
11. E. Candir, A. E. Ozdemir, O. Kamiloglu, E. M. Soylu, R. Dilbaz and D. Ustun, "Modified atmosphere packaging and ethanol vapor to control decay of 'Red Globe' table grapes during storage", *Postharv. Biol. Technol.*, **2012**, 63, 98-106.
12. M. E. Saltviet and F. Mencarelli, "Inhibition of ethylene synthesis and action in ripening tomato fruit by ethanol vapors". *J. Am. Soc. Hort. Sci.*, **1988**, 113, 572-576.
13. M. O. Kelly and M. E. Saltveit, "Effect of endogenously synthesized and exogenously applied ethanol on tomato fruit ripening", *Plant Physiol.*, **1988**, 88, 143-147.
14. J. Bai, E. A. Baldwin, R. C. S. Fortuny, J. P. Mattheis, R. Stanley, C. Perera and J. K. Brecht, "Effect of pretreatment of intact 'Gala' apple with ethanol vapor, heat, or 1-methylcyclopropene on quality and shelf life of fresh-cut slices", *J. Am. Soc. Hort. Sci.*, **2004**, 129, 583-593.
15. W. Utto, E. Onsaard and R. Chairat, "Development of controlled ethanol vapour release sachet prototype for fresh-cut ripen papaya", *King Mongkut's Agric. J.*, **2012**, 30, 39-49 (in Thai).
16. F. Charles, J. Sanchez and N. Gontard, "Active modified atmosphere packaging of fresh fruits and vegetables: Modeling with tomatoes and oxygen absorber." *J. Food Sci.*, **2003**, 68, 1736-1742.
17. I. Yamashita, Y. Nemoto and S. Yoshikawa, "Formation of volatile esters in strawberries", *Agric. Biol. Chem.*, **1975**, 39, 2303-2307.
18. Y. Suzuki, T. Uji and H. Terai, "Inhibition of senescence in broccoli florets with ethanol vapor from alcohol powder", *Postharv. Biol. Technol.*, **2004**, 31, 177-182.
19. M. L. Rooney, "Active packaging in polymer films", in "Active Food Packaging" (Ed. M. L. Rooney), Blackie Academic and Professional, Glasgow, **1995**, pp.74-110.

20. A. Plotto, J. Bai, J. A. Narciso, J. K. Brecht and E. A. Baldwin, "Ethanol vapor prior to processing extends fresh-cut mango storage by decreasing spoilage, but does not always delay ripening", *Postharv. Biol. Technol.*, **2006**, 39, 134-145.
21. T. Asoda, H. Terai, M. Kato and Y. Suzuki, "Effects of postharvest ethanol vapor treatment on ethylene responsiveness in broccoli". *Postharv. Biol. Technol.*, **2009**, 52, 216-220.
22. A. Fukasawa, Y. Suzuki, H. Terai and N. Yamauchi, "Effects of postharvest ethanol vapor treatment on activities and gene expression of chlorophyll catabolic enzymes in broccoli florets", *Postharv. Biol. Technol.*, **2010**, 55, 97-102.
23. W.-S. Zhang, X. Li, X.-X. Wang, G.-Y. Wang, J.-T. Zheng, D. C. Abeysinghe, I. B. Ferguson and K.-S. Chen, "Ethanol vapour treatment alleviates postharvest decay and maintains fruit quality in Chinese bayberry", *Postharv. Biol. Technol.*, **2007**, 46, 195-198.
24. C. Chervin, P. Westercamp and G. Monteils, "Ethanol vapours limit *Botrytis* development over the postharvest life of table grapes", *Postharv. Biol. Technol.*, **2005**, 36, 319-322.
25. J. P. Smith, B. Ooraikul, W. J. Koersen, F. R. van de Voort, E. D. Jackson and R. A. Lawrence, "Shelf life extension of a bakery product using ethanol vapor", *Food Microbiol.*, **1987**, 4, 329-337.
26. O. Levenspiel, "Chemical Reaction Engineering", Wiley, New York, **1972**, pp.1-7.
27. F. Johansson and A. Leufvén, "Influence of sorbed vegetable oil and relative humidity on the oxygen transmission rate through various polymer packaging films", *Packag. Technol. Sci.*, **1994**, 7, 275-281.
28. F. Johansson and A. Leufvén, "Food packaging polymer films as aroma vapor barriers at different relative humidities", *J. Food Sci.*, **1994**, 59, 1328-1331.
29. C. E. Rogers, "Permeation of gases and vapours in polymers", in "Polymer Permeability" (Ed. J. Comyn), Elsevier Applied Science, London, **1985**, Ch. 2.
30. M. Miyauchi, Y. Nakanishi and Y. Sagara, "Permeation of water and volatile flavors through packaging films", *Food Sci. Technol. Int. Tokyo*, **1996**, 2, 217-222.
31. N. H. Banks, K. M. Maguire and D. J. Tanner, "Innovation in postharvest handling systems", *J. Agric. Eng. Res.*, **2000**, 76, 285-295.
32. B. P. F. Day, "Extension of shelf-life of chilled foods", *Eur. Food Drink Rev.*, **1989**, 4, 47-56.
33. L. Jacxsens, F. Devlieghere and J. Debevere, "Temperature dependence of shelf-life as affected by microbial proliferation and sensory quality of equilibrium modified atmosphere packaged fresh produce", *Postharv. Biol. Technol.*, **2002**, 26, 59-73.
34. G. L. Robertson, "Food Packaging: Principles and Practice" Marcel Dekker, New York, **1993**, pp.73-110.
35. J. P. Smith, J. Hoshino and Y. Abe, "Interactive packaging involving sachet technology", in "Active Food Packaging" (Ed. M. L. Rooney), Blackie Academic and Professional, Glasgow, **1995**, pp.143-173.
36. A. Lichter, Y. Zutahy, T. Kaplunov, Z. Shacham, N. Aharoni and S. Lurie, "The benefits of modified atmosphere of ethanol-treated grapes", *Acta Hortic.*, **2005**, 682, 1739-1744.
37. J. R. Morris, O. L. Oswald, G. L. Main, J. N. Moore and J. R. Clark, "Storage of new seedless grape cultivar with sulfur dioxide generators", *Am. J. Enol. Vitic.*, **1992** 43, 230-232.
38. T. R. Hamilton-Kemp, D. D. Archbold, J. H. Loughrin, R. W. Collins and M. E. Byers, "Metabolism of natural volatile compounds by strawberry fruit", *J. Agric. Food Chem.*, **1996**, 44, 2802-2805.

39. J. Song, R. Leepipattanawit, W. M. Deng and R. M. Beaudry, "Hexanal vapor is a natural, metabolizable fungicide: Inhibition of fungal activity and enhancement of aroma biosynthesis in apple slices", *J. Am. Soc. Hort. Sci.*, **1996**, 121, 937-942.
40. J. J. Wolford, "Hexanal vapor to control decay of sliced apples in modified-atmosphere packages using metallocene film", *MS Thesis*, **1998**, Michigan State University, USA.
41. W. Utto, "Mathematical modelling of active packaging systems for horticultural products", *PhD Thesis*, **2008**, Massey University, New Zealand.
42. M. E. Saltveit and A. R. Sharaf, "Ethanol inhibits ripening of tomato fruit harvested at various degrees of ripeness without affecting subsequent quality", *J. Am. Soc. Hort. Sci.*, **1992**, 117, 793-798.
43. A. Rychter, H. W. Janes, C. K. Chin and C. Frenkel, "Effect of ethanol, acetaldehyde, acetic-acid, and ethylene on changes in respiration and respiratory metabolites in potato tubers", *Plant Physiol.*, **1979**, 64, 108-111.
44. K. L. Yam and D. S. Lee, "Design of modified atmosphere packaging for fresh produce", in "Active Food Packaging" (Ed. M. L. Rooney), Blackie Academic and Professional, Glasgow, **1995**, pp.55-73.
45. A. C. Cameron, P. C. Talasila and D. W. Joles, "Predicting film permeability needs for modified atmosphere packaging of lightly processed fruits and vegetables", *HortScience*, **1995**, 30, 25-34.
46. M. Serrano, D. Martinez-Romero, S. Castillo, F. Guillen and D. Valero, "The use of natural antifungal compounds improves the beneficial effect of MAP in sweet cherry storage", *Innov. Food Sci. Emerg. Technol.*, **2005**, 6, 115-123.
47. A. A. Kader, D. Zagory and E. L. Kerbel, "Modified atmosphere packaging of fruits and vegetables", *Crit. Rev. Food. Sci. Nutr.*, **1989**, 28, 1-30.

Maejo International Journal of Science and Technology

ISSN 1905-7873

Available online at www.mijst.mju.ac.th

Full Paper

On a fuzzy approach for the evaluation of golf players

Micael S. Couceiro^{1,2,*}, Fernando M. L. Martins^{3,4}, Filipe M. Clemente^{3,5}, Gonçalo Dias⁵ and Rui Mendes^{3,6}

¹Artificial Perception for Intelligent Systems and Robotics (AP4ISR), Institute of Systems and Robotics (ISR), University of Coimbra, Polo II, Coimbra, Portugal

²Ingeniarius, Lda., Mealhada, Portugal

³Polytechnic Institute of Coimbra, Coimbra College of Education, Department of Education, Portugal

⁴Institute of Telecommunications (Instituto de Telecomunicações) (IT), Covilhã, Portugal

⁵Faculty of Sport Sciences and Physical Education (FCDEF/CIDAF), University of Coimbra, Portugal

⁶Interdisciplinary Centre for the Study of Human Performance, Lisbon Technical University, Portugal

* Corresponding author, e-mail: micael@ingeniarius.pt

Received: 9 July 2013 / Accepted: 22 April 2014 / Published: 22 April 2014

Abstract: Athletes' performance may be complex to assess since multiple different metrics may be used to determine the overall performance. This paper proposes a novel fuzzy logic approach to evaluate players' accuracy in the golf putting context. This evaluation methodology merges three input parameters, namely the relative product metrics which are defined by the binary error, the radial error and the argument error. The proposed model herein is suitable to evaluate game context situations involving subjectivity, vagueness and imprecise information. Experimental results show that the evaluation of players' performance might be different than if we only had the aim of the golf game in mind, which involves placing the ball in the hole with as few shots as possible.

Keywords: golf, fuzzy logic approach, performance of golf players, golf putting

INTRODUCTION

Sports performance evaluation has been studied along diverse lines and within different disciplinary research frameworks, focusing on the analysis of players' behaviour (e.g. individual analysis) or teams who are part of a given competitive context (e.g. collective analysis) [1]. This has

afforded a broad scientific knowledge towards the development of new performance analysis methods [2].

However, the literature shows that sports evaluation is usually carried out in an analytical or standardised manner (e.g. batteries of physical tests or physiological and psychological analysis), or in a quantitative manner, viz. through technical-tactical indicators (e.g. match statistics). Despite their usefulness, these techniques are not enough to describe players' performance as a whole, bearing in mind that they only consider the 'cause-effect' linear actions resulting from athletes' actions or match situations [3]. For instance, one should better understand the meaning of having a golf ball finish before, after or in the vicinity of the hole, and to what extent this is truly meaningful and important for the putting performance. Moreover, it should be noted that the state of the art is scarce around this topic and does not clarify in any way the difference between a golf ball that stays in the $\pm 90^\circ$ lines or $\pm 180^\circ$ lines towards the hole. In other words, the literature does not provide any theoretical support for this research question, thus reinforcing the proposal of an alternative evaluation methodology.

It is important to further investigate these aspects that can be decisive in the golf-game outcome. Furthermore, this will demystify the role of the well-known *radial error* in the final evaluation of golf putting, as in many other sports movements, by merging it with other performance evaluation metrics, herein denoted as binary error and argument error. Since a unique, highly reliable and effective performance evaluation metric is crucial for assessing the athlete's potential and overall performance, a novel approach based on fuzzy logic has been introduced [4]. This metric merges all performance metrics relevant to achieve skill mastery and improve the execution of the task [5, 6].

Fuzzy logic was structured in 1965 by Zadeh [7] at the University of California, Berkeley to deal with and represent uncertainties. Fuzzy logic becomes important as our world is not made up of completely true or false facts and contemplates intermediate logical values between 'False' (0) and 'True' (1). This means that a diffuse logical value may be found in values between 0 and 1 [8]. Fuzzy logic has been used in several applications as a multiple-criteria analysis tool. The successful development of a fuzzy model is a complex multi-step process, in which the designer is faced with a large number of alternative implementation strategies and attributes [9]. Fuzzy logic addresses such applications perfectly as it resembles human decision-making, which can generate precise solutions from certain or approximate information.

This paper covers a large set of practical applications within the golf putting and proposes a fuzzified metric that can provide both quantitative and qualitative information. This metric shows that one can devise a 'memory' that objectively provides a trend of players' performance during the execution of a given task. In this case, the player is able to monitor the motor skill progress and correct product errors resulting from the putting performance. Furthermore, the proposed approach is extremely useful for measuring the performance fluctuations and irregularities of players, as well as assessing their individual motor skill characteristics.

Notation

N	Number of trials
n_i	Binary value of putting <i>Success</i>
η_B	Binary error metric
ε_i^x	Lateral error
ε_i^y	Longitudinal error

$\dot{\epsilon}_i$	Polar error
ϵ_i	Radial error module
θ_i	Argument error
μ_R	Radial error arithmetic mean
ϵ_{max}	Maximum radial error
η_R	Radial error metric
ρ_s	Spearman's rank correlation coefficient
η_θ	Argument error metric
μ_n	Binary error membership function
μ_ϵ	Radial error membership function
μ_θ	Argument error module membership function
μ_p	Consequent function of the putting performance

PERFORMANCE METRICS

This section presents three metrics to evaluate the golf putting accuracy, namely the binary error, the radial error and the argument error. The literature considers solely and explicitly the radial error as a strict measure of performance [10, 11]. The other metrics, namely the binary error and the argument error, are complementary to the radial error. The formalisation of these metrics aims at providing a comparison of the golf putting performance of various players.

Binary Error Evaluation

One way to evaluate the golf putting accuracy consists in computing the *binary error*. Despite not being denoted as such in the literature, this metric may be formalised based on theoretical assumptions around the disciplines of engineering, notably in the concepts inherent to binary logic [12]. Applying this logic to the golf putting performance, it is possible to evaluate the players' performance by quantifying the number of times that the ball entered the hole over the total number of trials of motor practice. For example, according to the binary logic (e.g. values 0 and 1), if the player succeeded in placing the ball into the hole, 1 would be regarded as *Success*; otherwise, the score value would be 0, i.e. *Failure*. In other words, this metric does not contemplate intermediate values [12].

In this work, we formalise this metric as:

$$\eta_B = \frac{1}{N} \sum_{i=1}^N r_i \quad (1)$$

where N is the total number of trials and r_i is the binary value that represents putting *Success*. That is, if the ball enters the hole, $r_i = 1$; otherwise, $r_i = 0$. However, considering the metric η_B , if the player scores as many times as he/she fails, the evaluation will be 0.5, thus completely disregarding how much he/she failed. Therefore, this result does not take into account the consistency of the player's performance, as he/she might still obtain a high score even if some of the trials were highly inaccurate.

Radial Error Evaluation

In recent studies focusing on the analysis of golf putting [6, 13, 14], the *radial error* has been used to examine the product measures derived from the motor performance of players. Through the analysis of both longitudinal and lateral errors, the studies obtained quantitative measures to evaluate the distance between the final position of the ball and the centre of the hole. When the player is able to place the ball into the hole, the error is considered 0 in both longitudinal and lateral components and consequently, the radial error is also 0.

In this context, a performance metric can be defined as the arithmetic mean of the radial error obtained in each trial:

$$\mu_R = \frac{1}{N} \sum_{i=1}^N \varepsilon_i \quad (2)$$

where ε_i is the radial error of trial i [15], which can be obtained from the application of the Pythagorean Theorem (Figure 1) as:

$$\varepsilon_i = \sqrt{(\varepsilon_i^x)^2 + (\varepsilon_i^y)^2} \quad (3)$$

Through the analysis of metric μ_R , we can conclude that the higher its value, the worse the putting accuracy performance becomes. From Figure 1 we can observe that the legs of the triangle are defined by the lateral error ε_i^x and the longitudinal error ε_i^y while the hypotenuse corresponds to the radial error ε_i .

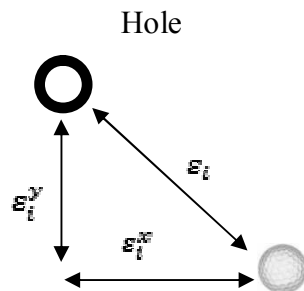


Figure 1. Representation of the three measured errors

However, by representing this metric as an absolute value, the inter-subject comparison is far from straightforward (cf. Results section). One way to overcome this constraint was presented in a previous study [15], which applied a normalised measure based on a maximum radial error ε_{max} , which depends on the evaluative and normative criteria (e.g. handicap, green limits and the player’s distance to the hole), being always superior or equal to the radial error ε_i for any trial i of any player, i.e. $\varepsilon_i \leq \varepsilon_{max} \forall i$. Thus, the relative metric η_R is obtained through the expression:

$$\eta_R = \frac{1}{N} \sum_{i=1}^N \left(1 - \frac{\varepsilon_i}{\varepsilon_{max}} \right) \quad (4)$$

Contrary to the previous metric from equation (1), η_R provides an ‘analogical’ evaluation of the putting accuracy, i.e. being not solely represented by the *Success* or *Failure* of this movement. It should be noted that a trial that promotes the placement of the ball inside the hole tends to be considered only slightly better than another which results in a ball close to it. This evaluation metric does not take into account all the ‘dynamics’ of the putting performance since the radial error may lead to an erroneous evaluation, thus concealing the obtained results. Unlike other

gestures (e.g. javelin throw), in golf putting the lateral error ε_i^x may not carry the same ‘weight’ as the longitudinal error ε_i^y in terms of putting performance.

Argument Error Evaluation

The concept adopted in this section dates back to the pioneering studies conducted by Isaac Newton, which paved the way to research around polar coordinates as we know them today [16]. From an operational point of view, a semi-straight line starting at the origin and any other point in the Cartesian plane (x, y) may be represented in the polar plane as a module (distance) and an argument (angle) [16]. In order to evaluate the putting accuracy performance, we herein propose a new evaluation metric that considers the radial error as the module (absolute value) of an error (denoted as polar error) represented in the polar coordinate system as:

$$\tilde{\varepsilon}_i = \varepsilon_i \angle \theta_i \quad (5)$$

where the argument θ_i is obtained through the conversion of the Cartesian coordinate system $(\varepsilon_i^x, \varepsilon_i^y)$ into the polar coordinate system $(\varepsilon_i, \theta_i)$, θ_i being obtained with the arc tangent variation *atan2* function.

Through the conversion from Cartesian coordinates to polar coordinates, one can obtain the quadrant where the ball is located at the end of each trial of motor practice, as well as the circular positions around the origin (hole), as shown in Figure 2. It should be noted that the y -axis is aligned with the line defined by the exit point of the ball (i.e. where the moment of the putter’s impact with the ball takes place) and the centre of the hole. On the other hand, the x -axis is perpendicular to the y -axis and aligned with the centre of the hole.

Considering the example from Figure 2, one can observe that balls 1 and 2 are of the same distance from the hole, i.e. $\varepsilon_1 = \varepsilon_2$. However, ball 2 is located in the first quadrant, closer to the 0° line with $\theta_2 = 10^\circ$, while ball 1 is located in the second quadrant, closer to the 90° line with $\theta_1 = 100^\circ$. The question is which of the two situations represents a better performance in terms of putting accuracy.

The metrics defined in equations (2) and (4) represent the same accuracy for the example depicted in Figure 2: in neither of the two cases did the balls enter the hole and both are at the same distance from it. Nevertheless, although not explicitly discussed in the literature [9, 10, 17], a player’s performance tends to be considered ‘worse’ when the ball finishes closer to the line that separates the first quadrant from the fourth and the second quadrant from the third, i.e. the x -axis line. Put it differently, it is preferable to obtain angles closer to 90° rather than angles closer to $\pm 180^\circ$.

As previously stated, the lateral error ε_i^x proves to be more ‘critical’ than the positive longitudinal error ε_i^y . This means that combining the analysis of both the radial error ε_i and the argument of radial error θ_i , it is possible to determine whether the accuracy of a given trial is better than the other. Given the same example from Figure 2, we can conclude that the putting accuracy represented by ball 1 is higher than that represented by ball 2. It may also be observed that the putting accuracy represented by ball 3 is lowest, even taking into account that $\varepsilon_3 < \varepsilon_1$, as this ball is placed in the fourth quadrant with $\theta_3 = 280^\circ$.

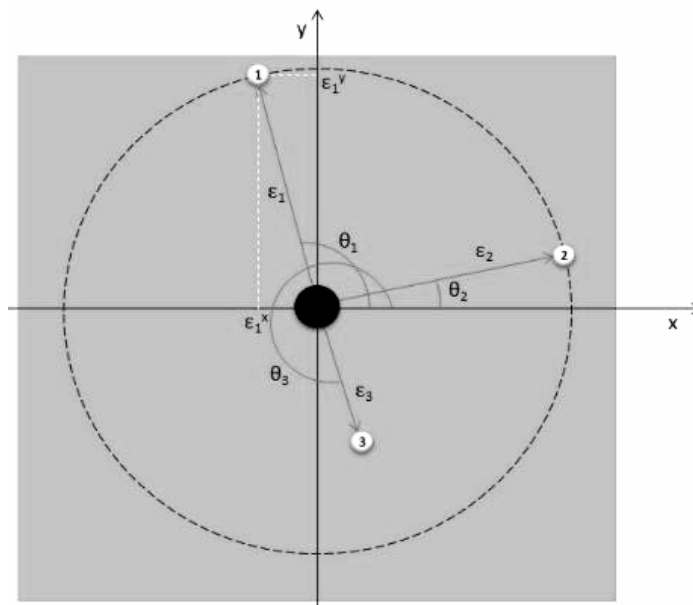


Figure 2. Graphic representation of Cartesian and polar coordinate systems around the centre of the hole

In order to compare the accuracy performance using the argument error, as before, a novel relative metric is proposed:

$$\eta_{\theta} = \frac{1}{N} \sum_{i=1}^N \left(1 - \frac{||\theta_i| - 90|}{90} \right) \quad (6)$$

To further improve the feasibility of this proposed approach, a Spearman’s rank correlation test [18] was carried out between 10 golf players’ handicap and their argument error, η_{θ} . This study consisted of 30 trials performed by each player at 4 metres from the hole without any constraints. A Spearman’s rank correlation coefficient of $\rho_s = -0.4893$ was obtained, thus allowing the observation of a decreasing monotonic trend between players’ handicap and their accuracy performance through the angular position of the balls. In other words, one can consider that as handicap decreases, putters finish closer to the 90° line.

Nevertheless, the fact that there are multiple evaluation metrics to determine a player’s performance increases the complexity of the selection process. Due to the ‘dynamics’ of the putting performance, it may not be sufficient to consider each evaluation metric independently. It is therefore extremely important to find a way to evaluate a player’s performance and simultaneously ponder the binary metric (if the ball enters the hole or not), the radial error (if it does not enter the hole, how far is it), and the argument error (if the ball does not enter the hole, what is its angular location?). Consequently, it is based on a fuzzy approach, introduced in the next section, that we will evaluate the overall performance accuracy associated with the golf putting.

FUZZY APPROACH

In the specific case of this work, it is possible through fuzzy logic to transform quantitative variables into qualitative ones by describing not only the ‘total’ error obtained by the player, but also the extent of his/her failure in the same trial. In order to do so, this research considers three inputs for the diffuse system, which are defined by the three measures previously introduced, namely binary error, radial error and argument error.

The membership function of the binary error is represented by a unitary crisp membership function as shown in equation (7) and Figure 3. In other words, the value 0 is ascribed for an unsuccessful shot (*Failure*) and for a successful one (*Success*) the value 1 is ascribed. It should be noted that this method has been used in the analysis of dynamic systems, namely artificial intelligence [9].

$$\mu_n(n_i) = \begin{cases} 0 & , n_i = 0 \\ 1 & , n_i = 1 \end{cases} \quad (7)$$

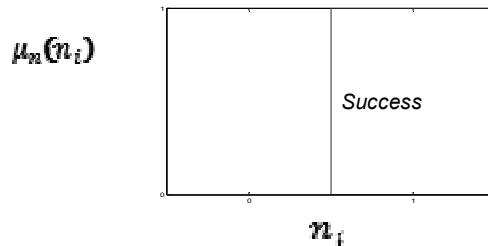


Figure 3. Binary error membership function

The membership function of the radial error may be represented as a special case of a triangular membership function (Figure 4). The smaller the radial error is, the closer the ball will be to the hole. This function may be represented as shown in equation (8):

$$\mu_\varepsilon(\varepsilon_i) = \begin{cases} \frac{\beta - \varepsilon_i}{\beta} & , \varepsilon_i \leq \beta \\ 0 & , \varepsilon_i > \beta \end{cases} \quad (8)$$

where parameter β is equal to ε_{max} (cf. equation (4)), which, as previously stated, may be related with the green's size or the highest radial error recorded from all trials.

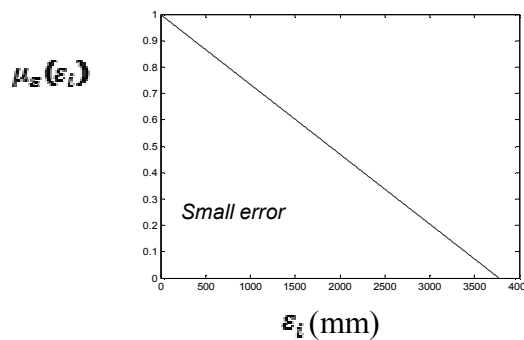


Figure 4. Radial error membership function

The membership function of the argument error is defined by a generalised bell-shaped function as shown in Figure 5. This function has one more parameter than the Gaussian function typically used:

$$\mu_\theta(|\theta_i|) = \frac{1}{\left[1 + \frac{(|\theta_i| - c)^2}{a}\right]^{ab}} \quad (9)$$

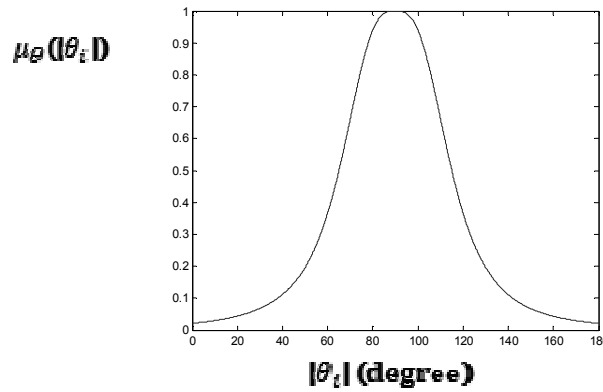


Figure 5. Argument error module membership function

We decided to use the absolute value of the argument error, $|\theta_i|$, as input, considering negative angles (third and fourth quadrants) as having the same evaluation as positive angles (first and second quadrants). Parameters a , b and c are defined considering that a ball situated on the 90° line (right angle) has the maximum performance value as to the argument error, whereas a ball closer to the 0° or 180° line (i.e. between the first and fourth quadrants and between the second and third quadrants respectively) represents a shot with a lower performance as to the argument error. Using Matlab's Fuzzy Logic Toolbox [1], equation (9) is parameterised with $a = 25$, $b = 1.5$, $c = 90$.

For defuzzification, we considered Mamdani's implication [7] with the lowest (first) of the maxima. Basically, two diffuse IF-THEN rules allow the classification of a given putting trial in terms of overall performance p_i as:

IF n_i is *Success* **THEN** p_i is *Accurate* with weight 1

ELSE-IF ε_i is *Small* **AND** $|\theta_i|$ is *Right* **THEN** p_i is *Accurate* with weight 0.8

The first rule is the most relevant to classifying the putting success as it represents the performance metric of the golf player, contemplating whether or not the ball enters the hole. If it does, $n_i = 1$; then all other variables are irrelevant and the shot will be classified as *Accurate*, i.e. $p_i = 1$. On the other hand, if the ball does not enter the hole, $n_i = 0$, and the radial error needs to be pondered. It was decided that the weight of this second rule should be 0.8: the moment the player does not hit the hole, the putting is considered to have, at best, an accuracy of 80%, i.e. $p_i = 0.8$.

As to the radial error, we know that the higher it is, the worse the player's performance becomes. However, this relation can only be considered linear if the argument error remains constant. If the argument error module comes close to the limits of $\pm 180^\circ$, the putting will be considered to have a lower performance and consequently a lower accuracy. The question here is: *How accurate will the putting be when the radial error argument varies?*

This relation cannot be considered linear because of the features inherent to the putting execution. This means that the **AND** connective cannot be considered as usual, viz. only by considering the minimum or the product between $\mu_\varepsilon(\varepsilon_i)$ and $\mu_\theta(|\theta_i|)$. A new **AND** connective is then proposed to relate both membership functions while maintaining the relation previously addressed:

$$\mathbf{AND} = \mu_\varepsilon(\varepsilon_i) \times \mu_\theta(|\theta_i|)^{1-\mu_\varepsilon(\varepsilon_i)} \quad (10)$$

As a result, the lower the radial error is, i.e. $\mu_\varepsilon(\varepsilon_i) \approx 1$, the lower the influence of the argument error module results, and vice-versa.

Finally, the consequent function is defined as follows:

$$\mu_p(p_i) = \begin{cases} p_i, & \varepsilon_i \geq 0 \\ 0, & \varepsilon_i < 0 \end{cases} \quad (11)$$

where $\mu_p(p_i)$ is the overall accuracy performance evaluation of trial i (Figure 6).

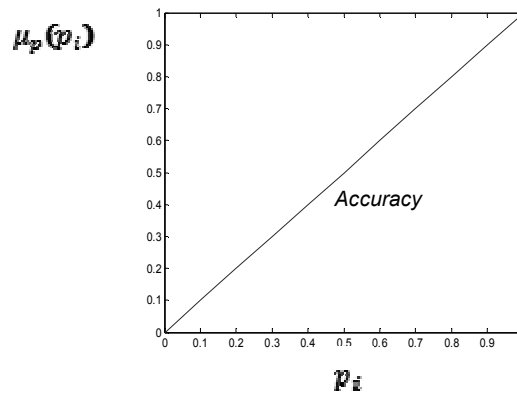


Figure 6. Consequent function of the putting performance

In order to understand the metric of the evaluation proposed, we shall consider the following example. Two golf players executed two trials each. Player 1 was able to hit the ball in the first trial: $\varepsilon_1^1 = 0$, but obtained the highest radial error of all the trials in the second shot, with an argument error of 0° : $\dot{\varepsilon}_2^1 = \varepsilon_{max} \angle 0^\circ$. Player 2 failed both trials with a radial error 10 times lower than ε_{max} , having obtained an argument error of 90° in the first trial and 0° in the second trial: $\dot{\varepsilon}_1^2 = \frac{\varepsilon_{max}}{10} \angle 90^\circ$ and $\dot{\varepsilon}_2^2 = \frac{\varepsilon_{max}}{10} \angle 0^\circ$.

In this situation the scenario would be the following. As regards the binary error, player 1 would have a higher performance than that of player 2, as he/she was able to place the first ball into the hole, viz. $\eta_B^1 = 0.5 > \eta_B^2 = 0$. As regards the radial error, player 2 would be the best, with $\eta_R^2 = 0.9 > \eta_R^1 = 0.5$. Both players would present the same performance as to the argument error, with $\eta_\theta^1 = \eta_\theta^2 = 0.5$.

Given the current context, by benefiting from the fuzzy evaluation proposed in this section, we obtain $\mu_p^1 = 0.5 > \mu_p^2 = 0.36$. This means that player 1 had a 14% higher performance than player 2.

The following section compares the performance of several expert players by benefiting from the diverse metrics presented in this work.

EXPERIMENTAL RESULTS

The performance metrics previously presented were evaluated considering 10 male golfers who were adults (aged 33.8 ± 11.9), volunteers, right-handed and experts (10.8 ± 5.4 handicap). An artificial plain green carpet 10 m long, 2 m wide and 4 mm thick [15] used by Minigolf professionals, rectangular with no flaws, quite similar to the green's natural surface texture was used.

A real golf hole was placed at 3.5 m from the carpet ending and 1 m from each lateral extremity. Three black dots marked the putting and were placed at 2 m ($D1$), 3 m ($D2$) and 4 m ($D3$). The dots were in the same direction as the hole at 1 m from each lateral extremity of the

carpet. A ramp 1 m long was placed under the carpet, levelling up the carpet surface to a height of 10 cm. A straight platform 4 m long was placed immediately after the ramp to keep that same height.

The ball's trajectory was tracked using a digital camera placed on a tripod 1.55 m high with an inclination of 22° pointing down. The camera was shot at 30 frames/sec. with a resolution of 1280×720 pixels and a focal length of 26 mm. In order to assist in the data analysis and convert the virtual into real coordinates, 13 reference points were marked on the carpet.

Three studies were designed. In the first study (*E1*), 30 trials were performed at 1, 2, 3 and 4 m away from the hole without any constraint (without ramp). In the second study (*E2*), 30 trials were performed at 2, 3 and 4 m away from the hole, with a constraint imposed by the ramp. In the third and last study (*E3*), 30 trials were performed at 2 m away from the hole with a constraint imposed by the ramp and an angle of 25° to the left and right of the hole.

Binary Evaluation

Figure 7 shows the players' performance throughout the 3 experimental studies by only considering the binary error metric. Player 1 shows the best performance. He obtained a success rate of 83%, succeeding in placing 83% of the balls into the hole. Player 1 is closely followed by players 4 and 9, while player 2 presents the worst performance.

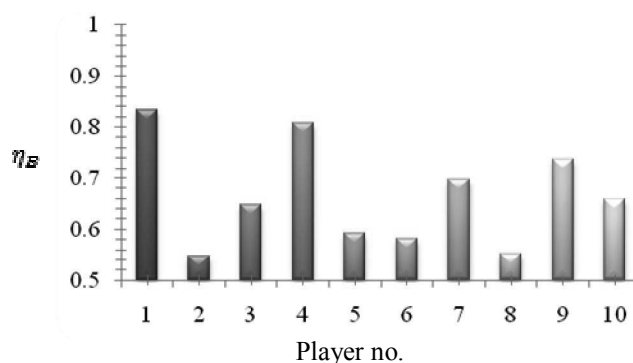


Figure 7. Binary evaluation of the players in 3 experimental studies

Radial Error Evaluation

Taking into account the radial error, Figure 8 shows the players' performance throughout the 3 experimental studies. In this study a maximum threshold value is found for player 8: $\beta = \epsilon_{max} = 3778 \text{ mm}$. The lowest radial error is found for player 4, who comes closer to 1. Players 9 and 1 closely follow player 4. Finally, player 8 clearly shows the worst performance.

Argument Error Evaluation

Figure 9 shows the players' performance throughout the 3 experimental studies by only considering the argument error. One may observe that player 1 shows the best performance, being closer to 1. Players 7 and 8 follow, with player 2 having the worst performance.

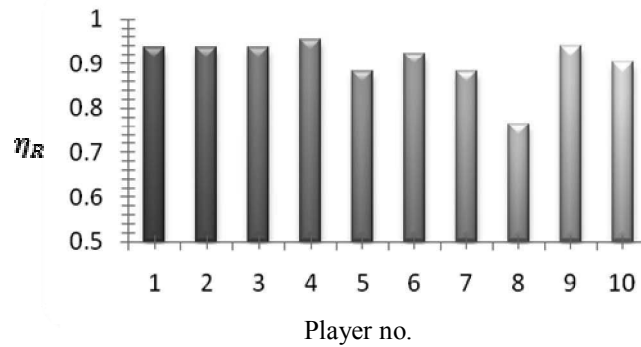


Figure 8. Radial error evaluation of the players in 3 experimental studies

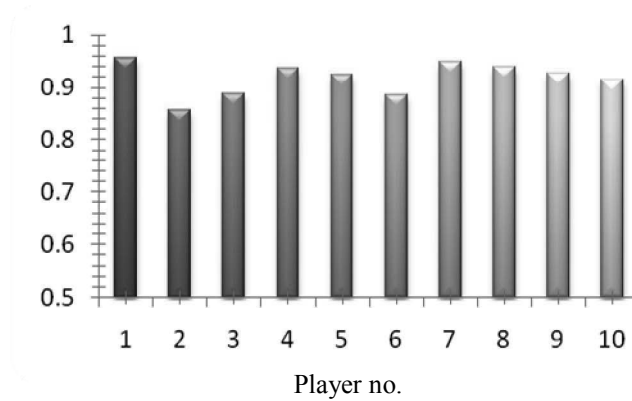


Figure 9. Argument error evaluation of the players in 3 experimental studies

Fuzzy Evaluation

To evaluate players using fuzzy logic, we benefited from the Fuzzy Inference System Editor of the Fuzzy Logic Toolbox [1]. Complementing the information previously presented, Figure 10 and Table 1 depict the players’ performance throughout the 3 experimental studies relying on diffuse information.

In the first study player 1 achieves the best performance, followed by players 4 and 9. Player 8 shows the worst performance. In the second study player 3 achieves the best performance, followed by players 10 and 4. The data also show that faced with a constraint (ramp/slope), the accuracy performance of player 1 tends to decrease considerably when compared with the performance of player 4. Player 8 shows the worst performance. In the last study player 5 shows the best performance, placing about 75% of the balls in the hole. Players 6 and 7 follow player 5. Again, player 8 shows the worst performance. Player 4 obtains the best performance in the 3 studies (Figure 10), followed by players 1 and 9. Finally, player 8 shows the worst performance (TOTAL row from Table 1).

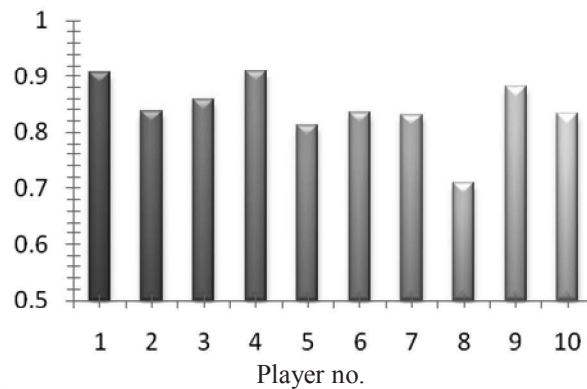


Figure 10. Fuzzy evaluation of players in 3 experimental studies

Table 1. Evaluation of fuzzy performance obtained by players throughout 3 experimental studies

Study	S01	S02	S03	S04	S05	S06	S07	S08	S09	S10
E1_1m	1.0000	1.0000	1.0000	1.0000	1.0000	1.0000	1.0000	1.0000	0.9787	1.0000
E1_2m	0.9847	0.8947	0.9517	0.9757	0.8590	0.8290	0.8807	0.7917	0.9640	0.8923
E1_3m	1.0000	0.7850	0.7700	0.9860	0.7260	0.7703	0.8510	0.7657	0.9530	0.8633
E1_4m	1.0000	0.7407	0.8050	0.9367	0.8047	0.7340	0.8503	0.4550	10.000	0.6267
E1	0.9962	0.8551	0.8817	0.9746	0.8474	0.8333	0.8955	0.7531	0.9739	0.8456
E2_2m	0.9413	0.9320	0.9610	0.9647	0.8400	0.9507	0.9277	0.8820	0.9493	0.9477
E2_3m	0.9273	0.8820	0.9847	0.9777	0.8323	0.8757	0.8270	0.6777	0.8587	0.9713
E2_4m	0.8657	0.8380	0.9033	0.8953	0.7133	0.8320	0.6153	0.5763	0.8307	0.9327
E2	0.9114	0.8840	0.9497	0.9459	0.7952	0.8861	0.7900	0.7120	0.8796	0.9506
E3_ang1	0.8237	0.7523	0.7843	0.6923	0.7763	0.7407	0.7710	0.6747	0.7447	0.6823
E3_ang2	0.6157	0.7027	0.5533	0.7553	0.7590	0.7827	0.7490	0.5550	0.6437	0.5753
E3	0.7197	0.7275	0.6688	0.7238	0.7677	0.7617	0.7600	0.6148	0.6942	0.6288
TOTAL	0.9065	0.8364	0.8570	0.9093	0.8123	0.8350	0.8302	0.7087	0.8803	0.8324

Note: E1_1m = study 1: 1 metre; E1_2m = study 1: 2 metres; E1_3m = study 1: 3 metres; E1_4m = study 1: 4 metres; E2_2m = study 2: 2 metres; E2_3m = study 2: 3 metres; E2_4m = study 2: 4 metres; E3_ang1 = study 3 (angle 1 – left); E3_ang2 = study 3 (angle 2 - right); S01 = player 1; S02 = player 2, etc.

DISCUSSION AND CONCLUSIONS

Considering the previously presented results, it is important to retrieve as much information as possible about the putting execution so as to understand how this methods can be applied to the sports training context. If we only consider the aim of the golf game in mind, which involves placing the ball in the hole with as few shots as possible, player 1 would be considered as the best performer (cf. binary error) followed by players 4 and 9. However, if one considers the performance evaluation as regards a fuzzy logic accuracy, viz. the simultaneous analysis of the binary error, the radial error and the argument error, player 4 is the one presenting the best performance, followed by players 1 and 9.

The use of the proposed metric is suitable in evaluating situations that involve subjectivity, vagueness and imprecise information. However, the success of a fuzzy-based engine relies on the experience of selecting an adequate membership function. Therefore, an expert knowledge about the task is required in order to validate the proposed rules and membership functions. In other

words, fuzzy systems need expert experience to strengthen the decision rules and to handle imprecise value in its reasoning.

This approach brings implications to the area of sports training since it aims at providing a deeper understanding of players' flaws [5]. The approach is truly important mainly in a coaching perspective to avoid overusing standard metrics that lack relevant information about a given gesture [19]. For instance, although player 1 was the best performing player most of the time, his overall performance significantly dropped when both ramp and slope constraints were added. In that sense, this multidisciplinary approach provides for the understanding of the golf putting and the acquisition of the necessary information during training and competition. Meanwhile, fuzzy logic has practical applications in other individual and team sports (e.g. tennis, football and basketball) that can benefit from this type of fuzzified metric with both quantitative and qualitative information, being mainly useful in following the performance trend of athletes' motor behaviour. Such techniques are equally effective in assessing how the athlete can stabilise his/her performance by exploring different levels of variability and complexity. Moreover, this approach is extremely useful for measuring the performance fluctuations and irregularities of both novices and experts, as well as for assessing their individual motor skill characteristics and profiles [17].

Operationally, this study introduces new evaluation metrics that are relevant in sports so as to measure the performance of athletes in laboratory and real situations for both teaching and learning. Specifically in the golf putting context, these metrics show that it is possible to devise a 'memory' that objectively provides a trend of players' performance during the execution of the task. In this case the player is able to monitor his/her motor progress and correct errors resulting from the putting performance. Moreover, the metrics also allow quantifying the result of the action and the direction of the error in the context of training and competition [17].

However, in order to consolidate the conclusions obtained in this work, it might be necessary to extend this type of metrics to other sports. In this case, and given the complexity of such extension, an interdisciplinary approach covering several areas of knowledge such as sport sciences, mathematics and engineering is proposed. The scientific contributions emerging from this interdisciplinary work can help to further understand the 'mechanics' connecting fuzzy logic to sports.

ACKNOWLEDGEMENTS

This work was supported by a PhD scholarship (SFRH/BD /73382/2010) granted to the first author by the Portuguese Foundation for Science and Technology (FCT) and the Institute of Systems and Robotics (ISR). The authors also thank the Coimbra College of Education (ESEC) and the Instituto de Telecomunicações (IT) for providing the facilities and equipment for this study. This work was also supported by the Instituto de Telecomunicações, granted by the Portuguese Foundation for Science and Technology (FCT) with the ref. PEst-OE/EEI/LA0008/2013.

REFERENCES

1. T. McGarry, D. I. Anderson, S. A. Wallace, M. D. Hughes and I. M. Franks, "Sport competition as a dynamical self-organizing system", *J. Sports Sci.*, **2002**, 20, 771-781.
2. P. O'Donoghue, "Time-motion analysis", in "The Essentials of Performance Analysis: An Introduction" (Ed. M. Hughes and I. Franks), Routledge, London, **2008**, pp.180-205.
3. M. Pidwirny, "Definitions of systems and models: fundamentals of physical geography", **2011**, <http://www.physicalgeography.net/fundamentals/4b.html> (Accessed: July 2011).

4. M. Othman, K. R. Ku-Mahamud and A. A. Bakar, "Fuzzy evaluation method using fuzzy rule approach in multicriteria analysis", *Yugosl. J. Oper. Res.*, **2008**, 18, 95-107.
5. B. Kolev, P. Chountas, I. Petrounias and V. Kodogiannis, "An application of intuitionistic fuzzy relational databases in football match result predictions", *Adv. Soft Comput.*, **2005**, 2, 281-289.
6. E. R. Komi, J. R. Roberts and S. J. Rothberg, "Measurement and analysis of grip force during a golf shot", *J. Sports Eng. Technol.*, **2008**, 222, 23-35.
7. L.A. Zadeh, "Fuzzy sets", *Inform. Control*, **1965**, 8, 338-353.
8. E. Cox, "The Fuzzy Systems Handbook: A Practitioner's Guide to Building, Using and Maintaining Fuzzy Systems", Academic Press, Boston, **1994**, pp.35-38.
9. W. Pedrycz and F. Gomide, "Fuzzy Systems Engineering: Toward Human-Centric Computing", Wiley-IEEE Press, **2007**, pp.67-99.
10. D. Pelz, "Putting Bible: The Complete Guide to Mastering the Green", Doubleday, New York, **2000**.
11. S. J. Mackenzie and D. B. Evans, "Validity and reliability of a new method for measuring putting stroke kinematics using the TOM11 system", *J. Sports Sci.*, **2010**, 8, 1-9.
12. J. M. Garibaldi and E. C. Ifeakor, "Application of simulated annealing fuzzy model tuning to umbilical cord acid-base interpretation", *IEEE Trans. Fuzzy Syst.*, **1999**, 7, 72-84.
13. N. C. A. da Costa, L. J. Henschen, J. J. Lu and V. S. Subrahmanian, "Automatic theorem proving in paraconsistent logics: Theory and implementation", Proceedings of 10th International Conference on Automated Deduction, New York, USA, **1990**, pp.72-86.
14. R. Mendes, R. Martins and G. Dias, "Effects of a contextual interference continuum on golf putting task", in "Book of Abstracts do XIII Annual Congress of the European College of Sport Science" (Ed. J. Cabri, F. Alves, D. Araújo, J. Barreiros, J. Diniz and A. Veloso), Faculty of Human Kinetics (University of Lisbon), Lisbon, **2008**, pp.325-326.
15. R. Mendes, G. Dias and S. Chiviawsky, "Contextual interference continuum on golf putting task", *Braz. J. Motor Behav.*, **2010**, 5, 21-22.
16. J. Stewart, "Calculus: Early Transcendental", McGraw Hill, New York, **2007**, pp.635-688.
17. M. S. Couceiro, G. Dias, F. M. L. Martins and J. M. A. Luz, "Towards a correction metric to the putting lip-out", Proceedings Symposium on Fractional Signals and Systems, **2011**, Coimbra, Portugal, Vol. 1, pp.138-146.
18. J. Pallant, "SPSS Survival Manual: A Step by Step Guide to Data Analysis Using the SPSS Program", Allen and Unwin, Crows Nest (Australia), **2011**, pp.102-120.
19. G. Dias and R. Mendes, "Effects of a contextual interference continuum on golf putting task", *Rev. Bras. Educ. Fís. Esporte*, **2010**, 24, 545-553.

Maejo International Journal of Science and Technology

ISSN 1905-7873

Available online at www.mijst.mju.ac.th

Full Paper

Cultivation options for indoor and outdoor growth of *Chaetoceros gracilis* with airlift photobioreactors

Watadta Ritcharoen¹, Puchong Sriouam¹, Piyanate Nakseedee¹, Patthama Sang¹, Sorawit Powtongsook², Kunn Kungvansaichol³ and Prasert Pavasant^{1,*}

¹ Chemical Engineering Research Unit for Value Adding of Bioresources, Department of Chemical Engineering, Faculty of Engineering, Chulalongkorn University, Bangkok, 10330, Thailand

² National Centre for Genetic Engineering and Biotechnology, National Science and Technology Development Agency, Phatum Thani 12120, Thailand

³ PTT Research and Technology Institute, PhraNakhon Si Ayutthaya, 13170, Thailand

* Corresponding author, email: prasert.p@chula.ac.th

Received: 12 February 2013 / Accepted: 24 April 2014 / Published: 29 April 2014

Abstract: Various configurations and modes of airlift photobioreactors were examined in the cultivation of *Chaetoceros gracilis*. Internal loop and external loop airlifts were cultivated in a batch mode in a controlled indoor environment. The external loop system provided a better performance than the internal loop system due to better light exposure. A continuous operation was conducted in an internal loop airlift photobioreactors-in-series. This was designed to minimise the effect of light blocking due to overgrown cells as the high-density culture was, in this configuration, only limited to the last airlift column in the series. Outdoor large-scale operation was conducted in a flat-panel airlift photobioreactor. Due to uneven light availability, the outdoor culture could not perform as well as the indoor one in terms of growth rate. Among the four systems investigated, the continuous culture in airlift photobioreactors-in-series provided the best performance with the highest cell density of 12.12×10^6 cells mL⁻¹. Cost analysis based on the maximum number of reactors that can be installed in one square metre indicates that the indoor system requires lowest operating cost per unit cultivation area, whereas the outdoor system provides highest profit as a result of the inherited large productivity.

Keywords: *Chaetoceros gracilis*, indoor culture, outdoor culture, airlift photobioreactor

INTRODUCTION

Chaetoceros gracilis is one of the most popular diatoms in Thailand and is used in feeding shrimp larvae. Conventionally, this diatom is cultivated in open pond systems in which an inherent

low specific growth rate allows an easy contamination by foreign, faster growing microorganisms. Closed bioreactor systems are often proposed as alternatives, where not only the well-defined environment facilitates the control of contaminants, but also the various important environment parameters (light intensity, temperature, etc.) can be manipulated to suit the growth of each individual species. Examples of such closed systems include flat plate/panel [1-3], tubular [4, 5], helical flow [6, 7] and airlift [8]. Airlift photobioreactors attract considerable attention as an alternative bioreactor for microorganisms such as *Tetrahymena thermophila* [9], *Haematococcus pluvialis* [10, 11] and *Chaetoceros calcitrans* [12, 13]. The use of airlift is recommended for the cultivation of algae as it allows a more effective circulation of cells, which enhances light exposure [12, 14] and effectively maintains microalgal suspension with reasonably low energy requirement [15, 16]. In addition, Issarapayup et al. [2] showed that a flat-panel airlift photobioreactor (FPAP) can be easily scaled up by extending the length of reactor without losing algal growth performance.

Outdoor cultivation of microalgae is suitable for large-scale culture and the future development of most microalgal applications will need to have a reliable and economical industrial-scale cultivation process. Sunlight as a light source reduces the operating cost and electricity consumption by as much as 2.5 times when compared with the system with artificial lighting [17, 18]. An outdoor pond may need a circulation cascade to increase light exposure of microalgae [19]. However, outdoor condition is still quite difficult to control, and the productivity of microalgae is typically variable with seasons [17, 19, 20]. The performance of the photobioreactors can still be improved by the design of the set-up and manipulation of the operation of the system. This work demonstrates how different designs of the airlift photobioreactor affect both indoor and outdoor cultivation of *Chaetoceros gracilis*.

MATERIALS AND METHODS

Preparation of Stock Culture

The original inoculum of *C. gracilis* was obtained from the Department of Aquaculture, Faculty of Fisheries, Kasetsart University. The stock culture was prepared by inoculating the diatom in the sterile modified F/2 medium incubated at 121°C [12]. The culture was then transferred to 250 mL of the medium in a 500-mL flask and inoculated until the cell concentration reached approximately 4×10^6 cells mL⁻¹. It was finally scaled up to 1,000 mL and 17 L and then transferred to the large-scale airlift photobioreactors.

Design Options for Indoor Cultivation

Batch culture

Two types of 17-L airlift photobioreactors were employed. They were made from clear acrylic plastic to allow light passage through the column. The internal-loop airlift photobioreactor (IAP) has a draft tube installed centrally within the outer column, which separates the downcomer from the riser (Figure 1(a) and Table 1). The 17-L external-loop airlift photobioreactor (EAP) consists of two vertical tubes operating as the riser and the downcomer, both with the height of 190 cm (Figure 1 (b)). The 5.4-cm-diameter riser is connected to the 10.4-cm-diameter downcomer near the top and the bottom of the system. Batch culture, both in IAP and EAP, was operated in a well-ventilated room where the temperature was maintained at 30±2°C. The system was sterilised using sodium dichloroisocyanurate. After two days, residual chlorine was neutralised with sodium thiosulphate. An initial cell concentration was prepared at 1×10^5 cells mL⁻¹ for all experiments. A calibrated flow meter (rotameter) was used to control the volume of gas flow supplied to the system

through a porous gas sparger attached to the base of the column, where the superficial gas velocity (u_{sg}) was controlled at 3 cm s^{-1} . Fluorescent light bulbs (36 watt) were provided on the outer surface of the column to supply light necessary for photosynthesis. The light intensity at the reactor surface was controlled at approximately 10,000 Lux ($135 \mu\text{mol photon m}^{-2}\text{s}^{-1}$). In this experiment, the light source was placed 10 cm away from the surface of the reactor and the intensity was adjusted by adding the shade between the light and the column. The light intensity was measured with a digital light meter (DT-1309, CEM, Shenzhen Everbest Machinery Industry Co. Ltd., China).

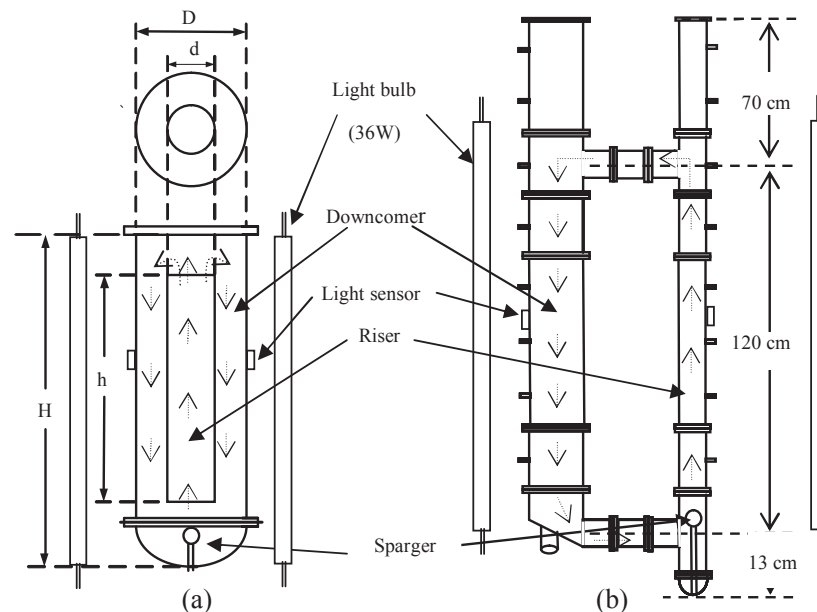


Figure 1. Experimental set-up for the cultivation of *C. gracilis* in airlift photobioreactor: (a) IAP and continuous airlift photobioreactor (CAP); (b) EAP. Arrows indicate flow direction.

Table 1. Dimensions of airlift photobioreactor (IAP and CAP)

Parameter	Dimension (cm)	
	IAP	CAP
Column outside diameter (D)	15	10
Draft tube outside diameter (d)	8	5
Column and draft tube thickness	0.3	0.3
Column height (H)	120	60
Draft tube height (h)	100	40

Continuous culture

The continuous airlift photobioreactor (CAP) with the size of 3 L (dimension given in Table 1) was used with fluorescent light bulbs (18 watt) being on both sides of the column with average light intensity at the centre of the column of approximately $135 \mu\text{mol photon m}^{-2}\text{s}^{-1}$. A few designs of CAP are proposed as illustrated in Figure 2. The first configuration is the single column (System I), which was used as a control experiment. System II is operated with two CAPs connected in series, whereas System III is one with three connected columns. In all configurations, the system was first cultivated as a batch culture with only the first CAP (Column I) operated with an initial cell concentration of approx $1 \times 10^5 \text{ cells mL}^{-1}$. When the growth of the diatom reached the mid-

exponential phase, the columns were then connected in series (two columns for System II and three for System III) and sterilised modified F/2 medium was fed into the first column using a peristaltic pump with the overflow stream to control the total volume at 3 L in each CAP. A medium feed rate was varied as indicated in Table 2. A calibrated flow meter (rotameter) was used to control the air volumetric flow rate supplied to the system through a porous gas sparger at the base of the column, with a superficial gas velocity (u_{sg}) of 3 cm s^{-1} .

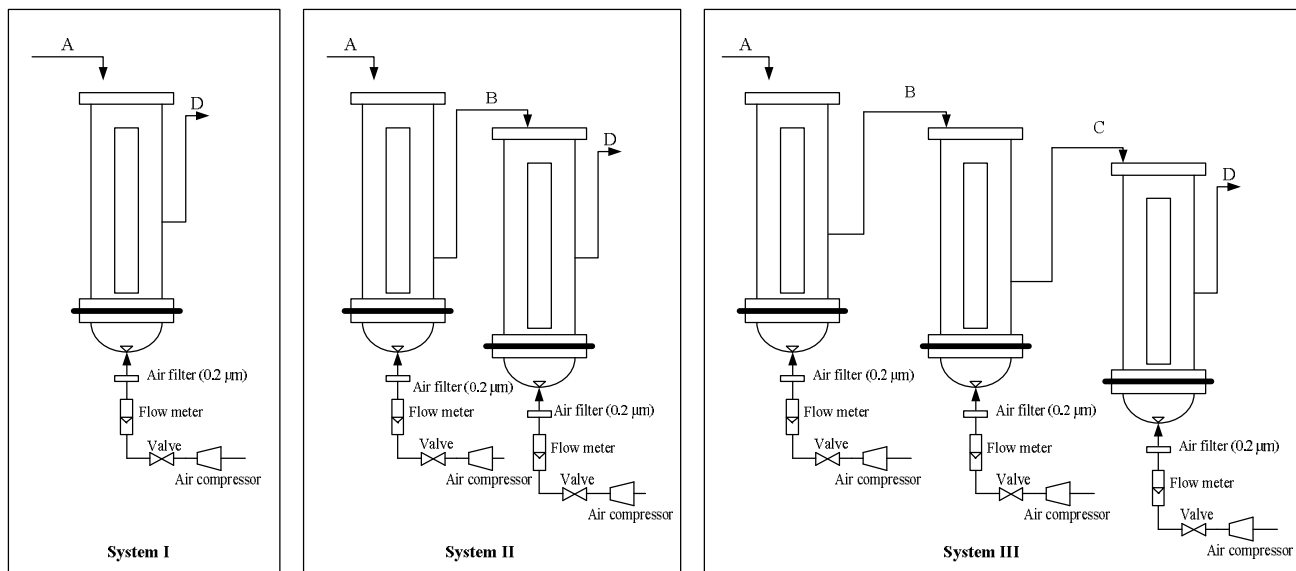


Figure 2. Experimental set-up for the cultivation of *C. gracilis* in CAPs-in-series

Table 2. Operating conditions for CAPs-in-series

Experiment	System	Medium feed rate (mL min^{-1})			
		Stream A	Stream B	Stream C	Stream D
Set 1	I	1	-	-	Overflow
Set 2	I	2	-	-	Overflow
Set 3	I	3	-	-	Overflow
Set 4	II	2	2	-	Overflow
Set 5	II	4	4	-	Overflow
Set 6	II	6	6	-	Overflow
Set 7	III	3	3	3	Overflow
Set 8	III	6	6	6	Overflow
Set 9	III	9	9	9	Overflow

Design Options for Outdoor Cultivation

Flat-panel (100 L) airlift photobioreactors (FPAPs) were set up as an outdoor IAP (Figure 3 and Table 3). Aeration with an overall superficial velocity (u_{sg}) of 3 cm s^{-1} was provided through a series of spargers which were installed 6 cm apart at the bottom of the reactor. The light intensity was measured with a light sensor (Vernier Labquest, with data logger), whereas the temperature was measured via a thermocouple (IP67, Hanna instrument Inc., with data logger). The operation of

these large-scale airlifts was carried out under three climate conditions, i.e. Period I (summer), Period II (rainy season) and Period III (winter).

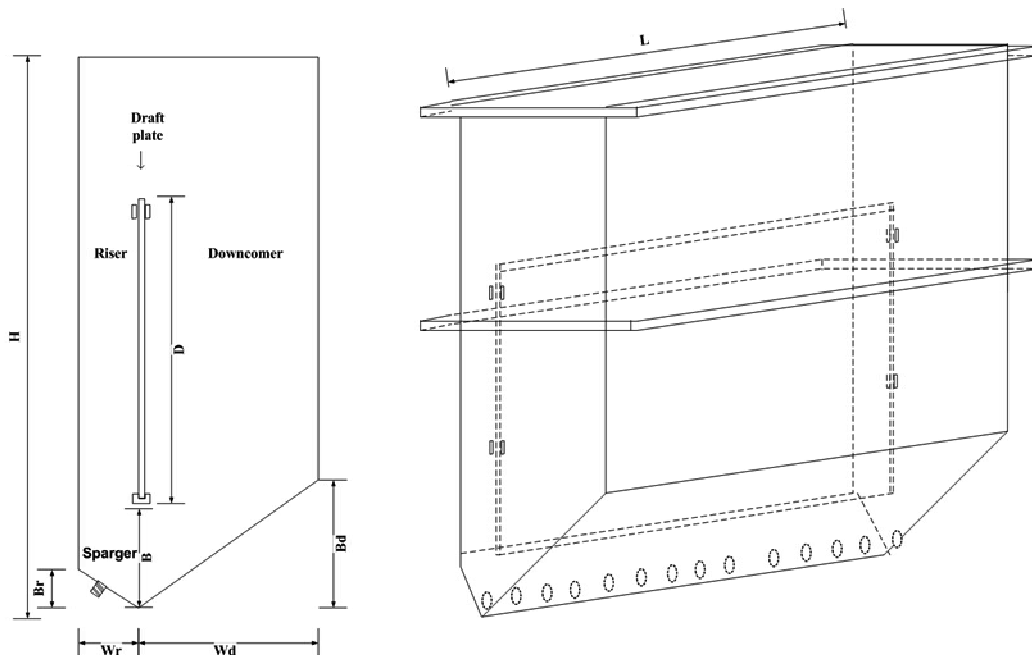


Figure 3. Experimental set-up for the cultivation of *C. gracilis* in flat-panel airlift photobioreactor (FPAP). Arrows indicate flow direction.

Table 3. Dimensions of FPAP

	cm
Reactor height (H)	100
Draft plate height (D)	30
Bottom clearance (B)	9
Riser bottom clearance (Br)	3
Downcomer bottom clearance (Bd)	10
Height of volume	50
Reactor length (L)	120
Riser width (Wr)	5
Downcomer width (Wd)	15

Calculations

The specific growth rate for batch cultivation can be obtained from the slope of plot between the natural logarithm of cell concentration during the exponential phase and cultivation time as follows:

$$\ln(N_2/N_1) = \mu(t_2 - t_1) \quad (1)$$

where μ is specific growth rate (h^{-1}), N_1 is cell concentration ($cells\ mL^{-1}$) at t_1 (first sampling time), and N_2 is cell concentration ($cells\ mL^{-1}$) at t_2 (second sampling time).

For continuous cultivation, the specific growth rate (μ) is equal to the dilution rate (D) at steady state, calculated from:

$$\mu = \frac{F}{V} \times 60 \quad (2)$$

where F is medium feed rate (mL min⁻¹) and V is volume of system (mL).

The productivity for batch culture is calculated from the overall growth period, which represents the average growth of the culture as follows:

$$P = \left(\frac{N_f - N_i}{t_f - t_i} \right) \times v \times 1000 \quad (3)$$

where P is productivity (cells h⁻¹), N_f is final cell concentration (cells mL⁻¹) at t_f, N_i is initial cell concentration (cells mL⁻¹) at t_i, and v is volume of system (mL).

For continuous cultivation, the productivity can be calculated from:

$$P = N \times F \times 60 \quad (4)$$

where N is final cell concentration in the last column of CAP-in-series (cells mL⁻¹) and F is medium feed rate (mL min⁻¹).

The average temperature under outdoor cultivation can be calculated from the average of the sum of maximum temperature and minimum temperature during the day. The average surface energy intensity is the integration over time of solar energy irradiating on the surface of one square metre (MJ m⁻²).

RESULTS AND DISCUSSION

Design Options for Indoor Cultivation

Batch culture: IAP and EAP

Figure 4 displays the growth of *C. gracilis* in both the IAP and EAP operating at u_{sg} of 3 cm s⁻¹. The final cell concentration obtained from the EAP was around 9.82×10^6 cells mL⁻¹ with a productivity of 1.76×10^9 cells h⁻¹ and a specific growth rate of 9.21×10^{-2} h⁻¹ at 94 h, while the IAP gave final cell concentration of 8.34×10^6 cells mL⁻¹, a productivity of 1.46×10^9 cells h⁻¹ and a specific growth rate of 8.56×10^{-2} h⁻¹ at 96 h. The performance of the EAP was better than that of the IAP, apparently due to a better light distribution throughout the column. As the riser and the downcomer of the EAP are separate columns, they are better exposed to light. Our test experiments demonstrated that the light intensities in the EAP system with and without aeration were not much different (measured at the centre of the riser and downcomer), indicating that there was no light shading effect from the bubbles. On the other hand, the light intensity at the centre of the riser in the IAP decreased about 9% after aeration, which lowered the light availability to the culture. In a normal cylindrical airlift configuration (like IAP), when the system is aerated with adequate gas throughput, more bubbles are dragged down the downcomer of the airlift, causing obstruction to light penetration. In addition, as the alga starts to bloom, dense cells in the downcomer further block light passage to the system, which even lowers the intensity for those cells in the riser section. This is why as much as 20% drop in cell productivity is observed in the IAP when compared with the EAP.

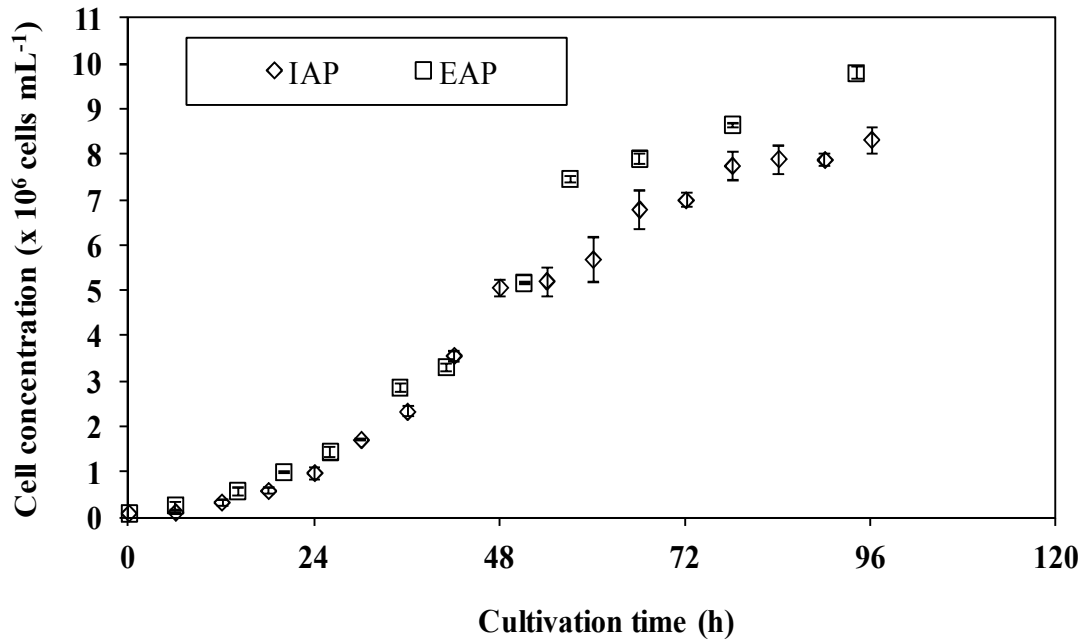


Figure 4. Growth of *C. gracilis* in 17-L IAP and EAP

Continuous culture

Although the IAP provides a lower performance when compared with the EAP, it was employed in the study on continuous culture due to its ease of set-up, maintaining and operating. A CAPs-in-series system is proposed to overcome the self-shading problem in which the over-grown culture obstructs light penetration to the system. In this set-up, cells are allowed to grow in separate compartments connected in series. The first compartment contains the culture at low concentration and therefore is exposed to high light intensity, and only the last compartment contains cells growing at high cell density and is subjected to light obstruction effect. Table 4 shows that an increasing dilution rate from 0.02 to 0.06 leads to a better productivity. Wash-out starts to take place at the dilution rate of 0.08. The productivity is enhanced by installing a series of reactor so that the next reactor is started with culture of higher cell density. However, such configuration in which reactors are installed in series means that the total volume of the system increases and this reduces the dilution rate. In Table 4 the dilution rate of each reactor is provided along with the overall dilution rate of the system where reactors are attached in series. The results indicate that the best productivity can be obtained from a series with 3 reactors, each being operated at a dilution rate of 0.06 (to prevent wash-out in the first column) with an overall dilution rate of 0.02.

Design Options for Outdoor Cultivation

Batch culture

FPAP was employed for outdoor cultivation with no control of light intensity or temperature. Figure 5 displays the profiles of light intensity and temperature during different cultivation periods. The daily maximum light intensity was around 60,000-100,000 Lux whilst the temperature varied between 30-40°C. Table 5 provides the average surface energy intensity and temperature for each season over the one-year period of this experiment. It can be seen that Periods I (summer) and III (winter) were subjected to very similar environmental conditions and both the

Table 4. Performance of CAPs-in-series systems in the cultivation of *C.gracilis*

Experiment	System	Medium feed rate (mL min ⁻¹)	Di [†] (h ⁻¹)	Do [‡] (h ⁻¹)	Final cell concentration (cells mL ⁻¹)	Productivity (cells h ¹)
Set 1	I	1	0.02	0.02	5.79 x 10 ⁶	0.35 x 10 ⁹
Set 2	I	2	0.04	0.04	4.54 x 10 ⁶	0.55 x 10 ⁹
Set 3	I	3	0.06	0.06	4.00 x10 ⁶	0.72 x 10 ⁹
Set 4	II	2	0.04	0.02	8.10 x 10 ⁶	0.97 x 10 ⁹
Set 5	II	4	0.08	0.04	Wash-out*	Wash-out*
Set 6	II	6	0.12	0.06	Wash-out*	Wash-out*
Set 7	III	3	0.06	0.02	12.12 x 10 ⁶	2.18 x 10 ⁹
Set 8	III	6	0.12	0.04	Wash-out*	Wash-out*
Set 9	III	9	0.18	0.06	Wash-out*	Wash-out*

[†] Dilution rate of individual reactor (D=medium feed rate/individual volume of reactor)

[‡] Overall dilution rate of system (D= medium feed rate /total volume)

* Wash-out from one reactor and transferred to the other in series

temperature and energy intensity were in a similar range. Due to the shading by clouds and rain, Period II (rainy season) exhibited lower culture temperature and energy intensity.

The cultivation was started with an initial cell concentration of 1×10^5 cells mL⁻¹ and the average growth of *C. gracilis* in each Period (I, II, III) is illustrated in Figure 6. A maximum cell concentration of 4.50×10^6 cells mL⁻¹ and specific productivity of 3.76×10^4 cells mL⁻¹ h⁻¹ (3.76×10^9 cells h⁻¹) were obtained from 117-h cultivation in Period I. The cultivation in Period II shows a decrease in maximum cell concentration to 3.45×10^6 cells mL⁻¹ and specific productivity to 2.36×10^4 cells mL⁻¹ h⁻¹ (2.36×10^9 cells h⁻¹) which occurred at 142 h. The maximum cell concentration further decreased to 3.05×10^6 cells mL⁻¹ with specific productivity of 3.12×10^4 cells mL⁻¹ h⁻¹ (3.12×10^9 cells h⁻¹) at 95 h when the alga was cultivated in Period III. Note that cell growth ceased after 95 h in Period III. The light exposure duration in Period I (summer) was 1.5 h longer than that in Period III (winter) and this could directly affect the extent of photosynthesis as observed.

Semi-continuous culture

For semi-continuous culture in 100-L FPAPs under the condition as specified in Period I (Figure 5), the maximum cell concentration was found to increase with increase in initial cell concentration as illustrated in Figure 7. The maximum cell concentration of 4.5×10^6 cells mL⁻¹ was obtained during the first round of cultivation with initial cell concentration of 0.1×10^6 cells mL⁻¹. This was equivalent to a specific productivity of 3.76×10^4 cells mL⁻¹ h⁻¹ (2.93×10^9 cells h⁻¹) at 117 h. Then the culture was partially harvested at the seventh day and replenished with fresh medium in a predefined volume such that the initial cell concentration for the second round became 1×10^6 cells mL⁻¹. In this consecutive batch, the maximum cell concentration increased to 7.1×10^6 cells mL⁻¹ after 96 h of cultivation, with a specific productivity of 6.50×10^4 cells mL⁻¹ h⁻¹ (5.59×10^9 cells h⁻¹). The culture was thereafter harvested with the same initial cell concentration for the next batch. The third batch could be harvested after three days at the same maximum cell concentration (7.2×10^6 cells mL⁻¹) but with a much higher specific productivity of 8.86×10^4 cells mL⁻¹ h⁻¹ (8.86×10^9

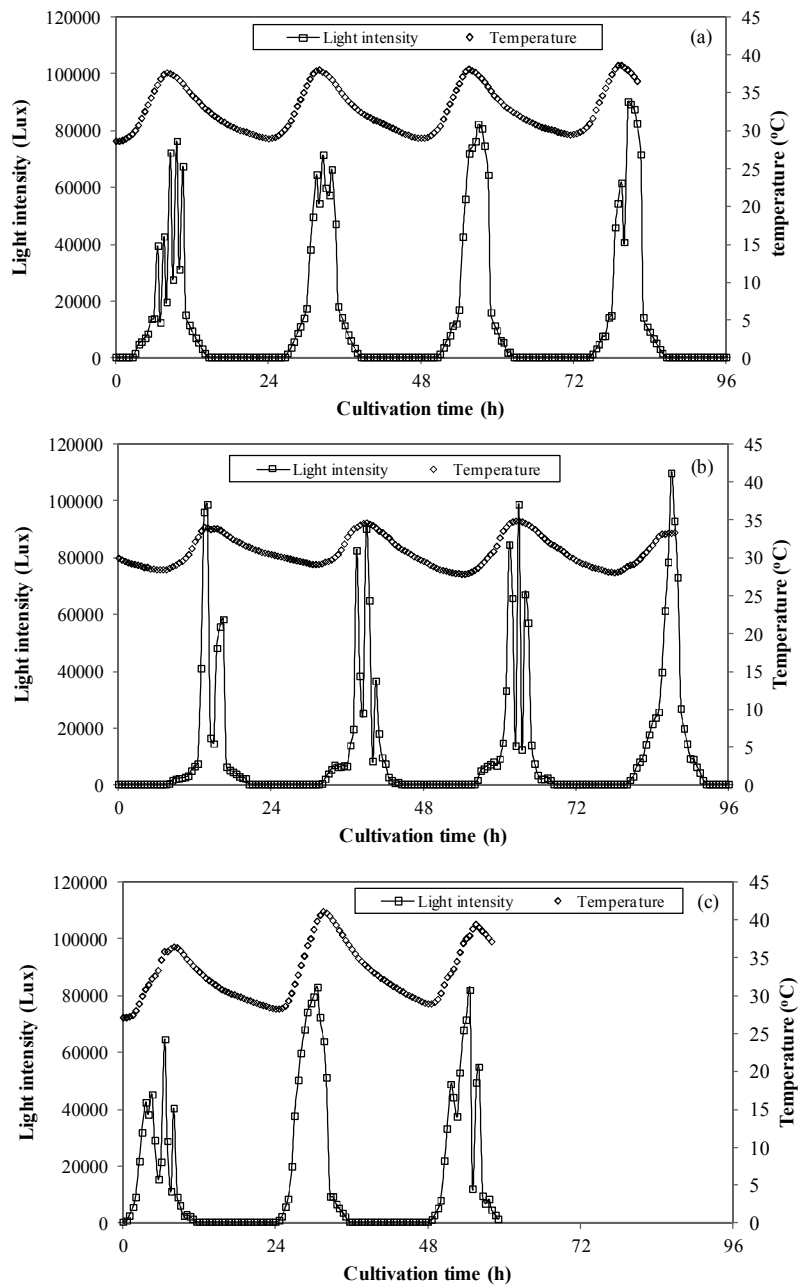


Figure 5. Profile of light intensity and temperature: (a) Period I (summer); (b) Period II (rainy season); (c) Period III (winter). The light intensity after Hour 60 in Period III was not reported due to equipment malfunction.

Table 5. Average surface energy intensity and average temperature during cultivation periods

Period	Average surface energy intensity (kWh m ⁻²)	Average temperature (°C)
Period I (summer)	0.53±0.07	33.7±0.4
Period II (rainy season)	0.40±0.05	31.4±0.5
Period III (winter)	0.50±0.07	33.6±1.6

cells h⁻¹). This results lead to the conclusion that the culture grows better if started with higher cell density as the low-density culture could be subjected to light inhibition during the initial stage. This result corresponds well to the reported cultivation of *Arthrospira platensis* [21] and *Tetraselmis chuii* [22].

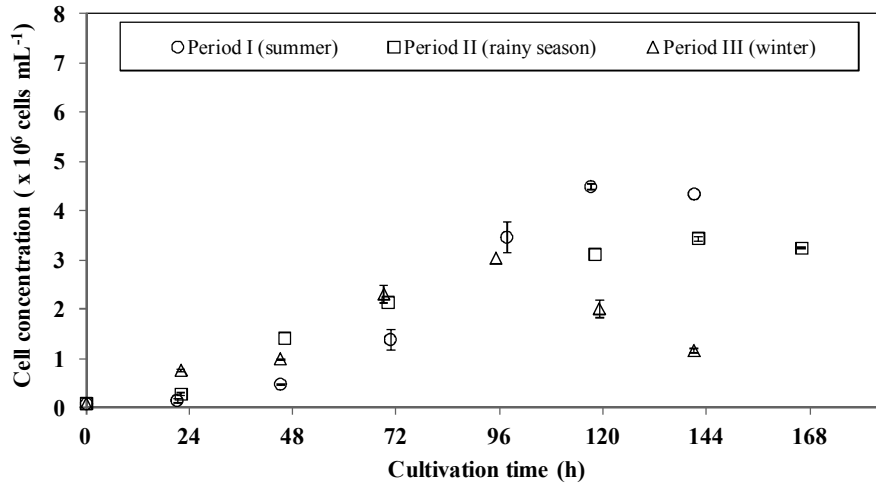


Figure 6. Growth of *C. gracilis* in 100-L FPAP in different seasons

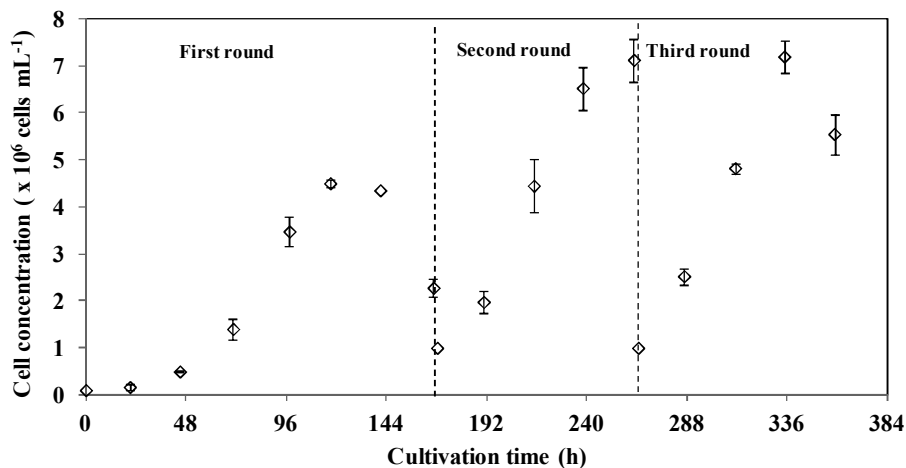


Figure 7. Growth of *C. gracilis* in semi-continuous 100-L FPAP

Economical Analysis

To conduct an economic analysis for the cultivation of *C. gracilis*, it is assumed that the target culture has a cell density of about 5×10^5 cells mL⁻¹ as this is a typical trading value in the Thai market. The cost estimates for *C. gracilis* cultivation using batch culture with different reactor types and sizes are based on the full utilisation of the area of 1.5×1.5 m² and the resulting cost distribution is depicted in Table 6. The estimates cover fixed costs and operating costs, i.e. nutrients, electricity and water, but labour is excluded. The fixed and operating costs are found to be around 40% and 60% respectively of the total cost. For the area of 1.5×1.5 m², the total number of IAP that can be installed is four whilst that of EAP or FPAP is two reactors. Note that the IAP is smaller and simpler in design so a large number can be fitted in the same area when compared with

Table 6. Annual costs estimation for cultivation of *C. gracilis* in indoor and outdoor airlift systems

	Unit	EAP (17L, indoor)	IAP (17L, indoor)	FPAP (100L, outdoor)
Initial cell concentration	cells mL ⁻¹	100,000	100,000	100,000
Max cell concentration	cells mL ⁻¹	9,820,000	8,340,000	3,670,000
Working volume	L reactor ⁻¹	17	17	100
Cultivation time	Days batch ⁻¹	4	4	5
Number of cycle (330 days year ⁻¹)	batches year ⁻¹	83	83	66
Final cell concentration	cells mL ⁻¹	500,000	500,000	500,000
Total product volume	L batch ⁻¹	334	284	734
Volume of brine water (30 ppt) for dilution	L batch ⁻¹	317	267	634
Productivity	L year ⁻¹	27,545	23,394	48,444
Operating costs				
- Nutrient requirements				
Nutrient cost	\$ L ⁻¹	0.0052	0.0052	0.0052
Nutrient charge	\$ year ⁻¹	7.28	7.28	34.24
-Electricity requirements				
1. Lighting	kWh Batch ⁻¹	10.37	10.37	
2. Compressor	kWh Batch ⁻¹	1.37	3.20	48.00
Total electricity requirements	kWh Batch ⁻¹	11.74	13.57	48.00
Electricity charge	\$ kWh ⁻¹	0.0938	0.0938	0.0938
Total Electricity Charge	\$ year ⁻¹	91	105	297
- Water/Brine requirements for medium preparation/dilution				
Volume of brine water (concentration)	L reactor ⁻¹	67	57	147
Brine water (concentration) charge	\$ L ⁻¹	0.0156	0.0156	0.0156
Total brine water (concentration) charge	\$ year ⁻¹	86.08	73.11	185.63
Tap water charge	\$ m ⁻³	0.3125	0.3125	0.3125
Total tap water Charge	\$ year ⁻¹	6.89	5.85	12.11
Total brine water (30 ppt) charge	\$ year ⁻¹	92.96	78.95	163.50
Total operating cost	\$ year⁻¹reactor⁻¹	191.04	191.17	494.74
Fixed costs				
Land and construction (assume 30% of operating cost)	\$ year ⁻¹	57	57	148
Reactor cost	\$ reactor ⁻¹	469	313	531
Reactor life time	year	5	5	5
Reactor charge	\$ year ⁻¹	94	63	106
Compressor	unist reactor ⁻¹	0.14	0.33	4
Compressor cost	\$ unit ⁻¹	81.25	81.25	81.25
Compressor life time	year	10	10	10
Compressor charge	\$ year ⁻¹	1.16	2.71	33
Total fixed cost	\$ year⁻¹reactor⁻¹	152.22	122.56	287.17
Total cost	\$ year⁻¹reactor⁻¹	343.26	313.73	781.91
Number of reactors per 1.5x1.5m ²		2	4	2
Total operating cost	\$ year ⁻¹ m ⁻²	170	340	440
Total fixed cost	\$ year ⁻¹ m ⁻²	135	218	255
Total cost	\$ year⁻¹m⁻²	305	558	695
Income (0.47 \$ L⁻¹)	\$ year⁻¹m⁻²	11,477	19,495	20,185
Profit	\$ year⁻¹m⁻²	11,172	18,937	19,490
Gain (profit/total cost)		37	34	28

Note: Electricity and water charges were based on current Thailand rates (2012): 1\$ = 32 THB.

other configurations. Figure 8 shows that the main operating costs are electricity and brine water. For indoor cultivation, the cost of lighting becomes the major cost which contributes to about 42% of the total cost. Electricity is also the major cost for large-scale outdoor cultivation with around 60% of the overall cost, and this is due to the use of compressors to supply aeration. Brine water is used to adjust the cell density after the harvest and this constitutes around 33-48% of the total cost. For large-scale and outdoor cultivation, the total costs are higher than a small-scale one owing to the effect of sizing. The total cost of FPAP (100 L) is around 695 US\$ year⁻¹m⁻², whereas the small-scale reactors cost about 305-558 US\$ year⁻¹m⁻². However, the large-scale cultivation provides better benefits in terms of return as it exhibits higher productivity provided that it is installed within

the same area. This analysis suggests that for high profitability, options like outdoor and large-scale cultivation should be considered, along with the reuse of brine water. However, the EAP provides the best gain, which suggests highest return per unit of investment.

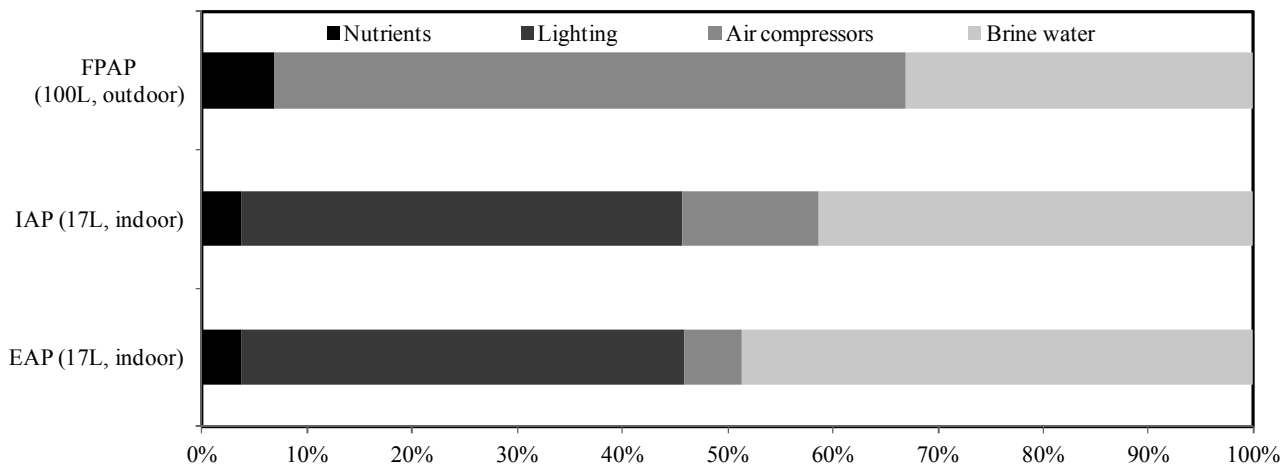


Figure 8. Proportion of operating costs for each airlift photobioreactor

CONCLUSIONS

An airlift photobioreactor has proven effective for the cultivation of *Chaetoceros gracilis*. For indoor cultivation, a good alternative design is achieved through the use of an external-loop airlift system, from which the final cell concentration of 9.82×10^6 cells mL⁻¹ from EAP can be obtained with a specific growth rate of 9.21×10^{-2} h⁻¹, which was higher than 8.34×10^6 cells mL⁻¹ and 8.56×10^{-2} h⁻¹ obtained from IAP. A continuous mode with reactor-in-series configuration provides a higher final cell concentration of 12.12×10^6 cells mL⁻¹. The growth rate in this case is limited by the wash-out condition, which occurs at the individual dilution rate of 0.08 h⁻¹. The outdoor operation, although suffering from uncontrolled environmental conditions, provides satisfactory growth performance. The higher maximum cell specific productivity obtained from indoor culture is counterbalanced by the economy of scale and the ease of operation of the outdoor system.

ACKNOWLEDGEMENTS

These studies were supported by the Thailand Research Fund (TRF) Royal Golden Jubilee Ph.D Programme and the Graduate School Fund, Chulalongkorn University.

REFERENCES

1. T. Göksan, Y. Durmaz and S. Gökpınar, "Effects of light path lengths and initial culture density on the cultivation of *Chaetoceros muelleri* (Lemmermann, 1898)", *Aquaculture*, **2003**, 217, 431-436.
2. K. Issarapayup, S. Powtongsook and P. Pavasant, "Flat panel airlift photobioreactors for cultivation of vegetative cell of microalga *Haematococcus pluvialis*", *J. Biotechnol.*, **2009**, 142, 227-232.
3. A. Richmond and Z. Cheng-Wu, "Optimization of a flat plate glass reactor for mass production of *Nannochloropsis* sp. outdoors", *J. Biotechnol.*, **2001**, 85, 259-269.

4. Y. K. Lee, S. Y. Ding, C. H. Hoe and C. S. Low, "Mixotrophic growth of *Chlorella sorokiniana* in outdoor enclosed photobioreactor", *J. Appl. Phycol.*, **1996**, 8, 163-169.
5. M. R. Tredici and G. C. Zittelli, "Efficiency of sunlight utilization: Tubular versus flat photobioreactors", *Biotechnol. Bioeng.*, **1998**, 57, 187-197.
6. D. O. Hall, F. G. Fernández, E. C. Guerrero, K. K. Rao and E. M. Grima, "Outdoor helical tubular photobioreactors for microalgal production: Modeling of fluid-dynamics and mass transfer and assessment of biomass productivity", *Biotechnol. Bioeng.*, **2003**, 82, 62-73.
7. C. Lu, K. Rao, D. Hall and A. Vonshak, "Production of eicosapentaenoic acid (EPA) in *Monodus subterraneus* grown in a helical tubular photobioreactor as affected by cell density and light intensity", *J. Appl. Phycol.*, **2001**, 13, 517-522.
8. J. C. Merchuk, M. Gluz and I. Mukmenev, "Comparison of photobioreactors for cultivation of the red microalga *Porphyridium* sp.", *J. Chem. Technol. Biotechnol.*, **2000**, 75, 1119-1126.
9. D. Hellenbroich, U. Valley, T. Ryll, R. Wagner, N. Tekkanat, W. Kessler, A. Ross and W. D. Deckwer, "Cultivation of *Tetrahymena thermophila* in a 1.5-m³ airlift bioreactor", *Appl. Microbiol. Biotechnol.*, **1999**, 51, 447-455.
10. K. Kaewpintong, A. Shotipruk, S. Powtongsook and P. Pavasant, "Photoautotrophic high-density cultivation of vegetative cells of *Haematococcus pluvialis* in airlift bioreactor", *Bioresour. Technol.*, **2007**, 98, 288-295.
11. R. Ranjbar, R. Inoue, T. Katsuda, H. Yamaji and S. Katoh, "High efficiency production of astaxanthin in an airlift photobioreactor", *J. Biosci. Bioeng.*, **2008**, 106, 204-207.
12. S. Krichnavaruk, W. Loataweesup, S. Powtongsook and P. Pavasant, "Optimal growth conditions and the cultivation of *Chaetoceros calcitrans* in airlift photobioreactor", *Chem. Eng. J.*, **2005**, 105, 91-98.
13. S. Krichnavaruk, S. Powtongsook and P. Pavasant, "Enhanced productivity of *Chaetoceros calcitrans* in airlift photobioreactors", *Bioresour. Technol.*, **2007**, 98, 2123-2130.
14. S. Y. Chiu, M. T. Tsai, C. Y. Kao, S. C. Ong and C. S. Lin, "The air-lift photobioreactors with flow patterning for high-density cultures of microalgae and carbon dioxide removal", *Eng. Life Sci.*, **2009**, 9, 254-260.
15. B. Ketheesan and N. Nirmalakhandan, "Development of a new airlift-driven raceway reactor for algal cultivation", *Appl. Energy*, **2011**, 88, 3370-3376.
16. B. Ketheesan and N. Nirmalakhandan, "Feasibility of microalgal cultivation in a pilot-scale airlift-driven raceway reactor", *Bioresour. Technol.*, **2012**, 108, 196-202.
17. J. A. López-Elías, D. Voltolina, F. Enríquez-Ocaña and G. Gallegos-Simental, "Indoor and outdoor mass production of the diatom *Chaetoceros muelleri* in a Mexican commercial hatchery", *Aquacult. Eng.*, **2005**, 33, 181-191.
18. C. Y. Chen, K. L. Yeh, R. Aisyah, D. J. Lee and J. S. Chang, "Cultivation, photobioreactor design and harvesting of microalgae for biodiesel production: A critical review", *Bioresour. Technol.*, **2011**, 102, 71-81.
19. M. Becerra-Dórame, J. A. López-Elías and L. R. Martínez-Córdova, "An alternative outdoor production system for the microalgae *Chaetoceros muelleri* and *Dunaliella* sp. during winter and spring in Northwest Mexico", *Aquacult. Eng.*, **2010**, 43, 24-28.
20. S. A. van Bergeijk, E. Salas-Leiton and J. P. Cañavate, "Low and variable productivity and low efficiency of mass cultures of the haptophyte *Isochrysis* aff. *galbana* (T-iso) in outdoor tubular photobioreactors", *Aquacult. Eng.*, **2010**, 43, 14-23.

21. P. Carlozzi, “Dilution of solar radiation through “culture” lamination in photobioreactor rows facing South-North: A way to improve the efficiency of light utilization by cyanobacteria (*Arthrospira platensis*)”, *Biotechnol. Bioeng.*, **2003**, 81, 305-315.
22. J. A. López-Elías, E. Esquer-Miranda, M. Martínez-Porchas, M. C. Garza-Aguirre, M. Rivas-Vega and N. Huerta-Aldaz, “The effect of inoculation time and inoculum concentration on the productive response of *Tetraselmis chuii* (Butcher, 1958) mass cultured in F/2 and 2-F media”, *Arch. Biol. Sci.*, **2011**, 63, 557-562.

© 2014 by Maejo University, San Sai, Chiang Mai, 50290 Thailand. Reproduction is permitted for noncommercial purposes.